The HKU Scholars Hub    The University of Hong Kong    香港大學學術庫

| Title | **Provenance and tectonic setting of the Neoproterozoic Yanbian Group, western Yangtze Block (SW China)** |
|---|---|
| Author(s) | **Sun, WH; Zhou, MF; Yan, DP; Li, JW; Ma, YX** |
| Citation | **Precambrian Research, 2008, v. 167 n. 1-2, p. 213-236** |
| Issued Date | **2008** |
| URL | **http://hdl.handle.net/10722/58670** |
| Rights | **Creative Commons: Attribution 3.0 Hong Kong License** |

1 Provenance and tectonic setting of the Neoproterozoic Yanbian

2 Group, western Yangtze Block (SW China)

3

4 Wei-Hua Sun [a,] [*], Mei-Fu Zhou [a], Dan-Ping Yan [b], Jian-Wei Li [c] and Yuxiao Ma [d]

5

6 [a] Department of Earth Sciences, University of Hong Kong, Hong Kong, China

7 [b] School of Earth Sciences and Resources, China University of Geosciences, Beijing 100083,

8 China

9 [c] State Key Laboratory of Geological Processes and Mineral Resources, and Faculty of Earth

10 Resources, China University of Geosciences, Wuhan 430074, China

11 [d] Department of Geochemistry, Chengdu University of Science and Technology, Chengdu, China

12

13 * Corresponding author. Tel.: +852 2859 8913; Fax: +852 2517 6912.

14 E-mail: weihua@hkusua.hku.hk

15 **Abstract**

16 Tectonic evolution of the Yangtze Block of South China during

17 Neoproterozoic time has been a major focus of debate and is important in the

18 reconstruction of the Rodinian supercontinent. The Yanbian Group in the western

19 margin of the Yangtze Block is a well-preserved Neoproterozoic volcanic-

20 sedimentary sequence and provides a rare opportunity to examine the

21 provenance and tectonic setting. It consists of a lower part composed of ~1500 m

22 thick basaltic lavas and an upper part with ~3500 m thick flysch deposits. The

23 flysch sequence contains typical deep marine turbidites consisting mainly of fine-

24 grained volcaniclastic sandstones and mudstones, indicating a submarine fan

25 depositional system. Detrital zircon dating yields ages ranging from ca. 865 Ma to

26    1000 Ma with two peaks at ca. 900 Ma and 920 Ma, respectively. The Yanbian

27    Group is intruded by the ~860- Ma Guandaoshan dioritic pluton, constraining its

28    depositional age at ca. 870 Ma. The sandstones contain abundant feldspar and

29    lithic fragments with minor amounts of quartz and have an average composition

30    of $Q_{16}F_{35}L_{49}$, suggesting a proximal source and an undissected to transitional arc

31    setting. The lithic fragments in the sandstones point to andesitic and felsic

32    volcanic rock sources. The sandstones and mudstones have intermediate

33    $SiO_2/Al_2O_3$ (typically 3-6), high $Fe_2O_3$+MgO contents (5-12 wt%), and moderate

34    to high $K_2O/Na_2O$ ratios (generally 0.1-1 and 1-10 for sandstones and mudstones,

35    respectively). In comparison with average upper continental crust, they show

36    strong Nb-Ta anomalies, slight depletion of Zr-Hf, La and Th, but moderate

37    enrichment of V, Cr, Ni, and Sc. These rocks show LREE enrichment

38    ($La/Yb_N$=5.3-7.4) with flat HREE, and pronounced negative Eu anomalies

39    (Eu/Eu*=0.6-0.74) in chondrite-normalized REE patterns, similar to post-Archean

40    shales. Geochemical data for these rocks suggest an arc setting and

41    intermediate-felsic volcanic source, consistent with a back-arc basin scenario for

42    the basaltic lavas in the lower Yanbian Group. Together with regional geological

43    evidence, the turbidites of the Yanbian Group strongly support a model in which

44    the western margin of the Yangtze Block was a major magmatic arc, active

45    probably from ~920 Ma to 740 Ma, a period of more than 180 million years.

46

47    **Key words**: turbidite, detrital zircon dating, geochemistry, provenance, Yanbian

48    Group, Yangtze Block

## 1. Introduction

Siliciclastic rocks are useful for investigating provenance and tectonic setting of sedimentary basins (Dickinson, 1970, 1985; Bhatia, 1983, 1985; Roser and Korsch, 1986, 1988; Floyd and Leveridge, 1987). Provenance regions, especially those at destructive plate margins, are rarely well preserved because of subsequent erosion and destruction. In such circumstances, studies of related sedimentary rocks have considerable potential for determining the source rocks and the history of ancient continental margins. A combination of traditional mineralogical (especially for sandstones) and geochemical methods and detrital zircon U-Pb analysis has greatly contributed to our understanding of the provenance, tectonic setting and tectonomagmatic evolution of sedimentary basins and their siliciclastic deposits (McLennan et al., 1990, 1995; Maas and McCulloch, 1991; Taylor and McLennan, 1995; Dickinson and Gehrels, 2000; DeGraaff-Surpless et al, 2002; Cope et al., 2005; She et al., 2006).

The tectonic evolution of the Yangtze Block of South China is of importance for the reconstruction of the supercontinent Rodinia and has been a matter of hot debate (Li Z.X. et al., 1999, 2003; Li X.H. et al., 2003, 2006; Zhou et al., 2002a, b, 2006a, b). Previous work has focused mainly on the Neoproterozoic igneous rocks, and studies of the associated sedimentary sequences are sparse. The Neoproterozoic Yanbian Group in the western margin of the Yangtze Block has been a subject of several recent studies (Du et al., 2005; Zhou et al., 2006a; Li X.H. et al., 2006; Sun et al., 2007), because it is not only one of the best-preserved volcano-sedimentary sequences in South China, but is spatially

72  associated with several contemporaneous intermediate to mafic plutons, making

73  it ideal for investigating the tectonic affinities of the Yangtze Block. Previous

74  studies on the volcanic rocks in the lower part of the Yanbian Group and the

75  related intrusive rocks have interpreted the Yanbian Group as a relict ophiolite

76  (Sun and Vuagnat, 1992) or a back-arc basin sequence (Du et al., 2005; Zhou et

77  al., 2006a; Li X.H. et al., 2006, Sun et al., 2007). So far, there is no agreement

78  about the depositional age of the Yanbian Group (Du et al., 2005; Zhou et al.,

79  2006a; Li X.H. et al., 2006), causing  additional ambiguity in its tectonic

80  interpretation. In particular, no studies are available regarding the chemical

81  composition and petrology of the sedimentary rocks, which are crucial to better

82  understanding the source rocks and tectonic setting.

83  In this paper, we present petrographic, detrital zircon U-Pb geochronological

84  and geochemical data for the upper siliciclastic rocks of the Yanbian Group, in an

85  attempt to constrain the age of the sediments and to infer their provenance and

86  tectonic setting. The results also provide insights into the tectonic evolution of the

87  Yangtze Block during Neoproterozoic time.

88

89  ## 2. Geological background

90  South China consists of the Yangtze Block in the northwest and the

91  Cathaysia Block in the southeast (Fig. 1). The Yangtze Block is separated from

92  the North China Craton by the Qinling-Dabie orogenic belt and is bounded to the

93  west by the Songpan-Ganze Terrane of the Tibetan Plateau. The Songpan-

94  Ganze Terrane is a prominent triangular region filled with Triassic deep-marine

95  flysch deposits (Zhou and Graham, 1996). The Yangtze Block comprises

96  metamorphic basement complexes and Neoproterozoic to Cenozoic cover

97  sequences (Yan D.P. et al., 2003). The basement complexes contain gneiss,

98  mica schist, amphibolite, marble and quartzite, whereas the cover sequences are

99  mainly composed of carbonate, clastic and volcanic rocks (SBGMR, 1991).

100  Along the western margin of the Yangtze Block, a ~1000-km-long, NS-

101  trending, Neoproterozoic igneous and metamorphic belt crops out from Kangding

102  in Sichuan Province to Yuanjiang in Yunnan Province (Fig. 1). This belt has been

103  recently interpreted as a major Neoproterozoic continental arc, named the

104  Hannan-Panxi arc, in which the igneous rocks have ages mostly ranging from

105  860 to 740 Ma (Zhou et al., 2002a, b, 2006a, b; Zhao and Zhou, 2007; Sun and

106  Zhou, 2008). The occurrence of this huge continental arc indicates an Andean-

107  type continental margin with oceanic crust being subducted eastward beneath

108  the western margin of the Yangtze Block during that time (Zhou et al., 2002b;

109  Sun and Zhou, 2008).

110  In the belt, the igneous plutons intrude high-grade (granitic gneisses and

111  amphibolite) and low-grade metamorphic rocks (Pan et al., 1987; Li  F.H. et al.,

112  1988). The high-grade metamorphic rocks, including the Kangding and

113  Dahongshan complexes, were traditionally considered to be late Archean to

114  Paleoproterozoic crystalline basement; the low-grade metamorphic rocks, such

115  as the Kunyang, Huili, Yanbian and Bikou Groups, were interpreted to be

116  Mesoproterozoic and to constitute the folded basement in this region (Chen and

117  Chen, 1987).

118    The Yanbian Group is unconformably overlain by Sinian (latest

119    Neoproterozoic) strata known as the Lieguliu Formation (Sun et al., 2007), which

120    is composed of glacial deposits, comparable to those of similar age on other

121    continents (Elsbacher, 1985). The Yanbian Group is intruded by a magmatic

122    association that consists of the ~860-Ma Guandaoshan dioritic pluton (Li X.H. et

123    al., 2003; Sun and Zhou, 2008), 810-820-Ma Tongde dioritic-gabbroic pluton (Li

124    Z.X. et al., 2003) and ~810-Ma Gaojiacun and Lengshuiqing mafic plutons (Zhou

125    et al., 2006a) (Fig. 1). These, together with the ~740 Ma Dadukou gabbroic

126    intrusion south of Tongde Town (Zhao and Zhou, 2007), have been interpreted

127    as part of the Hannan-Panxi arc along the western margin of the Yangtze Block

128    (Sun and Zhou, 2008).

129

## 130    3. Stratigraphy and depositional environment

131    Cropping out over an area of approximately 500 km$^2$, the Yanbian Group  is

132    composed of two principal units: a lower volcanic sequence ca. 1500 m thick,

133    known as the Fangtian Formation, and an upper flysch  more than 5000 m  thick,

134    comprising the Yumen, Xiaoping and Zagu Formations (Fig. 2)

135    The Fangtian Formation is composed of massive basalt, pillow basalt and

136    volcanic breccias with subordinate interbeds of chert, and pelitic and siliceous

137    slate. It is conformably overlain by the ca.1700-m-thick Yumen Formation, which

138    consists primarily of thin- to medium-bedded, dark-gray, carbonaceous and

139    siliceous slates with interbeds of fine- to coarse-grained sandstone (Fig. 3a).

140    Lenses of limestone are locally present. An ~5-cm-thick layer of black chert

141  marks the base of the Yumen Formation where it overlies the basaltic breccias of

142  the Fangtian Formation (Fig. 3a). The slates and sandstones have regular

143  parallel bedding, typical of distal turbidites. In this formation, turbidites generally

144  display $T_{bce}$ of the Bouma sequences.

145    The ~2200-m-thick Xiaoping Formation comprises dark gray slates,

146  carbonaceous slates, fine- to coarse-grained sandstones and siltstones,

147  representing turbidites and associated mudstones. The basal and top parts of the

148  succession are dominated by sandstones in beds up to 1.5 m thick, suggesting

149  small-scale channel-fill deposits. The sandstone channels usually display an

150  eroded base and a concave-upward morphology, with the grain size fining

151  upward.  Conglomerates are locally present as thin, discontinuous lag beds at

152  the base of the coarse sandstone layers. The sandstones have lenticular or flat

153  beds with thicknesses of 10-20 cm, but ranging from 2 to 50 cm. Sedimentary

154  structure, such as scours, slumps, and load and flame structure, are locally well

155  developed (Figs. 3b, c). Most sandstone beds are normally graded and follow the

156  Bouma sequence. Partial Bouma sequences are more common than complete

157  ones, with the $T_{abc}$ sequence being the most common, followed in abundance by

158  $T_{ae}$ (Fig. 3d). Thin limestone lenses and stromatolithic limestones are also

159  observed locally. Pyrite is common in the slates and siltstones, especially along

160  some layer boundaries.

161    The ~1300-m-thick Zagu Formation is composed of dark gray slates, black

162  dolomitic slates and dolomitic limestones. There is a thin (10-15 m) layer of

163  conglomerate and pebbly sandstone at the base, representing a medium-scale

164 channel-fill deposit. The conglomerate clasts are typically subangular to

165 subrounded, generally 2-4 cm in diameter, and consist mainly of intermediate-

166 felsic volcanic rocks (50-60%), chert (20-25%), fragments of carbonaceous rock

167 (10-15%) and siltstone (~10%). The conglomerates and sandstones are also well

168 graded. The Zagu Formation is unconformably overlain by the Sinian Lieguliu

169 Formation (Sun et al., 2007).

170 The Yanbian Group consists mainly of thin- to medium-bedded, fine-grained,

171 turbiditic volcaniclastic sandstones and mudstones with little variation in

172 sedimentary facies and minor input of coarse clastic material. These sedimentary

173 rocks most likely represent submarine fan deposits, especially mid-fan deposits.

174 This thick turbidite package lacking shallow-water deposits indicates a marine

175 environment below wave base. The presence of limestones throughout the

176 section indicates that the seafloor was above the carbonate compensation depth

177 and suggests a low-latitude, warm-water environment.

178

179 **4. Sandstone petrography**

180 The sandstones are mostly fine- to medium-grained, poorly sorted and

181 contain angular to subangular grains of low to moderate sphericity. They are

182 mainly composed of quartz, feldspar and lithic fragments. Quartz is relatively

183 minor in volume and is generally subangular to angular, mostly being

184 monocrystalline and lacking inclusions and undulatory extinction (Fig. 4a).

185 Subrounded feldspar is the dominant mineral and is partly altered to saussurite

186 and sericite. Plagioclase is much more common than alkali feldspar (Fig. 4b).

187 Lithic fragments are dominantly rhyolite and andesite with felsitic and microlitic

188 textures, although sedimentary and metamorphic varieties are also present (Figs.

189 4c,d,e).

190 Biotite and muscovite occur as elongate laths or short plates and are locally

191 accompanied by chlorite and glauconite. Sparse heavy minerals include

192 magnetite, zircon, apatite, titanite, pyrite, rutile and tourmaline. Most of these

193 grains are angular to subangular, although some are well-rounded. Amphibole

194 and pyroxene grains are locally present but extremely rare (Fig. 4f).

195 The matrix of the sandstones consists of clay minerals, comminuted and

196 altered lithic and feldspathic fragments, fine-grained quartz, micas, opaque

197 minerals, carbonate and some aphanitic material. Matrix is commonly between

198 10 to 15%, but may be overestimated due to the pseudomatrix problem

199 (Dickinson, 1970). Silica is the dominant cement in these rocks but calcite is also

200 common.

201 Thirty-one medium-grained sandstones were selected for petrographic study

202 using the Gazzi-Dickinson method (Ingersoll et al., 1984). About five to six

203 hundred framework grains were counted from each sample. Matrix (<~0.03 mm)

204 and cement were not counted. The Gazzi-Dickinson method divides volcanic

205 lithic clasts into various textural types (Dickinson, 1970), which is especially

206 significant in magmatic-arc settings, where volcaniclastic components may

207 constitute as much as 100% of the sand fraction (Marsaglia and Ingersoll, 1992).

208 Point-count categories and recalculated parameters are defined in Table 1.

209    The modal point-count data are shown in Table 2 and Figure 5. In general,

210    the sandstones are characterized by low quartz (Q), moderate feldspar (F) and

211    high lithic (L) abundances, with L/F ratios of 1-3, indicating that the sandstones

212    were derived almost exclusively from volcanic sources (Dickinson, 1970). The

213    Yumen, Xiaoping and Zagu Formations have average compositions of $Q_{22}F_{30}L_{48}$,

214    $Q_{15}F_{36}L_{49}$, and $Q_{14}F_{34}L_{52}$, respectively. In the discrimination diagrams (Fig. 5),

215    they plot in the magmatic-arc field, indicating an undissected-transitional arc

216    provenance.

217

218    **5.  Geochronology and geochemistry**

219    **5.1. Detrital zircon geochronology**

220    Single-grain U-Pb dating were performed using the laser ablation ICP-MS

221    technique at China University of Geosciences (Wuhan). The detailed analytical

222    procedures follow Yuan et al. (2004). A GeoLas 2005M laser-ablation system

223    equipped with a 193 nm ArF-excimer laser was used in connection with an

224    Agilent 7500 ICP-MS. Helium was used as the carrier gas to enhance the

225    transport efficiency of the ablated material. The spot diameter was 32 μm. Raw

226    data were processed using the Glitter program (Jackson et al., 2004). All

227    measurements were normalized relative to standard zircon 91500. Standard

228    silicate glass NIST SRM610 was used to calculate U and Th concentrations. The

229    data were processed using the ISOPLOT program (Ludwig, 1999).

230    Zircons from these rocks are commonly transparent to orange in color, 100-

231    200 μm in size and subrounded to subangular. A total of two hundred and ninety-

232    eight analyses were performed on zircon grains from five samples (Table 3). Of

233    those, 40 analyses with a degree of discordance >3% were discarded. However,

234    only a very few of these discordant analyses yield ages outside the range defined

235    by the remaining relatively concordant analyses. $^{207}Pb/^{206}Pb$ and $^{206}Pb/^{238}U$ ages

236    were applied for zircons older and younger than 1000 Ma, respectively. The

237    dataset yields ages mainly of ~900-920 Ma with only a very minor, statistically

238    insignificant, component of older continental-derived zircons in the Yumen and

239    Xiaoping Formations. The Zagu Formation, on the other hand, has a relatively

240    high content of older continental material (Fig. 6).

241    **5.1.1. Yumen Formation**

242    Sample F38, a coarse-grained sandstone specimen, was collected near the

243    base of the Yumen Formation (N26.53.39, E101.30.80) for zircon dating. Of the

244    60 grains analyzed, 4 were highly discordant and thus were discarded. The

245    remaining forty-six grains yielded $^{206}Pb/^{238}U$ apparent ages ranging from 865 to

246    975 Ma, with a single peak at 917±6 Ma (Fig. 6).

247    Sample F3, consisting of coarse-grained, feldspar-lithic sandstone, was

248    collected from the upper part of the Yumen Formation (N26.54.47, E101.28.89).

249    Of 58 spot analyses, 41 have concordant ages ranging from 860 to 990 Ma with

250    a weighted mean of 918±8 Ma. Only one concordant grain has a significantly

251    older age of ~2000 Ma (Fig. 6). The remaining 16 analyses are highly discordant

252    but have ages within the younger age population. Thus, the age distribution of

253    zircons from the Yumen Formation suggests uniform source rocks.

254

**5.1.2. Xiaoping Formation**

A medium- to coarse-grained, feldspar-lithic sandstone, sample F4, was collected from the middle part of the Xiaoping Formation (N26.55.96, E101.27.45). Of the 60 grains analyzed, 45 concordant grains yielded apparent $^{206}Pb/^{238}U$ ages between 850 and 960 Ma, with a prominent peak at ~920 Ma. Three concordant grains gave much older ages from ~2200 to 2600 Ma (Fig. 6). This age spectrum is very similar to that of samples F38 and F3 of the Yumen Formation. However, half of the remaining 12 analyses with varying degrees of discordance (>3%) yield older ages of around 2200-2600, suggesting a somewhat greater input of older material input relative to the Yumen Formation. Several concordant ages are as young as ~850 Ma (Fig. 6).

Sample F26 (N26.58.76, E101.32.17) was collected near the top of the Xiaoping Formation. 42 of 60 spot analyses have concordant ages ranging from 860 to 970 Ma, with two peaks of 897±6 Ma and 934±5 Ma, respectively (Fig. 6). The remaining 18 discordant analyses also show similar age ranges.

**5.1.3. Zagu Formation**

A pebbly sandstone, sample F23 (N26.58.96, E101.32.17), was collected from the base of the Zagu Formation. Of 60 grains analyzed, 46 are concordant. This sample yields an age distribution mainly between~ 870 Ma and 930 Ma, but it is characterized by sharp increase of older zircons with several minor peaks at 1800, 2000, 2600 and 3000 Ma (Fig. 6). Coupled with a rapid coarsening in the stratigraphic section, this suggests increased uplift and erosion in the source terrane.

## 5.2. Whole rock geochemistry

Major oxides and selected trace elements of whole-rock samples were determined by X-ray fluorescence (XRF) on fused glass beads at the University of Hong Kong. Trace elements were analyzed with a VG PQ Excell ICP-MS, also at the University of Hong Kong. The samples for ICP-MS analysis were prepared in closed beakers in high-pressure bombs to ensure complete digestion (Qi et al., 2000). We used pure elemental standards for external calibration, and BHVO-1 (basalt) and SY-4 (syenite) as reference materials for all analyses. Accuracies of the XRF analyses are estimated to be better than 1% for $SiO_2$, better than 2% for major oxides present in concentrations greater than 0.5 wt% and 5% for trace elements. The ICP-MS analyses yielded accuracies better than 5%.

### 5.2.1. Major elements

The majority of the Yanbian Group sandstones and mudstones have intermediate $SiO_2$ (55-73 wt%), high $Fe_2O_3$+MgO (usually 5-12 wt%; total Fe as $Fe_2O_3$) and $TiO_2$ (0.6-1.2 wt%) and low CaO (mostly <1 wt%) (Table 4). In general, $SiO_2$ increases whereas $TiO_2$, $Al_2O_3$, $Fe_2O_3$, MnO, MgO, CaO, and $Na_2O$ decrease with enhanced mineralogical maturity, indicating an increase in the quartz content and a decrease in chemically unstable detrital grains (e.g., feldspar and volcanic rock fragments) (Bhatia, 1983). There are no systematic stratigraphic variations from the Yumen through Xiaoping to Zagu Formations, possibly reflecting inadequate sampling from the Yumen and Zagu Formations.

300      Due to enrichment in clay minerals, the mudstones generally have higher

301    $K_2O$ and $Al_2O_3$ and lower $Na_2O$ contents, resulting in much higher $K_2O/Na_2O$

302    ratios (typically 1-10) than those of the corresponding sandstones (commonly

303    0.1-1). Most sandstone samples are immature, with $SiO_2/Al_2O_3$ ratios between 3

304    to 6 and $Na_2O/K_2O$ ratios between 1 to 3.5, and plot within the graywacke field in

305    the plot of Pettijohn (1987) (Fig. 7).

306    **5.2.2. Trace elements**

307    Rocks from the three Formations are virtually indistinguishable in their trace

308    element contents, and are characterized by variable contents of Rb (7-140 ppm),

309    Sr (10-377 ppm), Cs (0.4-8 ppm), Ba (80-1200 ppm), Th (2.6-12 ppm) and U

310    (0.5-3.2 ppm) (Table 4). In comparison with average upper continental crust, they

311    show strong Nb-Ta, anomalies, slight depletion of Zr-Hf, La and Th, but moderate

312    enrichment of V (17-257 ppm), Cr (15-185 ppm), Ni (<80 ppm), and Sc (8-22

313    ppm) (Fig. 8a). In addition, the mudstones commonly have higher Rb, Ba, Th, U

314    and Cs contents than the sandstones (Fig 8a), likely reflecting the abundance of

315    clay minerals (e.g., illite and sericite) in these rocks (McLennan et al., 1983).

316    Both the sandstones and mudstones exhibit subparallel chondrite-

317    normalized REE patterns, characterized by moderate fractionation between light

318    REE and heavy REE ($La/Yb_N$=5.3-7.4), with obvious negative Eu anomalies

319    ($Eu/Eu^*$=0.6-0.74) (Fig. 8b), features typical of post-Archean sedimentary rocks

320    (Taylor and McLennan, 1985). Moreover, the mudstones generally have slightly

321    more fractionated REE patterns than the sandstones and ~20% higher total REE

322    abundances.

323

## 6. Discussion

### 6.1. Age of the Yanbian Group

The depositional age of the unfossiliferous Yanbian Group has long been debated. It was traditionally thought to be Mesoproterozoic (Pan et al., 1987; SBGMR, 1991). However, newly obtained SHRIMP U-Pb zircon ages of 782±53 Ma (Du et al., 2005) for the basaltic lavas of the lower Yanbian Group strongly suggest a Neoproterozoic age. Similarly, Zhou et al. (2006a) reported a maximum depositional age of 837±6 Ma based on LA-ICP-MS detrital zircon dating. By contrast, Li X.H. et al. (2003, 2006) proposed a minimum age of 857±13 Ma, inferred from the emplacement age of the Guandaoshan pluton that intrudes the Yanbian Group. Thus the depositional age of the Yanbian Group should be no younger than 857 ± 13 Ma. The present geochronological results provide reliable and tight constraints on the maximum depositional age of the Yanbian Group. Although eight youngest zircons from the Yanbian Group give ages as young as 852±6 Ma (Fig. 6), we adopt here a somewhat older age of 868±6 Ma defined by another ten youngest zircon dates in the concordant dataset (Table 3). The ten zircons are from different samples but yield similar ages within quoted errors. We therefore suggest that the Yanbian Group was most likely not older than ~870 Ma. Furthermore, the Yanbian Group was probably deposited in a syn-magmatic basin, based on the short time delay between deposition of the sediments and emplacement of the 857±13 Ma Guandaoshan pluton.

## 6.2. Effect of chemical weathering

Chemical weathering strongly affects the mineralogy and major element geochemistry of siliciclastic sediments (Nesbitt and Young, 1982, 1996). The chemical index of alteration (CIA) is very useful in evaluating effects of weathering on sedimentary rock composition and is defined by Nesbitt and Young (1982) as:

$$CIA = [Al_2O_3/(Al_2O_3+CaO^*+Na_2O+K_2O)] \times 100$$

Where CaO* represents Ca in the silicate minerals only (i.e. excluding calcite, dolomite and apatite) (Fedo et al., 1995). High CIA values reflect the removal of labile cations (e.g., $Na^+$, $K^+$ and $Ca^+$) in preference to relatively stable residual constituents (e.g. $Al^+$), corresponding to high degrees of chemical weathering. The values vary from about 50 for the average upper continental crust to about 100 for residual clays. Shales typically have intermediate values of about 70-75, indicating that weathering did not proceed to the stage where alkali and alkaline earth elements were substantially removed from the clay minerals (Nesbitt and Young, 1982). The Yanbian sandstones have CIA values ranging broadly from 49 to 73 and the mudstones from 57 to 84 (Table 4 and Fig. 9). In turbidites, physical sorting during transport and deposition would yield mudstone with high concentration of fine-grained, aluminous clay minerals of high-CIA value (e.g., kaolinite, gibbsite) derived from the upper parts of weathering profiles, and sandstone relatively enriched in coarse-grained low-CIA residue (e.g., quartz, vestigial feldspars) derived from the lower parts of weathering profiles (Nesbitt et al., 1996). The CIA values of mudstones, therefore, will give a better

369 understanding of the intensity of weathering in the source. Most mudstones have

370 CIA values ranging from 65 to 77, reflecting only moderate source weathering.

371 However, 6 mudstone samples in the Xiaoping Formation and 1 sample from the

372 Zagu Formation having much higher CIA values in the range of 79-84 than

373 typical shales of 70-75. If these values were corrected for K metasomatism (Fedo

374 et al., 1995), their CIA values would be even greater than 90 (Fig. 9), indicative of

375 severe weathering in the source. One possible explanation for the higher CIA

376 values in the few samples from the Xiaoping and Zagu Formations may indicate

377 a contribution of a greater proportion of distal high-CIA detritus from older

378 cratonic source, which is consistent with our detrital zircon data.

379    The A-CN-K ($Al_2O_3$-CaO*+$Na_2O$-$K_2O$) triangular plot can also be used to

380 constrain the initial compositions of the source rocks (Fedo et al., 1995). The

381 sandstones and mudstones from the Yanbian Group form a linear trend, which is

382 generally subparallel to the A-CN join, but is slightly below the predicted

383 weathering trend, especially for the fine-grained mudstones (Fig. 9). This

384 probably indicates that the mudstones were more profoundly affected by

385 illitization. Their weathering trends suggest a provenance of tonalitic or

386 granodioritic rocks for the Yanbian sediments.

387 Differential        weathering        at        the        source        and        subsequent

388 diagenesis/metamorphism tend to mobilize and change the relative abundance of

389 large-ion lithophile elements (Nesbitt et al., 1980). However, the Yanbian

390 sandstones and mudstones commonly show linear correlation in the elemental

391 plots of K vs. Rb, K vs. Ba, Ce vs. Sm and U vs. Th (Fig. 10), indicating that

392   these elements were probably not changed significantly. Moreover, because the

393   sandstones studied here are relatively uniform in grain size, we believe that the

394   grain-size effect is not important.

395   **6.3. Tectonic setting of the Yanbian Group**

396   The pillow basalts and marine sedimentary rocks of the Yanbian Group, and

397   the spatially associated Gaojiacun and Lengshuiqing mafic intrusions, were

398   previously regarded as the Yanbian ophiolite (Sun and Vuagnat, 1992). However,

399   recent studies suggest that the mafic plutons postdate the Yanbian volcano-

400   sedimentary sequence, arguing against an ophiolite model (Zhou et al., 2006a).

401   Based on the geochemistry of the basaltic lavas, the Yanbian Group has been

402   reinterpreted as a back-arc basin sequence (Du et al., 2005; Li X.H. et al., 2006;

403   Sun et al., 2007), but evidence from the sedimentary sequence was not available.

404   Our new geochronological, petrographical and geochemical data thus provide

405   new constraints on a back-arc basin scenario.

406   The Yanbian Group was deposited at ~870 Ma and derived from a proximal

407   magmatic arc with ages generally between 900 and 920 Ma (Figs. 5 and 6). The

408   presence of almost contemporaneous volcanic arc magmatism indicates an

409   active continental margin setting (DeGraaf-Surpless et al., 2002), in contrast to a

410   passive continental margin where sediments are commonly derived from

411   weathering of older continental crust (Goodge et al., 2002). The immature

412   volcaniclastic graywackes, turbidites of the Yanbian Group are also consistent

413   with an active margin setting (Crook, 1974; Pettijohn et al., 1987), where such

414   rocks are commonly associated with pillow lavas or 'greenstones' (Pettijohn et al.,

415  1987 and references therein) and are commonly observed in modern back-arc

416  basins.

417      The sandstones from the Yanbian Group have about 15% modal quartz with

418  mostly 60-73 wt% $SiO_2$ and $K_2O/Na_2O$ ratios <1, and are quartz-intermediate,

419  indicating a mixed provenance and depositional setting typical of an active

420  continental margin (Crook, 1974). Roser and Korsch (1986) examined the

421  $K_2O/Na_2O$-$SiO_2$ systematics of sandstone-mudstone suites from passive

422  continental margins (PM), active continental margins (ACM) and oceanic island

423  arcs (ARC), and found that the chemistry of the fine-grained members, and the

424  coupled sand-mud trends, were more useful indicators of tectonic setting than

425  the sandstones alone. Sandstones from the Yanbian Group plot exclusively in

426  the ARC and ACM fields, whereas most mudstones plot in the ACM field (Fig.

427  11). The coupled sand-mud trends (chain-dashed tie lines in Fig. 11) show one

428  trend parallel to the field boundaries and the other perpendicular to the first,

429  indicating a back-arc basin setting (Roser and Korsch, 1986). Using Bhatia's

430  (1983) scheme, the majority of samples from the Yanbian Group plot in the

431  oceanic island arc (OIA) to continental island arc (CIA) fields (Fig. 12). The

432  observed scatter of some points is probably due to a combination of sandstone

433  maturity and interelement variation.

434      The trace-element geochemistry of fine-grained clastic sediments has also

435  been widely used to determine tectonic setting (Bhatia and Crook, 1986; Floyd et

436  al., 1991). On the La-Th-Sc and Th-Sc-Zr/10 ternary plots (Fig. 13), most of the

437  Yanbian Group sandstones also fall within the OIA and CIA fields.  The elemental

438 compositions of different greywackes can be most easily compared by utilizing

439 upper continental crust-normalized, multi-element patterns. As shown in Figure

440 8a, the Yanbian rocks have pronounced negative Nb-Ta anomalies, clearly

441 indicative of subduction-related magmatic rock source (Floyd et al., 1991). For

442 further comparison, the data were also normalized to the standard tectonic

443 setting values and the results show that the Yanbian rocks are mostly affiliated

444 with a continental arc+active margin (Fig. 14).

445 REE patterns of clastic rocks are mainly controlled by provenance (Taylor

446 and McLennan, 1985; McLennan, 1989) and are believed to be faithfully

447 preserved in flysch deposited by turbidity currents and mass-flow processes

448 (Hiscott and Gill, 1992). The Yanbian rocks have REE elements and ratios

449 similar to those of continental arc settings (Table 5), in good agreement with the

450 proposed back-arc basin scenario.

451 **6.4. Provenance of the Yanbian Group**

452 Petrographic, geochronological and geochemical evidence not only indicates

453 that rocks of the Yanbian Group rocks were mainly derived from a magmatic arc,

454 but also provides important constraints for the nature of this arc, which was not

455 preserved in the modern exposures.

456 High feldspar contents (generally >30%) of the Yanbian sandstones indicates

457 derivation directly from crystalline rocks (Boggs, 2001), because feldspars are

458 chemically and physically unstable and thus less likely to survive recycling than a

459 mineral like quartz. Presence of other unstable minerals such as magnetite,

460 pyroxene and amphibole also support this view. The poorly sorted and immature

461 nature of the Yanbian greywackes, and their deposition in a back-arc basin,

462 further points to a proximal arc source with short transport distance and little or

463 no reworking.

464     The source area for the Yanbian Group sediments was an undissected to

465 transitional volcanic arc, in which only minor plutonic rocks were exposed. This

466 interpretation is supported by the abundance of volcanic rock fragments in the

467 sediments, the dominance of plagioclase over K-feldspar and the presence of

468 only minor quartz (Fig. 5 a, b and c). It is also consistent with the negative Zr-Hf

469 anomalies of these rocks relative to the average continent upper crust, reflecting

470 a lack of zircon input from silicic plutonic rocks (Fig. 8a).

471     The abundant intermediate and felsic volcanic rock fragments and sparse

472 mafic rock clasts in the Yanbian sandstones provide the most direct evidence for

473 the composition of these volcanic rocks (Table 2). Moreover, the trace element

474 characteristics of the sediments provide additional constraints on the nature of

475 the provenance. Because silicic rocks are significantly richer in La and Th, and

476 poorer in Sc, Cr, and Co than mafic rocks (Cullers, 1994 and references therein),

477 La/Sc, Th/Sc, Th/Co, and Cr/Th ratios are good indicators of the source rocks.

478 The Yanbian rocks have relatively low and constant La/Th ratios with an average

479 of 1.5 but more variable Co/Th ratios (Fig. 15a), suggesting mixing of felsic and

480 intermediate components. Similarly, a plot of La/Th against Hf also points to

481 mixed sources (Fig. 15b). In addition, the Yanbian rocks mostly have Cr/Th ratios

482 of 5-25 (Table 4), clearly indicative of silicic-intermediate source rocks (Cullers,

483 1994). The low Cr (mostly<150 ppm) and Ni (<80 ppm) of the Yanbian rocks and

484     slight V-Cr-Ni anomalies (Fig. 8a) is also consistent with minor mafic-ultramafic

485     input from the source area (Floyd et al., 1991; Garver et al., 1996).

486     **6.5. An integrated tectonic model**

487     Although the tectonic affinity of the western margin of the Yangtze Block

488     during the Neoproterozoic has been a matter of debate, it has been confirmed

489     that a number of plutons in this region were subduction-related. In the Yanbian

490     area, these intrusions include the ~860-Ma Guandaoshan dioritic pluton (Sun and

491     Zhou, 2008), the ~810-Ma Gaojiacun and Lengshuiqing mafic intrusions (Zhou et

492     al., 2006a) and the ~740-Ma Dadukou gabbroic pluton (Zhao and Zhou, 2007).

493     Determination of the age and tectonic provenance of the Yanbian Group has

494     significant implications for the regional tectonic evolution during Neoproterozoic

495     time. This study provides a window into a Neoproterozoic magmatic arc on the

496     western margin of the Yangtze Block, and reveals the presence of a ~900-920

497     Ma felsic and intermediate volcanic arc in this region, although such a feature

498     has not yet been widely identified directly.

499     Available data allow us to propose a model involving the development of a

500     volcanic arc and formation of the Yanbian back-arc basin and the closely

501     associated subduction-related plutons in this region (Fig. 16). Subduction-related

502     volcanic rocks of mainly felsic and intermediate composition were produced at ca.

503     900-920 Ma owing to the eastward subduction of oceanic lithosphere along the

504     western margin of the Yangtze Block (Fig. 16a). Rifting occurred as a

505     consequence of diapiric upwelling of metasomatized mantle to create the

506     Yanbian back-arc basin and generate the basaltic lavas of the Fangtian

507 Formation (Fig. 16b). According to Crawford et al. (1981), arc volcanism appears

508 to cease around the time that back-arc opening commences. This basin was built

509 on the ~900-920 Ma volcanic arc sequence which provided materials to fill the

510 adjacent Yanbian basin above the lavas, to form the Yumen, Xiaoping and Zagu

511 Formations (Fig. 16b). With continued erosion, the relief of the source region

512 decreased and hence slowed down the supply of materials for the basin,

513 resulting in biochemical deposition of the carbonates in the Zagu Formation (Fig.

514 16b). Subduction-related magmatism was then re-activated to generate the

515 subduction-related plutons (Fig. 16c). The oldest pluton is the ~860-Ma

516 Guandaoshan dioritic pluton, followed by the ~810-Ma Gaojiacun and

517 Lengshuiqing and the youngest ~740 Ma Dadukou gabbroic plutons (Fig. 16c).

518 This period of igneous activity suggests continuous subduction along the western

519 margin of the Yangtze Block between about 920 and 740 Ma. This arc was thus

520 active for at least ~180 million years. Eventually, this region probably became a

521 passive margin and the Sinian Lieguliu Formation was unconformably deposited

522 over the Yanbian Group, marking the termination of the arc setting (Fig. 16d).

523    The subduction-related environment may extend along the entire western

524 margin of the Yangtze Block. Similar sequences also occurred in the northwest

525 margin including the Bikou Group (Fig. 1), which has detrital zircon ages ranging

526 from 700 to 850 Ma and has been interpreted as fore-arc basin deposits (Yan

527 Q.R. et al., 2004; Druschke et al., 2006). Thus our proposed model implies that

528 the western margin of the Yangtze Block was a major continental arc during the

529 Neoproterozoic, and thus probably flanked the Rodinia supercontinent.

530

## 7. Conclusions

532     The Yanbian Group is a typical deep marine, volcaniclastic succession

533     deposited in a back-arc basin. Detrital zircon dating and geological constraints

534     indicate that the Yanbian Group was formed at ~870 Ma. The immature nature of

535     the Yanbian sandstones indicates a proximal arc source with ages of ~900-920

536     Ma. The Yanbian Group and spatially associated subduction-related plutons in

537     the Yanbian region make up a typical arc assemblage, being part of a major

538     continental arc along the western margin of the Yangtze Block for at least 180

539     m.y. (920-740 Ma). We infer that the Yangtze Block probably flanked the Rodinia

540     supercontinent.

541

## Acknowledgments

550 **References**

551 Bhatia, M.R., 1983. Plate tectonics and geochemical composition of sandstones.

552     J. Geol. 91, 611-627.

553 Bhatia, M.R., 1985. Rare earth element geochemistry of Australian Paleozoic

554     graywackes and mudstones: Provenance and tectonic control. Sediment.

555     Geol. 45, 97-113.

556 Bhatia, M.R., Crook, K.A.W., 1986. Trace element characteristics of graywackes

557     and tectonic setting discrimination of sedimentary basins. Contrib. Mineral.

558     Petrol. 92, 181-193.

559 BGMRSP (Bureau of Geology and Mineral Resources of the Sichuan Province),

560     1972. Regional Geological Survey of People's Republic of China, the Yanbian

561     Sheet (G-47-XII; geological part), scale 1:200,000 (in Chinese).

562 Boggs, S., 2001. Principles of sedimentology and stratigraphy (Third editon).

563     New Jersey, Prentice-Hall, 726p.

564 Chen, Z.L., Chen, S.Y., 1987. On the tectonic evolution of the west margin of the

565     Yangzi block. Chongqing, China, Chongqing Publishing House, 172p. (in

566     Chinese).

567 Cope, T., Ritts, B.D., Darby, B.J., Fildani, A., Graham, S.A., 2005. Late Paleozoic

568     Sedimentation on the Northern Margin of the North China Block: Implications

569     for Regional Tectonics and Climate Change. Int. Geol. Rev. 47, 270-296.

570 Crawford, A.J., Beccaluva, L., Serri, G., 1981. Tectono-magmatic evolution of the

571     west Philippine-Mariana region and the origin of boninites. Earth Planet. Sci.

572     Lett.   54, 346-356.

573   Crook, K.A.W., 1974. Lithogenesis and geotectonics: The significance of

574       compositional variations in flysch arenites (graywackes). In: Dott, R.H.,

575       Shaver, R.H. (Eds.), Modern and Ancient Geosynclinal Sedimentation. SEPM

576       Spec. Publ. 19, pp. 304-310.

577   Cullers, R.L., 1994. The controls on the major and trace element variation of

578       shales, siltstones, and sandstones of Pennsylvanian-Permian age from

579       uplifted continental blocks in Colorado to platform sediment in Kansas, USA.

580       Geochim. Cosmochim. Acta 58, 4955-4972.

581   DeGraaff-Surpless, K., Graham, S.A., Wooden, J.L., McWilliams, M.O., 2002.

582       Detrital zircon provenance analysis of the Great Valley Group, California:

583       Evolution of an arc-forearc system. Geol. Soc. Am. Bull. 114, 1564-1580.

584   Dickinson, W.R., 1970. Interpreting detrital modes of graywacke and arkose. J.

585       Sediment. Petrol. 40, 695-707.

586   Dickinson, W.R., 1985. Interpreting provenance relations from detrital modes of

587       sandstones. In: Zuffa, G.G. (Eds.), Provenance of arenites. NATO ASI Series

588       C: Mathematical and Physical Sciences 48, D. Reidel Publishing Company,

589       pp. 333-361.

590   Dickinson, W.R., Gehrels, G.E., 2000. Sandstone petrofacies of detrital zircon

591       samples from Paleozoic and Triassic strata in suspect terranes of northern

592       Nevada and California. In: Soreghan, M.J., Gehrels, G.E. (Eds.), Paleozoic

593       and Triassic paleogeography and tectonics of western Nevada and northern

594       California. Boulder, Colorado, Geol. Soc. Am. Special Paper 347, pp. 151-171.

595     Druschke, P., Hanson, A.D., Yan, Q., Wang, Z., Wang, T., 2006. Stratigraphic

596          and U-Pb SHRIMP detrital zircon evidence for a Neoproterozoic continental

597          arc, Central China: Rodinia implications. J. Geol. 114, 627-636.

598     Du, L.L., Geng, Y.S., Yang, C.H., Wang, X.S., Ren, L.D., Zhou, X.W., Shi, Y.Y.,

599          Yang, Z.S., 2005. Geochemistry and SHRIMP U-Pb zircon chronology of

600          basalts from the Yanbian group in the western Yangtze Block. Acta Geologica

601          Sinica 76, 805-813 (in Chinese with English abstract).

602     Eisbacher, G.H., 1985. Late Proterozoic rifting, glacial sedimentation, and

603          sedimentary cycles in the light of Windermere deposition, western Canada.

604          Palaeogeogr. Palaeoclimatol. Palaeoecol. 51, 231-254.

605     Fedo, C.M., Nesbitt, H.W., Young, G.M., 1995. Unraveling the effects of

606          potassium metasomatism in sedimentary rocks and paleosols, with

607          implications for weathering conditions and provenance. Geology 23, 921-924.

608     Floyd, P.A., Leveridge, B.E., 1987. Tectonic environment of the Devonian

609          Gramscatho Basin, South Cornwall: Framework mode and geochemical

610          evidence from turbiditic sandstones. J. Geol. Soc. London 144, 531-542.

611     Floyd, P.A., Shail, R., Leveridge. B.E., Franke, W., 1991. Geochemistry and

612          provenance of Rhenohercynian synorogenic sandstones: implications for

613          tectonic environment discrimination. In: Morton, A.C., Todd, S.P., Haughton,

614          P.D.W. (Eds.), Developments in sedimentary provenance studies. Geol. Soc.

615          London, Spec. Publ. 57, 173-188.

616     Garver, J.I., Royce, P.R., Smick, T.A., 1996. Chromium and nickel in shale of the

617          Taconic Foreland: A case study for the provenance of fine-grained sediments

618      with an ultramafic source. J. Sediment. Res. 66, 100-106.

619    Goodge, J.W., Myrow, P., Williams, I.S., Bowring, S.A., 2002. Age and

620      provenance of the Beardmore Group, Antarctica: constraints on Rodinia

621      supercontinent breakup. J. Geol. 110, 393-406.

622    Gu, X.X., Liu, J.M., Zheng, M.H., Tang, J.X., Qi, L., 2002. Provenance and

623      tectonic setting of the Proterozoic turbidites in Hunan, South China:

624      geochemical evidence. J. Sediment. Res. 72, 393-407.

625    Hiscott, R.N., Gill, J.B., 1992. Major and trace element geochemistry of

626      Oligocene to Quaternary volcaniclastic sands and sandstones from the Izu-

627      Bonin arc. In: Taylor, B., Fujioka, K., et al. (Eds.), Proceedings of the Ocean

628      Drilling Program, Scientific Results 126. College Station, TX: Ocean Drilling

629      Program, pp. 467-485.

630    Ingersoll, R.V., Fullard, T.F., Ford, R.L., Grimm, J.P., Pickle, J.D., Sares, S.W.,

631      1984. The effect of grain size on detrital modes; a test of the Gazzi-Dickinson

632      point-counting method: J. Sediment. Petrol. 54, 103-116.

633    Jackson, S.E., Pearson, N.J., Griffin, W.L., Belousova, E.A., 2004. The

634      application of laser ablation-inductively coupled plasma-mass spectrometry

635      (LA-ICP-MS) to in-situ U-Pb zircon geochronology. Chem. Geol. 211, 331-335.

636    Li, F.H., Tan, J.M., Shen, Y.L., Yu, F.X., Zhou, G.F., Pan, X.N., Li, X.Z., 1988.

637      The pre-Sinian in the Kangdian area: Chongqing, China, Chongqing

638      Publishing House, 396p. (in Chinese).

639    Li, X.H., Li, Z.X., Zhou, H.W., Liu, Y., Liang, X.R., Li, W.X., 2003. SHRIMP U-Pb

640      zircon age, geochemistry and Nd isotope of the Guandaoshan pluton in SW

641      Sichuan: Petrogenesis and tectonic significance. Sci. China Ser. D (Supp.)

642      46, 73-83.

643    Li X.H., Li, Z.X., Sinclair, J.A., Li, W.X., Carter, G., 2006. Revisiting the "Yanbian

644      Terrane": implications for Neoproterozoic tectonic evolution of the western

645      Yangtze Block, South China. Precambrian Res. 151, 14-30.

646    Li, Z.X., Li, X.H., Kinny, P., Wang, J., 1999. The breakup of Rodinia: did it start

647      with a mantle plume beneath South China. Earth Planet. Sci. Lett. 173, 171-

648      181.

649    Li, Z.X., Li, X.H., Kinny, P.D., Wang, J., Zhang, S., Zhou, H., 2003.

650      Geochronology of Neoproterozoic syn-rift magmatism in the Yangtze Craton,

651      South China and correlations with other continents: evidence for a mantle

652      superplume that broke up Rodinia. Precambrian Res. 122, 85-109.

653    Ludwig, K. R., 1999. Isoplot/Ex version 2.06: A geochronological tool kit for

654      Microsoft Excel. Berkeley Geochronology Center, Spec. Publ. 1a.

655    Maas, R., McCulloch, M.T., 1991. The provenance of Archean clastic

656      metasediments in the Narryer Geniss Complex, Western Australia: trace

657      element geochemistry, Nd isotopes, and U-Pb ages for detrital zircons.

658      Geochim. Cosmochim. Acta 55, 1915-1932.

659    Marsaglia, K.M., Ingersoll, R.V., 1992. Compositional trends in arc-related, deep-

660      marine sand and sandstone: a reassessment of magmatic-arc provenance.

661      Geol. Soc. Am. Bull. 104, 1637-1649.

662    McLennan, S.M., 1989. Rare earth elements in sedimentary rocks: Influence of

663      provenance and sedimentary processes. Rev. Mineral. Geochem. 21, 169-200.

664 McLennan, S.M., 1993. Weathering and Global Denudation. J. Geol. 101, 295-
665     303.

666 McLennan, S.M., Taylor, S.R., Eriksson, K.A., 1983. Geochemistry of Archean
667     shales from the Pilbara Supergroup, Western Australia. Geochim.
668     Cosmochim. Acta 47, 1211-1222.

669 McLennan, S.M., Taylor, S.R., McCulloch, M.T., Maynard, J.B., 1990.
670     Geochemical and Nd-Sr isotopic composition of deep-sea turbidites: Crustal
671     evolution and plate tectonic associations. Geochim. Cosmochim. Acta 54,
672     2015-2050.

673 McLennan, S.M., Hemming, S.R., Taylor, S.R., Eriksson, K.A., 1995. Early
674     Proterozoic crustal evolution: Geochemical and Nd-Pb isotopic evidence from
675     metasedimentary rocks, southwestern North America. Geochim. Cosmochim.
676     Acta 59, 1153-1177.

677 Nesbitt, H.W., Markovics, G., Price, R.C., 1980. Chemical processes affecting
678     alkalies and alkaline earths during continental weathering: Geochim.
679     Cosmochim. Acta 44, 1659-1666.

680 Nesbitt, H.W., Young, G.M., 1982. Early Proterozoic climates and plate motions
681     inferred from major element chemistry of lutites. Nature 299, 715-717.

682 Nesbitt, H.W., Young, G.M., 1996. Petrogenesis of sediments in the absence of
683     chemical weathering: effects of abrasion and sorting on bulk composition and
684     mineralogy. Sedimentology 43, 341-358.

685    Nesbitt, H.W., Young, G.M., McLennan, S.M., and Keays, R.R., 1996. Effects of

686        chemical weathering and sorting on the petrogenesis of siliciclastic sediments,

687        with implications for  provenance studies. J. Geol. 104, 525-542.

688    Pettijohn, F.J., Potter, P.E., Siever, R., 1987. Sand and sandstone (Second

689        editon), Springer-Verkag, 553p.

690    Pan, X.N., Zhao, J.X., Zhan, X.Y., Zhen, H.X., Yan, Z.H., Zhou, G.F., Tao, D.L.,

691        1987. Tectonics and rifting in the Kangdian area: Chongqing, China,

692        Chongqing Publishing House, 295p. (in Chinese).

693    Qi, L., Hu, J., Gregoire, D.C., 2000. Determination of trace elements in granites

694        by inductively coupled plasma-mass spectrometry. Talanta 51, 507-513.

695    Roser, B.P., Korsch, R.J., 1986. Determination of tectonic setting of sandstone-

696        mudstone suites using $SiO_2$ content and $K_2O/Na_2O$ ratio. J. Geol. 94, 635-650.

697    Roser, B.P., Korsch, R.J., 1988. Provenance signatures of sandstone-mudstone

698        suites determined using discriminant function analysis of major-element data.

699        Chem. Geol. 67, 119-139.

700    SBGMR (Sichuan Bureau of Geology and Mineral Resources). 1991. Regional

701        Geology of Sichuan Province. Beijing, China, Geological Memoirs 23.

702        Geological Publishing House (in Chinese with English summary).

703    She, Z.B., Ma, C.Q., Mason, R., Li, J.W., Wang, G.C., Lei, Y.H., 2006.

704        Provenance of the Triassic Songpan-Ganzi flysch, west China. Chem. Geol.

705        231, 159-175.

706    Sun, C.M., Vuagnat, M., 1992. Proterozoic ophiolites from Yanbian and Shimian

707        (Sichuan Province, China): Petrography, geochemistry, petrogenesis, and

708    geotectonic environment. Schweiz. Mineral. Petrograph. Mitt. 72, 389-413.

709    Sun, W.H., Zhou, M.-F., Zhao J.H., 2007. Geochemistry and tectionic

710    significance of basaltic lavas in the Neoproterozoic Yanbian Group (Southern

711    Sichuan Province, SW China). Int. Geol. Rev. 49, 554-571.

712    Sun, W.H., Zhou, M.-F., 2008. The ~860-Ma, Cordilleran-type Guandaoshan

713    dioritic pluton in the Yangtze Block, SW China: Implications for the origin of

714    Neoproterozoic magmatism. J. Geol. 116, 238-253.

715    Taylor, S.R., McLennan, S.M., 1985. The Continental Crust; Its Composition and

716    Evolution. London, Blackwell, 312 p.

717    Taylor, S.R., McLennan, S.M., 1995. The Geochemical Evolution of the

718    Continental Crust. Rev. Geophys. 33, 241-265.

719    Yan, D.P., Zhou, M.-F., Song, H. L., Wang, X.W., Malpas, J., 2003. Origin and

720    tectonic significance of a Mesozoic multi-layer over-thrust within the Yangtze

721    block (South China). Tectonophysics 361, 239-254.

722    Yan, Q.R., Hanson, A.D., Wang, Z.Q., Druschke, P.A., Yan, Z., Wang, T., Liu,

723    D.Y., Song, B., Pan, P., Zhou, H., Jiang, C.F., 2004. Late Proterozoic

724    subduction and rifting on the northern margin of the Yangtze Plate, China:

725    implications for Rodinia reconstruction. Int. Geol. Rev. 46, 817-832.

726    Yuan, H.L., Gao, S., Liu, X.M., Li, H.M., Gunther, D.,Wu, F.Y., 2004. Accurate U-

727    Pb age and trace element determinations of zircon by laser ablation-

728    inductively coupled plasma-mass spectrometry. Geostandard. Geoanal. Res.

729    28, 353-370.

730    Zhao, J.H., Zhou, M.-F., 2007. Geochemistry of Neoproterozoic mafic intrusions

731       in the Panzhihua district (Sichuan Province, SW China): implications for

732       subduction-related metasomatism in the upper mantle. Precambrian Res. 152,

733       27-47.

734    Zhou, M.-F., Kennedy, A.K., Sun, M., Malpas, J., Lesher, C.M., 2002a. Late

735       Proterozoic arc-related mafic intrusions along the northern margin of South

736       China: implications for the accretion of Rodinia. J. Geol. 110, 611-618.

737    Zhou, M.-F., Yan, D.P., Kennedy, A.K., Li, Y.Q., Ding, J., 2002b. SHRIMP U-Pb

738       zircon geochronological and geochemical evidence for Late Proterozoic arc-

739       magmatism along the western margin of the Yangtze Block, South China.

740       Earth Planet. Sci. Lett. 196, 51-67.

741    Zhou, M.-F., Ma, Y.X., Yan, D.P., Xia, X.P., Zhao, J.H., Sun, M., 2006a. The

742       Yanbian Terrane (Southern Sichuan Province, SW China): A Late Proterozoic

743       arc assemblage in the western margin of the Yangtze Block. Precambrian

744       Res. 144, 19-38.

745    Zhou, M.-F., Yan, D.P., Wang, C.L., Qi, L., Kennedy, A., 2006b. Subduction-

746       related origin of the 750 Ma Xuelongbao adakitic complex (Sichuan Province,

747       China): Implications for the tectonic setting of the giant Neoproterozoic

748       magmatic event in South China. Earth Planet. Sci. Lett. 248, 286-300.

749    Zhou, D., Graham, S.A., 1996. The Songpan-Ganzi complex of the West Qinling

750       Shan as a Triassic remnant ocean basin.  In: Yin, A., Harrison, T.M. (Eds.),

751       The Tectonic Evolution of Asia. New York, Cambridge University Press, pp.

752       281-299.

**Figure captions**

754 Fig. 1. Simplified geological map of the Yanbian region, Sichuan Province, SW

755 China (after BGMRSP, 1972). The insert map showing the tectonic units of South

756 China and general distribution of Neoproterozoic rocks in the margins of the

757 Yangtze Block.

758 Fig. 2. Stratigraphy of the Yanbian Group based on a measured cross section

759 (BGMRSP, 1972) and our field mapping. Stars indicate samples for detrital zircon

760 analysis. The sandstone beds shown in the column are not strictly to scale

761 because they are typically thin layers interbedded with slate.

762 Fig. 3. (a) Contact between the clastic Yumen Formation and the volcanic

763 Fangtian Formation. (b) A scour structure in the Xiaoping Formation. (c) Slumped

764 siltstone in the Xiaoping Formation. (d) Well-exposed Bouma sequences in the

765 Xiaoping Formation.

766 Fig. 4. (a) Photomicrographs of grain types and features in the Yanbian

767 sandstones. (a) General view showing sub-angular monocrystalline quartz (Q)

768 (T3-3). (b) Sub-rounded plagioclase feldspar (Pl) and K-feldspar (Kf) grains (T3-

769 1-2). (c) A metamorphic grain (Lm) and volcanic grains (Lv) with felsitic and

770 microlitic texture (B11). (d) Siltstone fragments (Ls) (B11). (e) A typical volcanic

771 rock fragment with microlitic texture that we interpret to be derived from

772 intermediate composition (B9). (f) A clinopyroxene grain (Cpx) (F6). All samples

773 are in cross-polarized light. Scale bar in each photograph is 0.3 mm.

774 Fig. 5. Ternary plots of sandstone point count data for the Yanbian Group. (a)

775 QFL plot. (b) QmFLt plot. (c) QLvmLsm plot. (d) QmPK plot. Provenance fields

are from Dickinson (1985). The large open triangles represent arithmetic means of data and polygonal box represents one standard deviation.

Fig. 6. Detrital zircon data for the sandstone samples of the Yanbian Group. (a) Neoproterozoic (860-1000 Ma) detrital zircon age histogram and cumulative probability plot, showing number of grains analyzed and percentage of Neoproterozoic ages as a fraction of total discordant and concordant ages. (b) Histogram and cumulative probability plot of total concordant detrital zircon ages. Total number of concordant ages for each sample is shown, with number of analyses (concordant plus discordant ages) shown in parenthesis.

Fig. 7. (a) Geochemical classification of sandstones from the Yanbian Group (Pettijohn et al., 1987).

Fig. 8. (a) Upper crust-normalized, multi-element diagrams for the Yanbian samples; (b) Chondrite-normalized REE patterns of the Yanbian sandstones and mudstones. Post-Archean average Australian shale (PAAS) is also plotted as a heavy dashed line "+" for comparison. Values are from Taylor and McLennan (1985).

Fig. 9. CIA ternary diagram, A-CN-K=$Al_2O_3$ -CaO*+$Na_2O$-$K_2O$, after Nesbitt and Young (1982) showing Yanbian sandstones and mudstones as well as average compositions of tonalite and granodiorite (from Fedo et al., 1995). Approximate correction for carbonate content was made by assuming reasonable Ca/Na ratios in silicate material (McLennan, 1993). After correcting phosphate using $P_2O_5$, if the remaining mole fraction of CaO ≤$Na_2O$, then this value of CaO is adopted; if CaO >$Na_2O$, CaO* is assumed to be equivalent to $Na_2O$. Due to relatively low

799 carbonate contents in most samples, however, the calculated proportions are

800 thus very close to actual values.

801 Fig. 10. Plots of K vs. Rb, K vs. Ba, Ce vs. Sm, and U vs. Th, showing linear

802 correlations.

803 Fig 11. $K_2O/Na_2O$-$SiO_2$ plot for the Yanbian rocks. PM = passive margin; ACM =

804 active continental margin; ARC = oceanic island arc. (after Roser and Korsch,

805 1986).

806 Fig.12. Tectonic discrimination diagrams for the Yanbian Group sandstones: PM

807 = passive margin; ACM = active continental margin; CIA = continental island arc;

808 OIA =oceanic island arc (after Bhatia, 1983).

809 Fig. 13. Triangular trace element plots for Yanbian sandstones (after Bhatia and

810 Crook, 1986). Abbreviations as in Fig. 11.

811 Fig. 14. Normalized multi-element diagrams for the Yanbian sandstones. CAAM

812 = continental arc+active margin; OIA = oceanic island arc; PM = passive margin;

813 OWP = oceanic within-plate. Normalizing values are from Floyd et al. (1991).

814 Fig. 15. Source rock discrimination diagrams for the Yanbian rocks; (a) Co/Th vs.

815 La/Sc diagram (after Gu et al., 2002), showing derivation from mixed felsic-basic

816 volcanic source, (b) La/Th vs. Hf diagram (after Floyd and Leveridge, 1987),

817 indicating mixed of felsic/basic source rocks.

818 Fig. 16. Model for the development of the Yanbian Group and the spatially

819 associated subduction-related intrusions in the Yanbian region, SW China.

1    Provenance and tectonic setting of the Neoproterozoic Yanbian

2    Group, western Yangtze Block (SW China)

3

4    Wei-Hua Sun [a, *], Mei-Fu Zhou [a], Dan-Ping Yan [b], Jian-Wei Li [c] and Yuxiao Ma [d]

5

6    [a] Department of Earth Sciences, University of Hong Kong, Hong Kong, China

7    [b] School of Earth Sciences and Resources, China University of Geosciences, Beijing 100083,

8    China

9    [c] State Key Laboratory of Geological Processes and Mineral Resources, and Faculty of Earth

10   Resources, China University of Geosciences, Wuhan 430074, China

11   [d] Department of Geochemistry, Chengdu University of Science and Technology, Chengdu, China

12

13   * Corresponding author. Tel.: +852 2859 8913; Fax: +852 2517 6912.

14   E-mail: weihua@hkusua.hku.hk

15   **Abstract**

16       Tectonic evolution of the Yangtze Block of South China during

17   Neoproterozoic time has been a major focus of debate and is important in the

18   reconstruction of the Rodinian supercontinent. The Yanbian Group in the western

19   margin of the Yangtze Block is a well-preserved Neoproterozoic volcanic-

20   sedimentary sequence and provides a rare opportunity to examine the

21   provenance and tectonic setting. It consists of a lower part composed of ~1500 m

22   thick basaltic lavas and an upper part with ~3500 m thick flysch deposits. The

23   flysch sequence contains typical deep marine turbidites consisting mainly of fine-

24   grained volcaniclastic sandstones and mudstones, indicating a submarine fan

25   depositional system. Detrital zircon dating yields ages ranging from ca. 865 Ma to

26    1000 Ma with two peaks at ca. 900 Ma and 920 Ma, respectively. The Yanbian

27    Group is intruded by the ~860- Ma Guandaoshan dioritic pluton, constraining its

28    depositional age at ca. 870 Ma. The sandstones contain abundant feldspar and

29    lithic fragments with minor amounts of quartz and have an average composition

30    of $Q_{16}F_{35}L_{49}$, suggesting a proximal source and an undissected to transitional arc

31    setting. The lithic fragments in the sandstones point to andesitic and felsic

32    volcanic rock sources. The sandstones and mudstones have intermediate

33    $SiO_2/Al_2O_3$ (typically 3-6), high $Fe_2O_3$+MgO contents (5-12 wt%), and moderate

34    to high $K_2O/Na_2O$ ratios (generally 0.1-1 and 1-10 for sandstones and mudstones,

35    respectively). In comparison with average upper continental crust, they show

36    strong Nb-Ta anomalies, slight depletion of Zr-Hf, La and Th, but moderate

37    enrichment of V, Cr, Ni, and Sc. These rocks show LREE enrichment

38    $(La/Yb_N=5.3-7.4)$ with flat HREE, and pronounced negative Eu anomalies

39    $(Eu/Eu^*=0.6-0.74)$ in chondrite-normalized REE patterns, similar to post-Archean

40    shales. Geochemical data for these rocks suggest an arc setting and

41    intermediate-felsic volcanic source, consistent with a back-arc basin scenario for

42    the basaltic lavas in the lower Yanbian Group. Together with regional geological

43    evidence, the turbidites of the Yanbian Group strongly support a model in which

44    the western margin of the Yangtze Block was a major magmatic arc, active

45    probably from ~920 Ma to 740 Ma, a period of more than 180 million years.

46

47    **Key words**:  turbidite, detrital zircon dating, geochemistry, provenance, Yanbian

48    Group, Yangtze Block

## 1. Introduction

Siliciclastic rocks are useful for investigating provenance and tectonic setting of sedimentary basins (Dickinson, 1970, 1985; Bhatia, 1983, 1985; Roser and Korsch, 1986, 1988; Floyd and Leveridge, 1987). Provenance regions, especially those at destructive plate margins, are rarely well preserved because of subsequent erosion and destruction. In such circumstances, studies of related sedimentary rocks have considerable potential for determining the source rocks and the history of ancient continental margins. A combination of traditional mineralogical (especially for sandstones) and geochemical methods and detrital zircon U-Pb analysis has greatly contributed to our understanding of the provenance, tectonic setting and tectonomagmatic evolution of sedimentary basins and their siliciclastic deposits (McLennan et al., 1990, 1995; Maas and McCulloch, 1991; Taylor and McLennan, 1995; Dickinson and Gehrels, 2000; DeGraaff-Surpless et al, 2002; Cope et al., 2005; She et al., 2006).

The tectonic evolution of the Yangtze Block of South China is of importance for the reconstruction of the supercontinent Rodinia and has been a matter of hot debate (Li Z.X. et al., 1999, 2003; Li X.H. et al., 2003, 2006; Zhou et al., 2002a, b, 2006a, b). Previous work has focused mainly on the Neoproterozoic igneous rocks, and studies of the associated sedimentary sequences are sparse. The Neoproterozoic Yanbian Group in the western margin of the Yangtze Block has been a subject of several recent studies (Du et al., 2005; Zhou et al., 2006a; Li X.H. et al., 2006; Sun et al., 2007), because it is not only one of the best-preserved volcano-sedimentary sequences in South China, but is spatially

72   associated with several contemporaneous intermediate to mafic plutons, making

73   it ideal for investigating the tectonic affinities of the Yangtze Block. Previous

74   studies on the volcanic rocks in the lower part of the Yanbian Group and the

75   related intrusive rocks have interpreted the Yanbian Group as a relict ophiolite

76   (Sun and Vuagnat, 1992) or a back-arc basin sequence (Du et al., 2005; Zhou et

77   al., 2006a; Li X.H. et al., 2006, Sun et al., 2007). So far, there is no agreement

78   about the depositional age of the Yanbian Group (Du et al., 2005; Zhou et al.,

79   2006a; Li X.H. et al., 2006), causing   additional ambiguity in its tectonic

80   interpretation. In particular, no studies are available regarding the chemical

81   composition and petrology of the sedimentary rocks, which are crucial to better

82   understanding the source rocks and tectonic setting.

83      In this paper, we present petrographic, detrital zircon U-Pb geochronological

84   and geochemical data for the upper siliciclastic rocks of the Yanbian Group, in an

85   attempt to constrain the age of the sediments and to infer their provenance and

86   tectonic setting. The results also provide insights into the tectonic evolution of the

87   Yangtze Block during Neoproterozoic time.

88

89   **2.  Geological background**

90      South China consists of the Yangtze Block in the northwest and the

91   Cathaysia Block in the southeast (Fig. 1). The Yangtze Block is separated from

92   the North China Craton by the Qinling-Dabie orogenic belt and is bounded to the

93   west by the Songpan-Ganze Terrane of the Tibetan Plateau. The Songpan-

94   Ganze Terrane is a prominent triangular region filled with Triassic deep-marine

flysch deposits (Zhou and Graham, 1996). The Yangtze Block comprises metamorphic basement complexes and Neoproterozoic to Cenozoic cover sequences (Yan D.P. et al., 2003). The basement complexes contain gneiss, mica schist, amphibolite, marble and quartzite, whereas the cover sequences are mainly composed of carbonate, clastic and volcanic rocks (SBGMR, 1991).

Along the western margin of the Yangtze Block, a ~1000-km-long, NS-trending, Neoproterozoic igneous and metamorphic belt crops out from Kangding in Sichuan Province to Yuanjiang in Yunnan Province (Fig. 1). This belt has been recently interpreted as a major Neoproterozoic continental arc, named the Hannan-Panxi arc, in which the igneous rocks have ages mostly ranging from 860 to 740 Ma (Zhou et al., 2002a, b, 2006a, b; Zhao and Zhou, 2007; Sun and Zhou, 2008). The occurrence of this huge continental arc indicates an Andean-type continental margin with oceanic crust being subducted eastward beneath the western margin of the Yangtze Block during that time (Zhou et al., 2002b; Sun and Zhou, 2008).

In the belt, the igneous plutons intrude high-grade (granitic gneisses and amphibolite) and low-grade metamorphic rocks (Pan et al., 1987; Li F.H. et al., 1988). The high-grade metamorphic rocks, including the Kangding and Dahongshan complexes, were traditionally considered to be late Archean to Paleoproterozoic crystalline basement; the low-grade metamorphic rocks, such as the Kunyang, Huili, Yanbian and Bikou Groups, were interpreted to be Mesoproterozoic and to constitute the folded basement in this region (Chen and Chen, 1987).

118    The Yanbian Group is unconformably overlain by Sinian (latest
119    Neoproterozoic) strata known as the Lieguliu Formation (Sun et al., 2007), which
120    is composed of glacial deposits, comparable to those of similar age on other
121    continents (Elsbacher, 1985). The Yanbian Group is intruded by a magmatic
122    association that consists of the ~860-Ma Guandaoshan dioritic pluton (Li X.H. et
123    al., 2003; Sun and Zhou, 2008), 810-820-Ma Tongde dioritic-gabbroic pluton (Li
124    Z.X. et al., 2003) and ~810-Ma Gaojiacun and Lengshuiqing mafic plutons (Zhou
125    et al., 2006a) (Fig. 1). These, together with the ~740 Ma Dadukou gabbroic
126    intrusion south of Tongde Town (Zhao and Zhou, 2007), have been interpreted
127    as part of the Hannan-Panxi arc along the western margin of the Yangtze Block
128    (Sun and Zhou, 2008).

129

## 3. Stratigraphy and depositional environment

131     Cropping out over an area of approximately 500 km$^2$, the Yanbian Group is
132    composed of two principal units: a lower volcanic sequence ca. 1500 m thick,
133    known as the Fangtian Formation, and an upper flysch more than 5000 m thick,
134    comprising the Yumen, Xiaoping and Zagu Formations (Fig. 2)
135    The Fangtian Formation is composed of massive basalt, pillow basalt and
136    volcanic breccias with subordinate interbeds of chert, and pelitic and siliceous
137    slate. It is conformably overlain by the ca.1700-m-thick Yumen Formation, which
138    consists primarily of thin- to medium-bedded, dark-gray, carbonaceous and
139    siliceous slates with interbeds of fine- to coarse-grained sandstone (Fig. 3a).
140    Lenses of limestone are locally present. An ~5-cm-thick layer of black chert

141 marks the base of the Yumen Formation where it overlies the basaltic breccias of

142 the Fangtian Formation (Fig. 3a). The slates and sandstones have regular

143 parallel bedding, typical of distal turbidites. In this formation, turbidites generally

144 display $T_{bce}$ of the Bouma sequences.

145   The ~2200-m-thick Xiaoping Formation comprises dark gray slates,

146 carbonaceous slates, fine- to coarse-grained sandstones and siltstones,

147 representing turbidites and associated mudstones. The basal and top parts of the

148 succession are dominated by sandstones in beds up to 1.5 m thick, suggesting

149 small-scale channel-fill deposits. The sandstone channels usually display an

150 eroded base and a concave-upward morphology, with the grain size fining

151 upward.  Conglomerates are locally present as thin, discontinuous lag beds at

152 the base of the coarse sandstone layers. The sandstones have lenticular or flat

153 beds with thicknesses of 10-20 cm, but ranging from 2 to 50 cm. Sedimentary

154 structure, such as scours, slumps, and load and flame structure, are locally well

155 developed (Figs. 3b, c). Most sandstone beds are normally graded and follow the

156 Bouma sequence. Partial Bouma sequences are more common than complete

157 ones, with the $T_{abc}$ sequence being the most common, followed in abundance by

158 $T_{ae}$ (Fig. 3d). Thin limestone lenses and stromatolithic limestones are also

159 observed locally. Pyrite is common in the slates and siltstones, especially along

160 some layer boundaries.

161   The ~1300-m-thick Zagu Formation is composed of dark gray slates, black

162 dolomitic slates and dolomitic limestones. There is a thin (10-15 m) layer of

163 conglomerate and pebbly sandstone at the base, representing a medium-scale

channel-fill deposit. The conglomerate clasts are typically subangular to subrounded, generally 2-4 cm in diameter, and consist mainly of intermediate-felsic volcanic rocks (50-60%), chert (20-25%), fragments of carbonaceous rock (10-15%) and siltstone (~10%). The conglomerates and sandstones are also well graded. The Zagu Formation is unconformably overlain by the Sinian Lieguliu Formation (Sun et al., 2007).

The Yanbian Group consists mainly of thin- to medium-bedded, fine-grained, turbiditic volcaniclastic sandstones and mudstones with little variation in sedimentary facies and minor input of coarse clastic material. These sedimentary rocks most likely represent submarine fan deposits, especially mid-fan deposits. This thick turbidite package lacking shallow-water deposits indicates a marine environment below wave base. The presence of limestones throughout the section indicates that the seafloor was above the carbonate compensation depth and suggests a low-latitude, warm-water environment.

## 4. Sandstone petrography

The sandstones are mostly fine- to medium-grained, poorly sorted and contain angular to subangular grains of low to moderate sphericity. They are mainly composed of quartz, feldspar and lithic fragments. Quartz is relatively minor in volume and is generally subangular to angular, mostly being monocrystalline and lacking inclusions and undulatory extinction (Fig. 4a). Subrounded feldspar is the dominant mineral and is partly altered to saussurite and sericite. Plagioclase is much more common than alkali feldspar (Fig. 4b).

187 Lithic fragments are dominantly rhyolite and andesite with felsitic and microlitic

188 textures, although sedimentary and metamorphic varieties are also present (Figs.

189 4c,d,e).

190 Biotite and muscovite occur as elongate laths or short plates and are locally

191 accompanied by chlorite and glauconite. Sparse heavy minerals include

192 magnetite, zircon, apatite, titanite, pyrite, rutile and tourmaline. Most of these

193 grains are angular to subangular, although some are well-rounded. Amphibole

194 and pyroxene grains are locally present but extremely rare (Fig. 4f).

195 The matrix of the sandstones consists of clay minerals, comminuted and

196 altered lithic and feldspathic fragments, fine-grained quartz, micas, opaque

197 minerals, carbonate and some aphanitic material. Matrix is commonly between

198 10 to 15%, but may be overestimated due to the pseudomatrix problem

199 (Dickinson, 1970). Silica is the dominant cement in these rocks but calcite is also

200 common.

201 Thirty-one medium-grained sandstones were selected for petrographic study

202 using the Gazzi-Dickinson method (Ingersoll et al., 1984). About five to six

203 hundred framework grains were counted from each sample. Matrix (<~0.03 mm)

204 and cement were not counted. The Gazzi-Dickinson method divides volcanic

205 lithic clasts into various textural types (Dickinson, 1970), which is especially

206 significant in magmatic-arc settings, where volcaniclastic components may

207 constitute as much as 100% of the sand fraction (Marsaglia and Ingersoll, 1992).

208 Point-count categories and recalculated parameters are defined in Table 1.

209     The modal point-count data are shown in Table 2 and Figure 5. In general,

210    the sandstones are characterized by low quartz (Q), moderate feldspar (F) and

211    high lithic (L) abundances, with L/F ratios of 1-3, indicating that the sandstones

212    were derived almost exclusively from volcanic sources (Dickinson, 1970). The

213    Yumen, Xiaoping and Zagu Formations have average compositions of $Q_{22}F_{30}L_{48}$,

214    $Q_{15}F_{36}L_{49}$, and $Q_{14}F_{34}L_{52}$, respectively. In the discrimination diagrams (Fig. 5),

215    they plot in the magmatic-arc field, indicating an undissected-transitional arc

216    provenance.

217

## 5. Geochronology and geochemistry

### 5.1. Detrital zircon geochronology

220    Single-grain U-Pb dating were performed using the laser ablation ICP-MS

221    technique at China University of Geosciences (Wuhan). The detailed analytical

222    procedures follow Yuan et al. (2004). A GeoLas 2005M laser-ablation system

223    equipped with a 193 nm ArF-excimer laser was used in connection with an

224    Agilent 7500 ICP-MS. Helium was used as the carrier gas to enhance the

225    transport efficiency of the ablated material. The spot diameter was 32 μm. Raw

226    data were processed using the Glitter program (Jackson et al., 2004). All

227    measurements were normalized relative to standard zircon 91500. Standard

228    silicate glass NIST SRM610 was used to calculate U and Th concentrations. The

229    data were processed using the ISOPLOT program (Ludwig, 1999).

230    Zircons from these rocks are commonly transparent to orange in color, 100-

231    200 μm in size and subrounded to subangular. A total of two hundred and ninety-

232    eight analyses were performed on zircon grains from five samples (Table 3). Of

233    those, 40 analyses with a degree of discordance >3% were discarded. However,

234    only a very few of these discordant analyses yield ages outside the range defined

235    by the remaining relatively concordant analyses. $^{207}Pb/^{206}Pb$ and $^{206}Pb/^{238}U$ ages

236    were applied for zircons older and younger than 1000 Ma, respectively. The

237    dataset yields ages mainly of ~900-920 Ma with only a very minor, statistically

238    insignificant, component of older continental-derived zircons in the Yumen and

239    Xiaoping Formations. The Zagu Formation, on the other hand, has a relatively

240    high content of older continental material (Fig. 6).

241    **5.1.1. Yumen Formation**

242    Sample F38, a coarse-grained sandstone specimen, was collected near the

243    base of the Yumen Formation (N26.53.39, E101.30.80) for zircon dating. Of the

244    60 grains analyzed, 4 were highly discordant and thus were discarded. The

245    remaining forty-six grains yielded $^{206}Pb/^{238}U$ apparent ages ranging from 865 to

246    975 Ma, with a single peak at 917±6 Ma (Fig. 6).

247    Sample F3, consisting of coarse-grained, feldspar-lithic sandstone, was

248    collected from the upper part of the Yumen Formation (N26.54.47, E101.28.89).

249    Of 58 spot analyses, 41 have concordant ages ranging from 860 to 990 Ma with

250    a weighted mean of 918±8 Ma. Only one concordant grain has a significantly

251    older age of ~2000 Ma (Fig. 6). The remaining 16 analyses are highly discordant

252    but have ages within the younger age population. Thus, the age distribution of

253    zircons from the Yumen Formation suggests uniform source rocks.

254

### 5.1.2. Xiaoping Formation

A medium- to coarse-grained, feldspar-lithic sandstone, sample F4, was collected from the middle part of the Xiaoping Formation (N26.55.96, E101.27.45). Of the 60 grains analyzed, 45 concordant grains yielded apparent $^{206}Pb/^{238}U$ ages between 850 and 960 Ma, with a prominent peak at ~920 Ma. Three concordant grains gave much older ages from ~2200 to 2600 Ma (Fig. 6). This age spectrum is very similar to that of samples F38 and F3 of the Yumen Formation. However, half of the remaining 12 analyses with varying degrees of discordance (>3%) yield older ages of around 2200-2600, suggesting a somewhat greater input of older material input relative to the Yumen Formation. Several concordant ages are as young as ~850 Ma (Fig. 6).

Sample F26 (N26.58.76, E101.32.17) was collected near the top of the Xiaoping Formation. 42 of 60 spot analyses have concordant ages ranging from 860 to 970 Ma, with two peaks of 897±6 Ma and 934±5 Ma, respectively (Fig. 6). The remaining 18 discordant analyses also show similar age ranges.

### 5.1.3. Zagu Formation

A pebbly sandstone, sample F23 (N26.58.96, E101.32.17), was collected from the base of the Zagu Formation. Of 60 grains analyzed, 46 are concordant. This sample yields an age distribution mainly between~ 870 Ma and 930 Ma, but it is characterized by sharp increase of older zircons with several minor peaks at 1800, 2000, 2600 and 3000 Ma (Fig. 6). Coupled with a rapid coarsening in the stratigraphic section, this suggests increased uplift and erosion in the source terrane.

## 5.2. Whole rock geochemistry

Major oxides and selected trace elements of whole-rock samples were determined by X-ray fluorescence (XRF) on fused glass beads at the University of Hong Kong. Trace elements were analyzed with a VG PQ Excell ICP-MS, also at the University of Hong Kong. The samples for ICP-MS analysis were prepared in closed beakers in high-pressure bombs to ensure complete digestion (Qi et al., 2000). We used pure elemental standards for external calibration, and BHVO-1 (basalt) and SY-4 (syenite) as reference materials for all analyses. Accuracies of the XRF analyses are estimated to be better than 1% for $SiO_2$, better than 2% for major oxides present in concentrations greater than 0.5 wt% and 5% for trace elements. The ICP-MS analyses yielded accuracies better than 5%.

### 5.2.1. Major elements

The majority of the Yanbian Group sandstones and mudstones have intermediate $SiO_2$ (55-73 wt%), high $Fe_2O_3$+MgO (usually 5-12 wt%; total Fe as $Fe_2O_3$) and $TiO_2$ (0.6-1.2 wt%) and low CaO (mostly <1 wt%) (Table 4). In general, $SiO_2$ increases whereas $TiO_2$, $Al_2O_3$, $Fe_2O_3$, MnO, MgO, CaO, and $Na_2O$ decrease with enhanced mineralogical maturity, indicating an increase in the quartz content and a decrease in chemically unstable detrital grains (e.g., feldspar and volcanic rock fragments) (Bhatia, 1983). There are no systematic stratigraphic variations from the Yumen through Xiaoping to Zagu Formations, possibly reflecting inadequate sampling from the Yumen and Zagu Formations.

300       Due to enrichment in clay minerals, the mudstones generally have higher

301    $K_2O$ and $Al_2O_3$ and lower $Na_2O$ contents, resulting in much higher $K_2O/Na_2O$

302    ratios (typically 1-10) than those of the corresponding sandstones (commonly

303    0.1-1). Most sandstone samples are immature, with $SiO_2/Al_2O_3$ ratios between 3

304    to 6 and $Na_2O/K_2O$ ratios between 1 to 3.5, and plot within the graywacke field in

305    the plot of Pettijohn (1987) (Fig. 7).

306    **5.2.2. Trace elements**

307       Rocks from the three Formations are virtually indistinguishable in their trace

308    element contents, and are characterized by variable contents of Rb (7-140 ppm),

309    Sr (10-377 ppm), Cs (0.4-8 ppm), Ba (80-1200 ppm), Th (2.6-12 ppm) and U

310    (0.5-3.2 ppm) (Table 4). In comparison with average upper continental crust, they

311    show strong Nb-Ta, anomalies, slight depletion of Zr-Hf, La and Th, but moderate

312    enrichment of V (17-257 ppm), Cr (15-185 ppm), Ni (<80 ppm), and Sc (8-22

313    ppm)  (Fig. 8a). In addition, the mudstones commonly have higher Rb, Ba, Th, U

314    and Cs contents than the sandstones (Fig 8a), likely reflecting the abundance of

315    clay minerals (e.g., illite and sericite) in these rocks (McLennan et al., 1983).

316       Both the sandstones and mudstones exhibit subparallel chondrite-

317    normalized REE patterns, characterized by moderate fractionation between light

318    REE and heavy REE ($La/Yb_N$=5.3-7.4), with obvious negative Eu anomalies

319    (Eu/Eu*=0.6-0.74) (Fig. 8b), features typical of post-Archean sedimentary rocks

320    (Taylor and McLennan, 1985). Moreover, the mudstones generally have slightly

321    more fractionated REE patterns than the sandstones and ~20% higher total REE

322    abundances.

## 6. Discussion

### 6.1. Age of the Yanbian Group

The depositional age of the unfossiliferous Yanbian Group has long been debated. It was traditionally thought to be Mesoproterozoic (Pan et al., 1987; SBGMR, 1991). However, newly obtained SHRIMP U-Pb zircon ages of 782±53 Ma (Du et al., 2005) for the basaltic lavas of the lower Yanbian Group strongly suggest a Neoproterozoic age. Similarly, Zhou et al. (2006a) reported a maximum depositional age of 837±6 Ma based on LA-ICP-MS detrital zircon dating. By contrast, Li X.H. et al. (2003, 2006) proposed a minimum age of 857±13 Ma, inferred from the emplacement age of the Guandaoshan pluton that intrudes the Yanbian Group. Thus the depositional age of the Yanbian Group should be no younger than 857 ± 13 Ma. The present geochronological results provide reliable and tight constraints on the maximum depositional age of the Yanbian Group. Although eight youngest zircons from the Yanbian Group give ages as young as 852±6 Ma (Fig. 6), we adopt here a somewhat older age of 868±6 Ma defined by another ten youngest zircon dates in the concordant dataset (Table 3). The ten zircons are from different samples but yield similar ages within quoted errors. We therefore suggest that the Yanbian Group was most likely not older than ~870 Ma. Furthermore, the Yanbian Group was probably deposited in a syn-magmatic basin, based on the short time delay between deposition of the sediments and emplacement of the 857±13 Ma Guandaoshan pluton.

## 6.2. Effect of chemical weathering

Chemical weathering strongly affects the mineralogy and major element geochemistry of siliciclastic sediments (Nesbitt and Young, 1982, 1996). The chemical index of alteration (CIA) is very useful in evaluating effects of weathering on sedimentary rock composition and is defined by Nesbitt and Young (1982) as:

$$CIA = [Al_2O_3/(Al_2O_3+CaO^*+Na_2O+K_2O)]\times 100$$

Where CaO* represents Ca in the silicate minerals only (i.e. excluding calcite, dolomite and apatite) (Fedo et al., 1995). High CIA values reflect the removal of labile cations (e.g., $Na^+$, $K^+$ and $Ca^+$) in preference to relatively stable residual constituents (e.g. $Al^+$), corresponding to high degrees of chemical weathering. The values vary from about 50 for the average upper continental crust to about 100 for residual clays. Shales typically have intermediate values of about 70-75, indicating that weathering did not proceed to the stage where alkali and alkaline earth elements were substantially removed from the clay minerals (Nesbitt and Young, 1982). The Yanbian sandstones have CIA values ranging broadly from 49 to 73 and the mudstones from 57 to 84 (Table 4 and Fig. 9). In turbidites, physical sorting during transport and deposition would yield mudstone with high concentration of fine-grained, aluminous clay minerals of high-CIA value (e.g., kaolinite, gibbsite) derived from the upper parts of weathering profiles, and sandstone relatively enriched in coarse-grained low-CIA residue (e.g., quartz, vestigial feldspars) derived from the lower parts of weathering profiles (Nesbitt et al., 1996). The CIA values of mudstones, therefore, will give a better

369 understanding of the intensity of weathering in the source. Most mudstones have

370 CIA values ranging from 65 to 77, reflecting only moderate source weathering.

371 However, 6 mudstone samples in the Xiaoping Formation and 1 sample from the

372 Zagu Formation having much higher CIA values in the range of 79-84 than

373 typical shales of 70-75. If these values were corrected for K metasomatism (Fedo

374 et al., 1995), their CIA values would be even greater than 90 (Fig. 9), indicative of

375 severe weathering in the source. One possible explanation for the higher CIA

376 values in the few samples from the Xiaoping and Zagu Formations may indicate

377 a contribution of a greater proportion of distal high-CIA detritus from older

378 cratonic source, which is consistent with our detrital zircon data.

379 The A-CN-K ($Al_2O_3$-CaO*+$Na_2O$-$K_2O$) triangular plot can also be used to

380 constrain the initial compositions of the source rocks (Fedo et al., 1995). The

381 sandstones and mudstones from the Yanbian Group form a linear trend, which is

382 generally subparallel to the A-CN join, but is slightly below the predicted

383 weathering trend, especially for the fine-grained mudstones (Fig. 9). This

384 probably indicates that the mudstones were more profoundly affected by

385 illitization. Their weathering trends suggest a provenance of tonalitic or

386 granodioritic rocks for the Yanbian sediments.

387 Differential weathering at the source and subsequent

388 diagenesis/metamorphism tend to mobilize and change the relative abundance of

389 large-ion lithophile elements (Nesbitt et al., 1980). However, the Yanbian

390 sandstones and mudstones commonly show linear correlation in the elemental

391 plots of K vs. Rb, K vs. Ba, Ce vs. Sm and U vs. Th (Fig. 10), indicating that

392 these elements were probably not changed significantly. Moreover, because the

393 sandstones studied here are relatively uniform in grain size, we believe that the

394 grain-size effect is not important.

**6.3. Tectonic setting of the Yanbian Group**

396 The pillow basalts and marine sedimentary rocks of the Yanbian Group, and

397 the spatially associated Gaojiacun and Lengshuiqing mafic intrusions, were

398 previously regarded as the Yanbian ophiolite (Sun and Vuagnat, 1992). However,

399 recent studies suggest that the mafic plutons postdate the Yanbian volcano-

400 sedimentary sequence, arguing against an ophiolite model (Zhou et al., 2006a).

401 Based on the geochemistry of the basaltic lavas, the Yanbian Group has been

402 reinterpreted as a back-arc basin sequence (Du et al., 2005; Li X.H. et al., 2006;

403 Sun et al., 2007), but evidence from the sedimentary sequence was not available.

404 Our new geochronological, petrographical and geochemical data thus provide

405 new constraints on a back-arc basin scenario.

406 The Yanbian Group was deposited at ~870 Ma and derived from a proximal

407 magmatic arc with ages generally between 900 and 920 Ma (Figs. 5 and 6). The

408 presence of almost contemporaneous volcanic arc magmatism indicates an

409 active continental margin setting (DeGraaf-Surpless et al., 2002), in contrast to a

410 passive continental margin where sediments are commonly derived from

411 weathering of older continental crust (Goodge et al., 2002). The immature

412 volcaniclastic graywackes, turbidites of the Yanbian Group are also consistent

413 with an active margin setting (Crook, 1974; Pettijohn et al., 1987), where such

414 rocks are commonly associated with pillow lavas or 'greenstones' (Pettijohn et al.,

415  1987 and references therein) and are commonly observed in modern back-arc

416  basins.

417      The sandstones from the Yanbian Group have about 15% modal quartz with

418  mostly 60-73 wt% $SiO_2$ and $K_2O/Na_2O$ ratios <1, and are quartz-intermediate,

419  indicating a mixed provenance and depositional setting typical of an active

420  continental margin (Crook, 1974). Roser and Korsch (1986) examined the

421  $K_2O/Na_2O-SiO_2$ systematics of sandstone-mudstone suites from passive

422  continental margins (PM), active continental margins (ACM) and oceanic island

423  arcs (ARC), and found that the chemistry of the fine-grained members, and the

424  coupled sand-mud trends, were more useful indicators of tectonic setting than

425  the sandstones alone. Sandstones from the Yanbian Group plot exclusively in

426  the ARC and ACM fields, whereas most mudstones plot in the ACM field (Fig.

427  11). The coupled sand-mud trends (chain-dashed tie lines in Fig. 11) show one

428  trend parallel to the field boundaries and the other perpendicular to the first,

429  indicating a back-arc basin setting (Roser and Korsch, 1986). Using Bhatia's

430  (1983) scheme, the majority of samples from the Yanbian Group plot in the

431  oceanic island arc (OIA) to continental island arc (CIA) fields (Fig. 12). The

432  observed scatter of some points is probably due to a combination of sandstone

433  maturity and interelement variation.

434      The trace-element geochemistry of fine-grained clastic sediments has also

435  been widely used to determine tectonic setting (Bhatia and Crook, 1986; Floyd et

436  al., 1991). On the La-Th-Sc and Th-Sc-Zr/10 ternary plots (Fig. 13), most of the

437  Yanbian Group sandstones also fall within the OIA and CIA fields.  The elemental

438  compositions of different greywackes can be most easily compared by utilizing

439  upper continental crust-normalized, multi-element patterns. As shown in Figure

440  8a, the Yanbian rocks have pronounced negative Nb-Ta anomalies, clearly

441  indicative of subduction-related magmatic rock source (Floyd et al., 1991). For

442  further comparison, the data were also normalized to the standard tectonic

443  setting values and the results show that the Yanbian rocks are mostly affiliated

444  with a continental arc+active margin (Fig. 14).

445      REE patterns of clastic rocks are mainly controlled by provenance (Taylor

446  and McLennan, 1985; McLennan, 1989) and are believed to be faithfully

447  preserved in flysch deposited by turbidity currents and mass-flow processes

448  (Hiscott and Gill, 1992). The Yanbian rocks have REE elements and ratios

449  similar to those of continental arc settings (Table 5), in good agreement with the

450  proposed back-arc basin scenario.

451  **6.4. Provenance of the Yanbian Group**

452      Petrographic, geochronological and geochemical evidence not only indicates

453  that rocks of the Yanbian Group rocks were mainly derived from a magmatic arc,

454  but also provides important constraints for the nature of this arc, which was not

455  preserved in the modern exposures.

456      High feldspar contents (generally >30%) of the Yanbian sandstones indicates

457  derivation directly from crystalline rocks (Boggs, 2001), because feldspars are

458  chemically and physically unstable and thus less likely to survive recycling than a

459  mineral like quartz. Presence of other unstable minerals such as magnetite,

460  pyroxene and amphibole also support this view. The poorly sorted and immature

461  nature of the Yanbian greywackes, and their deposition in a back-arc basin,

462  further points to a proximal arc source with short transport distance and little or

463  no reworking.

464      The source area for the Yanbian Group sediments was an undissected to

465  transitional volcanic arc, in which only minor plutonic rocks were exposed. This

466  interpretation is supported by the abundance of volcanic rock fragments in the

467  sediments, the dominance of plagioclase over K-feldspar and the presence of

468  only minor quartz (Fig. 5 a, b and c).  It is also consistent with the negative Zr-Hf

469  anomalies of these rocks relative to the average continent upper crust, reflecting

470  a lack of zircon input from silicic plutonic rocks (Fig. 8a).

471      The abundant intermediate and felsic volcanic rock fragments and sparse

472  mafic rock clasts in the Yanbian sandstones provide the most direct evidence for

473  the composition of these volcanic rocks (Table 2). Moreover, the trace element

474  characteristics of the sediments provide additional constraints on the nature of

475  the provenance. Because silicic rocks are significantly richer in La and Th, and

476  poorer in Sc, Cr, and Co than mafic rocks (Cullers, 1994 and references therein),

477  La/Sc, Th/Sc, Th/Co, and Cr/Th ratios are good indicators of the source rocks.

478  The Yanbian rocks have relatively low and constant La/Th ratios with an average

479  of 1.5 but more variable Co/Th ratios (Fig. 15a), suggesting mixing of felsic and

480  intermediate components. Similarly, a plot of La/Th against Hf also points to

481  mixed sources (Fig. 15b). In addition, the Yanbian rocks mostly have Cr/Th ratios

482  of 5-25 (Table 4), clearly indicative of silicic-intermediate source rocks (Cullers,

483  1994). The low Cr (mostly<150 ppm) and Ni (<80 ppm) of the Yanbian rocks and

484 slight V-Cr-Ni anomalies (Fig. 8a) is also consistent with minor mafic-ultramafic

485 input from the source area (Floyd et al., 1991; Garver et al., 1996).

**6.5. An integrated tectonic model**

487 Although the tectonic affinity of the western margin of the Yangtze Block

488 during the Neoproterozoic has been a matter of debate, it has been confirmed

489 that a number of plutons in this region were subduction-related. In the Yanbian

490 area, these intrusions include the ~860-Ma Guandaoshan dioritic pluton (Sun and

491 Zhou, 2008), the ~810-Ma Gaojiacun and Lengshuiqing mafic intrusions (Zhou et

492 al., 2006a) and the ~740-Ma Dadukou gabbroic pluton (Zhao and Zhou, 2007).

493 Determination of the age and tectonic provenance of the Yanbian Group has

494 significant implications for the regional tectonic evolution during Neoproterozoic

495 time. This study provides a window into a Neoproterozoic magmatic arc on the

496 western margin of the Yangtze Block, and reveals the presence of a ~900-920

497 Ma felsic and intermediate volcanic arc in this region, although such a feature

498 has not yet been widely identified directly.

499 Available data allow us to propose a model involving the development of a

500 volcanic arc and formation of the Yanbian back-arc basin and the closely

501 associated subduction-related plutons in this region (Fig. 16). Subduction-related

502 volcanic rocks of mainly felsic and intermediate composition were produced at ca.

503 900-920 Ma owing to the eastward subduction of oceanic lithosphere along the

504 western margin of the Yangtze Block (Fig. 16a). Rifting occurred as a

505 consequence of diapiric upwelling of metasomatized mantle to create the

506 Yanbian back-arc basin and generate the basaltic lavas of the Fangtian

507 Formation (Fig. 16b). According to Crawford et al. (1981), arc volcanism appears

508 to cease around the time that back-arc opening commences. This basin was built

509 on the ~900-920 Ma volcanic arc sequence which provided materials to fill the

510 adjacent Yanbian basin above the lavas, to form the Yumen, Xiaoping and Zagu

511 Formations (Fig. 16b). With continued erosion, the relief of the source region

512 decreased and hence slowed down the supply of materials for the basin,

513 resulting in biochemical deposition of the carbonates in the Zagu Formation (Fig.

514 16b). Subduction-related magmatism was then re-activated to generate the

515 subduction-related plutons (Fig. 16c). The oldest pluton is the ~860-Ma

516 Guandaoshan dioritic pluton, followed by the ~810-Ma Gaojiacun and

517 Lengshuiqing and the youngest ~740 Ma Dadukou gabbroic plutons (Fig. 16c).

518 This period of igneous activity suggests continuous subduction along the western

519 margin of the Yangtze Block between about 920 and 740 Ma. This arc was thus

520 active for at least ~180 million years. Eventually, this region probably became a

521 passive margin and the Sinian Lieguliu Formation was unconformably deposited

522 over the Yanbian Group, marking the termination of the arc setting (Fig. 16d).

523 The subduction-related environment may extend along the entire western

524 margin of the Yangtze Block. Similar sequences also occurred in the northwest

525 margin including the Bikou Group (Fig. 1), which has detrital zircon ages ranging

526 from 700 to 850 Ma and has been interpreted as fore-arc basin deposits (Yan

527 Q.R. et al., 2004; Druschke et al., 2006). Thus our proposed model implies that

528 the western margin of the Yangtze Block was a major continental arc during the

529 Neoproterozoic, and thus probably flanked the Rodinia supercontinent.

## 7. Conclusions

The Yanbian Group is a typical deep marine, volcaniclastic succession deposited in a back-arc basin. Detrital zircon dating and geological constraints indicate that the Yanbian Group was formed at ~870 Ma. The immature nature of the Yanbian sandstones indicates a proximal arc source with ages of ~900-920 Ma. The Yanbian Group and spatially associated subduction-related plutons in the Yanbian region make up a typical arc assemblage, being part of a major continental arc along the western margin of the Yangtze Block for at least 180 m.y. (920-740 Ma). We infer that the Yangtze Block probably flanked the Rodinia supercontinent.

**References**

Bhatia, M.R., 1983. Plate tectonics and geochemical composition of sandstones. J. Geol. 91, 611-627.

Bhatia, M.R., 1985. Rare earth element geochemistry of Australian Paleozoic graywackes and mudstones: Provenance and tectonic control. Sediment. Geol. 45, 97-113.

Bhatia, M.R., Crook, K.A.W., 1986. Trace element characteristics of graywackes and tectonic setting discrimination of sedimentary basins. Contrib. Mineral. Petrol. 92, 181-193.

BGMRSP (Bureau of Geology and Mineral Resources of the Sichuan Province), 1972. Regional Geological Survey of People's Republic of China, the Yanbian Sheet (G-47-XII; geological part), scale 1:200,000 (in Chinese).

Boggs, S., 2001. Principles of sedimentology and stratigraphy (Third editon). New Jersey, Prentice-Hall, 726p.

Chen, Z.L., Chen, S.Y., 1987. On the tectonic evolution of the west margin of the Yangzi block. Chongqing, China, Chongqing Publishing House, 172p. (in Chinese).

Cope, T., Ritts, B.D., Darby, B.J., Fildani, A., Graham, S.A., 2005. Late Paleozoic Sedimentation on the Northern Margin of the North China Block: Implications for Regional Tectonics and Climate Change. Int. Geol. Rev. 47, 270-296.

Crawford, A.J., Beccaluva, L., Serri, G., 1981. Tectono-magmatic evolution of the west Philippine-Mariana region and the origin of boninites. Earth Planet. Sci. Lett. 54, 346-356.

573     Crook, K.A.W., 1974. Lithogenesis and geotectonics: The significance of

574         compositional variations in flysch arenites (graywackes). In: Dott, R.H.,

575         Shaver, R.H. (Eds.), Modern and Ancient Geosynclinal Sedimentation. SEPM

576         Spec. Publ. 19, pp. 304-310.

577     Cullers, R.L., 1994. The controls on the major and trace element variation of

578         shales, siltstones, and sandstones of Pennsylvanian-Permian age from

579         uplifted continental blocks in Colorado to platform sediment in Kansas, USA.

580         Geochim. Cosmochim. Acta 58, 4955-4972.

581     DeGraaff-Surpless, K., Graham, S.A., Wooden, J.L., McWilliams, M.O., 2002.

582         Detrital zircon provenance analysis of the Great Valley Group, California:

583         Evolution of an arc-forearc system. Geol. Soc. Am. Bull. 114, 1564-1580.

584     Dickinson, W.R., 1970. Interpreting detrital modes of graywacke and arkose. J.

585         Sediment. Petrol. 40, 695-707.

586     Dickinson, W.R., 1985. Interpreting provenance relations from detrital modes of

587         sandstones. In: Zuffa, G.G. (Eds.), Provenance of arenites. NATO ASI Series

588         C: Mathematical and Physical Sciences 48, D. Reidel Publishing Company,

589         pp. 333-361.

590     Dickinson, W.R., Gehrels, G.E., 2000. Sandstone petrofacies of detrital zircon

591         samples from Paleozoic and Triassic strata in suspect terranes of northern

592         Nevada and California. In: Soreghan, M.J., Gehrels, G.E. (Eds.), Paleozoic

593         and Triassic paleogeography and tectonics of western Nevada and northern

594         California. Boulder, Colorado, Geol. Soc. Am. Special Paper 347, pp. 151-171.

595    Druschke, P., Hanson, A.D., Yan, Q., Wang, Z., Wang, T., 2006. Stratigraphic

596        and U-Pb SHRIMP detrital zircon evidence for a Neoproterozoic continental

597        arc, Central China: Rodinia implications. J. Geol. 114, 627-636.

598    Du, L.L., Geng, Y.S., Yang, C.H., Wang, X.S., Ren, L.D., Zhou, X.W., Shi, Y.Y.,

599        Yang, Z.S., 2005. Geochemistry and SHRIMP U-Pb zircon chronology of

600        basalts from the Yanbian group in the western Yangtze Block. Acta Geologica

601        Sinica 76, 805-813 (in Chinese with English abstract).

602    Eisbacher, G.H., 1985. Late Proterozoic rifting, glacial sedimentation, and

603        sedimentary cycles in the light of Windermere deposition, western Canada.

604        Palaeogeogr. Palaeoclimatol. Palaeoecol. 51, 231-254.

605    Fedo, C.M., Nesbitt, H.W., Young, G.M., 1995. Unraveling the effects of

606        potassium metasomatism in sedimentary rocks and paleosols, with

607        implications for weathering conditions and provenance. Geology 23, 921-924.

608    Floyd, P.A., Leveridge, B.E., 1987. Tectonic environment of the Devonian

609        Gramscatho Basin, South Cornwall: Framework mode and geochemical

610        evidence from turbiditic sandstones. J. Geol. Soc. London 144, 531-542.

611    Floyd, P.A., Shail, R., Leveridge. B.E., Franke, W., 1991. Geochemistry and

612        provenance of Rhenohercynian synorogenic sandstones: implications for

613        tectonic environment discrimination. In: Morton, A.C., Todd, S.P., Haughton,

614        P.D.W. (Eds.), Developments in sedimentary provenance studies. Geol. Soc.

615        London, Spec. Publ. 57, 173-188.

616    Garver, J.I., Royce, P.R., Smick, T.A., 1996. Chromium and nickel in shale of the

617        Taconic Foreland: A case study for the provenance of fine-grained sediments

618      with an ultramafic source. J. Sediment. Res. 66, 100-106.

619    Goodge, J.W., Myrow, P., Williams, I.S., Bowring, S.A., 2002. Age and

620      provenance of the Beardmore Group, Antarctica: constraints on Rodinia

621      supercontinent breakup. J. Geol. 110, 393-406.

622    Gu, X.X., Liu, J.M., Zheng, M.H., Tang, J.X., Qi, L., 2002. Provenance and

623      tectonic setting of the Proterozoic turbidites in Hunan, South China:

624      geochemical evidence. J. Sediment. Res. 72, 393-407.

625    Hiscott, R.N., Gill, J.B., 1992. Major and trace element geochemistry of

626      Oligocene to Quaternary volcaniclastic sands and sandstones from the Izu-

627      Bonin arc. In: Taylor, B., Fujioka, K., et al. (Eds.), Proceedings of the Ocean

628      Drilling Program, Scientific Results 126. College Station, TX: Ocean Drilling

629      Program, pp. 467-485.

630    Ingersoll, R.V., Fullard, T.F., Ford, R.L., Grimm, J.P., Pickle, J.D., Sares, S.W.,

631      1984. The effect of grain size on detrital modes; a test of the Gazzi-Dickinson

632      point-counting method: J. Sediment. Petrol. 54, 103-116.

633    Jackson, S.E., Pearson, N.J., Griffin, W.L., Belousova, E.A., 2004. The

634      application of laser ablation-inductively coupled plasma-mass spectrometry

635      (LA-ICP-MS) to in-situ U-Pb zircon geochronology. Chem. Geol. 211, 331-335.

636    Li, F.H., Tan, J.M., Shen, Y.L., Yu, F.X., Zhou, G.F., Pan, X.N., Li, X.Z., 1988.

637      The pre-Sinian in the Kangdian area: Chongqing, China, Chongqing

638      Publishing House, 396p. (in Chinese).

639    Li, X.H., Li, Z.X., Zhou, H.W., Liu, Y., Liang, X.R., Li, W.X., 2003. SHRIMP U-Pb

640      zircon age, geochemistry and Nd isotope of the Guandaoshan pluton in SW

641    Sichuan: Petrogenesis and tectonic significance. Sci. China Ser. D (Supp.)

642    46, 73-83.

643    Li X.H., Li, Z.X., Sinclair, J.A., Li, W.X., Carter, G., 2006. Revisiting the "Yanbian

644    Terrane": implications for Neoproterozoic tectonic evolution of the western

645    Yangtze Block, South China. Precambrian Res. 151, 14-30.

646    Li, Z.X., Li, X.H., Kinny, P., Wang, J., 1999. The breakup of Rodinia: did it start

647    with a mantle plume beneath South China. Earth Planet. Sci. Lett. 173, 171-

648    181.

649    Li, Z.X., Li, X.H., Kinny, P.D., Wang, J., Zhang, S., Zhou, H., 2003.

650    Geochronology of Neoproterozoic syn-rift magmatism in the Yangtze Craton,

651    South China and correlations with other continents: evidence for a mantle

652    superplume that broke up Rodinia. Precambrian Res. 122, 85-109.

653    Ludwig, K. R., 1999. Isoplot/Ex version 2.06: A geochronological tool kit for

654    Microsoft Excel. Berkeley Geochronology Center, Spec. Publ. 1a.

655    Maas, R., McCulloch, M.T., 1991. The provenance of Archean clastic

656    metasediments in the Narryer Geniss Complex, Western Australia: trace

657    element geochemistry, Nd isotopes, and U-Pb ages for detrital zircons.

658    Geochim. Cosmochim. Acta 55, 1915-1932.

659    Marsaglia, K.M., Ingersoll, R.V., 1992. Compositional trends in arc-related, deep-

660    marine sand and sandstone: a reassessment of magmatic-arc provenance.

661    Geol. Soc. Am. Bull. 104, 1637-1649.

662    McLennan, S.M., 1989. Rare earth elements in sedimentary rocks: Influence of

663    provenance and sedimentary processes. Rev. Mineral. Geochem. 21, 169-200.

664 McLennan, S.M., 1993. Weathering and Global Denudation. J. Geol. 101, 295-
665     303.

666 McLennan, S.M., Taylor, S.R., Eriksson, K.A., 1983. Geochemistry of Archean
667     shales from the Pilbara Supergroup, Western Australia. Geochim.
668     Cosmochim. Acta 47, 1211-1222.

669 McLennan, S.M., Taylor, S.R., McCulloch, M.T., Maynard, J.B., 1990.
670     Geochemical and Nd-Sr isotopic composition of deep-sea turbidites: Crustal
671     evolution and plate tectonic associations. Geochim. Cosmochim. Acta 54,
672     2015-2050.

673 McLennan, S.M., Hemming, S.R., Taylor, S.R., Eriksson, K.A., 1995. Early
674     Proterozoic crustal evolution: Geochemical and Nd-Pb isotopic evidence from
675     metasedimentary rocks, southwestern North America. Geochim. Cosmochim.
676     Acta 59, 1153-1177.

677 Nesbitt, H.W., Markovics, G., Price, R.C., 1980. Chemical processes affecting
678     alkalies and alkaline earths during continental weathering: Geochim.
679     Cosmochim. Acta 44, 1659-1666.

680 Nesbitt, H.W., Young, G.M., 1982. Early Proterozoic climates and plate motions
681     inferred from major element chemistry of lutites. Nature 299, 715-717.

682 Nesbitt, H.W., Young, G.M., 1996. Petrogenesis of sediments in the absence of
683     chemical weathering: effects of abrasion and sorting on bulk composition and
684     mineralogy. Sedimentology 43, 341-358.

685    Nesbitt, H.W., Young, G.M., McLennan, S.M., and Keays, R.R., 1996. Effects of

686        chemical weathering and sorting on the petrogenesis of siliciclastic sediments,

687        with implications for  provenance studies. J. Geol. 104, 525-542.

688    Pettijohn, F.J., Potter, P.E., Siever, R., 1987. Sand and sandstone (Second

689        editon), Springer-Verkag, 553p.

690    Pan, X.N., Zhao, J.X., Zhan, X.Y., Zhen, H.X., Yan, Z.H., Zhou, G.F., Tao, D.L.,

691        1987. Tectonics and rifting in the Kangdian area: Chongqing, China,

692        Chongqing Publishing House, 295p. (in Chinese).

693    Qi, L., Hu, J., Gregoire, D.C., 2000. Determination of trace elements in granites

694        by inductively coupled plasma-mass spectrometry. Talanta 51, 507-513.

695    Roser, B.P., Korsch, R.J., 1986. Determination of tectonic setting of sandstone-

696        mudstone suites using $SiO_2$ content and $K_2O/Na_2O$ ratio. J. Geol. 94, 635-650.

697    Roser, B.P., Korsch, R.J., 1988. Provenance signatures of sandstone-mudstone

698        suites determined using discriminant function analysis of major-element data.

699        Chem. Geol. 67, 119-139.

700    SBGMR (Sichuan Bureau of Geology and Mineral Resources). 1991. Regional

701        Geology of Sichuan Province. Beijing, China, Geological Memoirs 23.

702        Geological Publishing House (in Chinese with English summary).

703    She, Z.B., Ma, C.Q., Mason, R., Li, J.W., Wang, G.C., Lei, Y.H., 2006.

704        Provenance of the Triassic Songpan-Ganzi flysch, west China. Chem. Geol.

705        231, 159-175.

706    Sun, C.M., Vuagnat, M., 1992. Proterozoic ophiolites from Yanbian and Shimian

707        (Sichuan Province, China): Petrography, geochemistry, petrogenesis, and

708        geotectonic environment. Schweiz. Mineral. Petrograph. Mitt. 72, 389-413.

709     Sun, W.H., Zhou, M.-F., Zhao J.H., 2007. Geochemistry and tectionic

710        significance of basaltic lavas in the Neoproterozoic Yanbian Group (Southern

711        Sichuan Province, SW China). Int. Geol. Rev. 49, 554-571.

712     Sun, W.H., Zhou, M.-F., 2008. The ~860-Ma, Cordilleran-type Guandaoshan

713        dioritic pluton in the Yangtze Block, SW China: Implications for the origin of

714        Neoproterozoic magmatism. J. Geol. 116, 238-253.

715     Taylor, S.R., McLennan, S.M., 1985. The Continental Crust; Its Composition and

716        Evolution. London, Blackwell, 312 p.

717     Taylor, S.R., McLennan, S.M., 1995. The Geochemical Evolution of the

718        Continental Crust. Rev. Geophys. 33, 241-265.

719     Yan, D.P., Zhou, M.-F., Song, H. L., Wang, X.W., Malpas, J., 2003. Origin and

720        tectonic significance of a Mesozoic multi-layer over-thrust within the Yangtze

721        block (South China). Tectonophysics 361, 239-254.

722     Yan, Q.R., Hanson, A.D., Wang, Z.Q., Druschke, P.A., Yan, Z., Wang, T., Liu,

723        D.Y., Song, B., Pan, P., Zhou, H., Jiang, C.F., 2004. Late Proterozoic

724        subduction and rifting on the northern margin of the Yangtze Plate, China:

725        implications for Rodinia reconstruction. Int. Geol. Rev. 46, 817-832.

726     Yuan, H.L., Gao, S., Liu, X.M., Li, H.M., Gunther, D.,Wu, F.Y., 2004. Accurate U-

727        Pb age and trace element determinations of zircon by laser ablation-

728        inductively coupled plasma-mass spectrometry. Geostandard. Geoanal. Res.

729        28, 353-370.

730    Zhao, J.H., Zhou, M.-F., 2007. Geochemistry of Neoproterozoic mafic intrusions

731        in the Panzhihua district (Sichuan Province, SW China): implications for

732        subduction-related metasomatism in the upper mantle. Precambrian Res. 152,

733        27-47.

734    Zhou, M.-F., Kennedy, A.K., Sun, M., Malpas, J., Lesher, C.M., 2002a. Late

735        Proterozoic arc-related mafic intrusions along the northern margin of South

736        China: implications for the accretion of Rodinia. J. Geol. 110, 611-618.

737    Zhou, M.-F., Yan, D.P., Kennedy, A.K., Li, Y.Q., Ding, J., 2002b. SHRIMP U-Pb

738        zircon geochronological and geochemical evidence for Late Proterozoic arc-

739        magmatism along the western margin of the Yangtze Block, South China.

740        Earth Planet. Sci. Lett. 196, 51-67.

741    Zhou, M.-F., Ma, Y.X., Yan, D.P., Xia, X.P., Zhao, J.H., Sun, M., 2006a. The

742        Yanbian Terrane (Southern Sichuan Province, SW China): A Late Proterozoic

743        arc assemblage in the western margin of the Yangtze Block. Precambrian

744        Res. 144, 19-38.

745    Zhou, M.-F., Yan, D.P., Wang, C.L., Qi, L., Kennedy, A., 2006b. Subduction-

746        related origin of the 750 Ma Xuelongbao adakitic complex (Sichuan Province,

747        China): Implications for the tectonic setting of the giant Neoproterozoic

748        magmatic event in South China. Earth Planet. Sci. Lett. 248, 286-300.

749    Zhou, D., Graham, S.A., 1996. The Songpan-Ganzi complex of the West Qinling

750        Shan as a Triassic remnant ocean basin.  In: Yin, A., Harrison, T.M. (Eds.),

751        The Tectonic Evolution of Asia. New York, Cambridge University Press, pp.

752        281-299.

**Figure captions**

754 Fig. 1. Simplified geological map of the Yanbian region, Sichuan Province, SW

755 China (after BGMRSP, 1972). The insert map showing the tectonic units of South

756 China and general distribution of Neoproterozoic rocks in the margins of the

757 Yangtze Block.

758 Fig. 2. Stratigraphy of the Yanbian Group based on a measured cross section

759 (BGMRSP, 1972) and our field mapping. Stars indicate samples for detrital zircon

760 analysis. The sandstone beds shown in the column are not strictly to scale

761 because they are typically thin layers interbedded with slate.

762 Fig. 3. (a) Contact between the clastic Yumen Formation and the volcanic

763 Fangtian Formation. (b) A scour structure in the Xiaoping Formation. (c) Slumped

764 siltstone in the Xiaoping Formation. (d) Well-exposed Bouma sequences in the

765 Xiaoping Formation.

766 Fig. 4. (a) Photomicrographs of grain types and features in the Yanbian

767 sandstones. (a) General view showing sub-angular monocrystalline quartz (Q)

768 (T3-3). (b) Sub-rounded plagioclase feldspar (Pl) and K-feldspar (Kf) grains (T3-

769 1-2). (c) A metamorphic grain (Lm) and volcanic grains (Lv) with felsitic and

770 microlitic texture (B11). (d) Siltstone fragments (Ls) (B11). (e) A typical volcanic

771 rock fragment with microlitic texture that we interpret to be derived from

772 intermediate composition (B9). (f) A clinopyroxene grain (Cpx) (F6). All samples

773 are in cross-polarized light. Scale bar in each photograph is 0.3 mm.

774 Fig. 5. Ternary plots of sandstone point count data for the Yanbian Group. (a)

775 QFL plot. (b) QmFLt plot. (c) QLvmLsm plot. (d) QmPK plot. Provenance fields

776    are from Dickinson (1985). The large open triangles represent arithmetic means

777    of data and polygonal box represents one standard deviation.

778    Fig. 6. Detrital zircon data for the sandstone samples of the Yanbian Group. (a)

779    Neoproterozoic (860-1000 Ma) detrital zircon age histogram and cumulative

780    probability plot, showing number of grains analyzed and percentage of

781    Neoproterozoic ages as a fraction of total discordant and concordant ages. (b)

782    Histogram and cumulative probability plot of total concordant detrital zircon ages.

783    Total number of concordant ages for each sample is shown, with number of

784    analyses (concordant plus discordant ages) shown in parenthesis.

785    Fig. 7. (a) Geochemical classification of sandstones from the Yanbian Group

786    (Pettijohn et al., 1987).

787    Fig. 8.  (a) Upper crust-normalized, multi-element diagrams for the Yanbian

788    samples; (b) Chondrite-normalized REE patterns of the Yanbian sandstones and

789    mudstones. Post-Archean average Australian shale (PAAS) is also plotted as a

790    heavy dashed line "+" for comparison. Values are from Taylor and McLennan

791    (1985).

792    Fig. 9. CIA ternary diagram, A-CN-K=$Al_2O_3$ -CaO*+$Na_2O$-$K_2O$, after Nesbitt and

793    Young (1982) showing Yanbian sandstones and mudstones as well as average

794    compositions of tonalite and granodiorite (from Fedo et al., 1995). Approximate

795    correction for carbonate content was made by assuming reasonable Ca/Na ratios

796    in silicate material (McLennan, 1993). After correcting phosphate using $P_2O_5$, if

797    the remaining mole fraction of CaO ≤$Na_2O$, then this value of CaO is adopted; if

798    CaO >$Na_2O$, CaO* is assumed to be equivalent to $Na_2O$. Due to relatively low

799 carbonate contents in most samples, however, the calculated proportions are

800 thus very close to actual values.

801 Fig. 10. Plots of K vs. Rb, K vs. Ba, Ce vs. Sm, and U vs. Th, showing linear

802 correlations.

803 Fig 11. $K_2O/Na_2O-SiO_2$ plot for the Yanbian rocks. PM = passive margin; ACM =

804 active continental margin; ARC = oceanic island arc. (after Roser and Korsch,

805 1986).

806 Fig.12. Tectonic discrimination diagrams for the Yanbian Group sandstones: PM

807 = passive margin; ACM = active continental margin; CIA = continental island arc;

808 OIA =oceanic island arc (after Bhatia, 1983).

809 Fig. 13. Triangular trace element plots for Yanbian sandstones (after Bhatia and

810 Crook, 1986). Abbreviations as in Fig. 11.

811 Fig. 14. Normalized multi-element diagrams for the Yanbian sandstones. CAAM

812 = continental arc+active margin; OIA = oceanic island arc; PM = passive margin;

813 OWP = oceanic within-plate. Normalizing values are from Floyd et al. (1991).

814 Fig. 15. Source rock discrimination diagrams for the Yanbian rocks; (a) Co/Th vs.

815 La/Sc diagram (after Gu et al., 2002), showing derivation from mixed felsic-basic

816 volcanic source, (b) La/Th vs. Hf diagram (after Floyd and Leveridge, 1987),

817 indicating mixed of felsic/basic source rocks.

818 Fig. 16. Model for the development of the Yanbian Group and the spatially

819 associated subduction-related intrusions in the Yanbian region, SW China.

**Table 1**

Table 1. Definition of point-count and recalculated mode parameters (after Dickinson, 1970; Ingersoll et al., 1984)

| Symbol | Definition |
| --- | --- |
| **Point-counting Categories** | |
| Qm | Monocrystalline quartz |
| Qpq | Polycrystalline quartz (not including chert) |
| Cht | Chert |
| P | Plagioclase feldspar |
| K | K-feldspar |
| Lvf | Volcanic-lithic with felsitic texture (mainly silicic volcanic rocks) |
| Lvm | Volcanic-lithic with microlitic texture (mainly intermediate lava) |
| Lvl | Volcanic-lithic with lathwork texture (mainly basaltic lava) |
| Lvv | Vitric volcanic-lithic grain |
| Lmv | Metavolcanic-lithic grain |
| Lms | Metamorphic-lithic grains except Lmv |
| Lss | Siltstone/shale sedimentary-lithic grain |
| Lsc | Carbonate grain |
| M | Phyllosilicates |
| Hv | Heavy minerals |
| FW | Total framework grains counted |
| | |
| **Recalculated Parameters** | |
| Qp | Polycrystalline quartz including chert (Qpq+Cht) |
| Q | Total quartzose grains (Qm+Qp) |
| F | Total feldspar grains (P+K) |
| Lvm | Total volcanic-lithic grains (Lvf+Lvm+Lvl+Lvv+Lmv) |
| Lsm | Total ~~volcanic~~ lithic grins (Lss+Lms) |
| L | Total unstable lithic grains (Lvm+Lsm) |
| Lt | Total lithics (L+Qp) |

Table2

Table 2 Modal Point-count Data for the Yanbian Group, SW China

| Fm. Sample | Qm | Qpq | Cht | P | K | Lvf | Lvm | Lvl | Lvv | Lmv | Lms | Lss | Lsc | M | Hv | FW | (Q-F-L) | | | (Qm-F-Lt) | | | (Qm-P-K) | | | (Qp-Lv-Ls) | | | Lv/L | P/F |
|---|---|---|---|---|---|---|---|---|---|---|---|---|---|---|---|---|---|---|---|---|---|---|---|---|---|---|---|---|---|---|
| | | | | | | | | | | | | | | | | | %Q | %F | %L | %Qm | %F | %Lt | %Qm | %P | %K | %Qp | %Lv | %Ls | | |
| ZG F22 | 48 | 1 | 1 | 126 | 67 | 127 | 67 | | | 1 | 3 | 120 | | 5 | 6 | 561 | 9 | 34 | 57 | 9 | 34 | 57 | 20 | 52 | 28 | 1 | 61 | 38 | 0.61 | 0.65 |
| ZG F23 | 50 | 2 | 1 | 119 | 96 | 122 | 39 | | | 1 | 2 | 157 | | 3 | 4 | 589 | 9 | 37 | 54 | 8 | 37 | 55 | 19 | 45 | 36 | 1 | 50 | 49 | 0.50 | 0.55 |
| ZG B15 | 50 | 1 | 6 | 172 | 51 | 156 | 110 | | | | | 14 | | 4 | 6 | 560 | 10 | 40 | 50 | 9 | 40 | 51 | 18 | 63 | 19 | 2 | 93 | 5 | 0.95 | 0.77 |
| ZG L18 | 59 | 6 | 32 | 122 | 41 | 155 | 56 | | | | | 61 | | 4 | 5 | 532 | 18 | 31 | 51 | 11 | 31 | 58 | 27 | 55 | 18 | 12 | 68 | 20 | 0.78 | 0.75 |
| ZG YM6 | 75 | 5 | 46 | 136 | 25 | 134 | 48 | | | | | 77 | | 4 | 9 | 546 | 23 | 29 | 47 | 14 | 29 | 57 | 32 | 58 | 11 | 16 | 59 | 25 | 0.70 | 0.84 |
| XP F20 | 27 | 1 | 5 | 148 | 19 | 126 | 207 | | | | | 9 | | 2 | 7 | 542 | 6 | 31 | 63 | 5 | 31 | 64 | 14 | 76 | 10 | 2 | 96 | 3 | 0.97 | 0.89 |
| XP B9 | 28 | 1 | 4 | 103 | 18 | 204 | 117 | 2 | | | 2 | 86 | | 3 | 9 | 563 | 6 | 21 | 73 | 5 | 21 | 74 | 19 | 69 | 12 | 1 | 78 | 21 | 0.79 | 0.85 |
| XP B10 | 27 | 1 | 5 | 128 | 21 | 176 | 195 | | | | 3 | 20 | | 4 | 7 | 576 | 6 | 26 | 68 | 5 | 26 | 69 | 15 | 73 | 12 | 2 | 93 | 6 | 0.94 | 0.86 |
| XP B11 | 13 | 1 | 4 | 94 | 5 | 125 | 185 | | | | 9 | 120 | | 3 | 6 | 556 | 3 | 18 | 79 | 2 | 18 | 80 | 12 | 84 | 4 | 1 | 70 | 29 | 0.71 | 0.95 |
| XP F4 | 73 | 2 | 69 | 215 | 3 | 138 | 8 | | | | 1 | 31 | 1 | 3 | 4 | 540 | 27 | 40 | 33 | 14 | 40 | 46 | 25 | 74 | 1 | 29 | 59 | 13 | 0.82 | 0.99 |
| XP F5 | 69 | 7 | 74 | 209 | 8 | 129 | 7 | | | | 2 | 53 | 1 | 3 | 7 | 558 | 27 | 39 | 34 | 12 | 39 | 49 | 24 | 73 | 3 | 30 | 50 | 20 | 0.71 | 0.96 |
| XP F6 | 19 | 1 | 19 | 222 | 5 | 18 | 228 | 1 | | | | 7 | 1 | 2 | 6 | 519 | 8 | 44 | 49 | 4 | 44 | 53 | 8 | 90 | 2 | 7 | 90 | 3 | 0.97 | 0.98 |
| XP F7 | 17 | 1 | 13 | 218 | 4 | 17 | 243 | | | | 1 | 3 | | 3 | 4 | 517 | 6 | 43 | 51 | 3 | 43 | 54 | 7 | 91 | 2 | 5 | 94 | 1 | 0.98 | 0.98 |
| XP F8 | 18 | 1 | 12 | 216 | 5 | 16 | 265 | | | | 3 | | | 1 | 7 | 536 | 6 | 41 | 53 | 3 | 41 | 55 | 8 | 90 | 2 | 4 | 95 | 1 | 0.99 | 0.98 |
| XP F9 | 61 | 2 | 82 | 193 | 8 | 83 | 34 | | | 1 | 1 | 123 | | 3 | 3 | 588 | 25 | 34 | 41 | 10 | 34 | 55 | 23 | 74 | 3 | 26 | 36 | 38 | 0.49 | 0.96 |
| XP F10 | 72 | 3 | 53 | 89 | 28 | 181 | 110 | | | | 3 | | | 1 | 5 | 539 | 24 | 22 | 55 | 13 | 22 | 65 | 38 | 47 | 15 | 16 | 83 | 1 | 0.99 | 0.76 |
| XP F11 | 79 | 4 | 21 | 215 | 12 | 102 | 124 | | | | | | | 1 | 4 | 557 | 19 | 41 | 41 | 14 | 41 | 45 | 26 | 70 | 4 | 10 | 90 | 0 | 1.00 | 0.95 |
| XP F14 | 11 | 1 | 1 | 125 | 4 | 3 | 373 | | | | 3 | 6 | 1 | 2 | 5 | 527 | 2 | 24 | 73 | 2 | 24 | 73 | 8 | 89 | 3 | 1 | 97 | 2 | 0.98 | 0.97 |
| XP F33 | 93 | 4 | 38 | 331 | 24 | 62 | 43 | | | | | 43 | | 3 | 3 | 638 | 21 | 56 | 23 | 15 | 56 | 30 | 21 | 74 | 5 | 22 | 55 | 23 | 0.71 | 0.93 |
| XP F34 | 89 | 3 | 39 | 218 | 21 | 168 | 47 | | | | | 56 | | 3 | 4 | 641 | 20 | 37 | 42 | 14 | 37 | 49 | 27 | 66 | 6 | 13 | 69 | 18 | 0.79 | 0.91 |
| XP S6 | 65 | 4 | 26 | 85 | 28 | 267 | 4 | | 15 | | | 2 | | 3 | 6 | 496 | 19 | 23 | 58 | 13 | 23 | 64 | 37 | 48 | 16 | 9 | 90 | 1 | 0.99 | 0.75 |
| XP S8 | 66 | 1 | 12 | 174 | 49 | 96 | 52 | | 1 | | 4 | 93 | | 4 | 4 | 548 | 14 | 41 | 45 | 12 | 41 | 47 | 23 | 60 | 17 | 5 | 58 | 37 | 0.61 | 0.78 |
| XP S3-1 | 87 | 4 | 19 | 203 | 18 | 164 | 31 | | 3 | | 1 | 2 | | 3 | 5 | 532 | 21 | 42 | 38 | 16 | 42 | 42 | 28 | 66 | 6 | 10 | 88 | 1 | 0.99 | 0.92 |
| XP S5 | 99 | 4 | 21 | 236 | 27 | 106 | 71 | | 1 | | | 12 | | 1 | 5 | 577 | 21 | 46 | 33 | 17 | 46 | 37 | 27 | 65 | 7 | 12 | 83 | 6 | 0.94 | 0.90 |
| XP S4 | 86 | 3 | 27 | 326 | 53 | 38 | 21 | | | | | | | 3 | 4 | 554 | 21 | 68 | 11 | 16 | 68 | 16 | 18 | 70 | 11 | 34 | 66 | 0 | 1.00 | 0.86 |
| XP B4 | 77 | 3 | 26 | 131 | 19 | 204 | 69 | | | | | 6 | | 3 | 4 | 535 | 20 | 28 | 52 | 14 | 28 | 58 | 34 | 58 | 8 | 9 | 89 | 2 | 0.98 | 0.87 |
| XP L6 | 43 | 3 | 38 | 84 | 26 | 225 | 44 | 1 | | | | 80 | | 3 | 6 | 543 | 15 | 20 | 64 | 8 | 20 | 72 | 28 | 55 | 17 | 10 | 69 | 20 | 0.77 | 0.76 |
| YM F3 | 41 | 2 | 58 | 196 | 1 | 93 | 5 | | | 1 | | 136 | | 2 | 7 | 533 | 19 | 37 | 44 | 8 | 37 | 55 | 17 | 82 | 0 | 20 | 34 | 46 | 0.42 | 0.99 |
| YM F38 | 74 | 5 | 27 | 96 | 19 | 113 | 73 | | | 1 | | 112 | | 2 | 5 | 520 | 20 | 22 | 58 | 14 | 22 | 64 | 39 | 51 | 10 | 10 | 56 | 34 | 0.63 | 0.83 |
| YM T3 | 128 | 1 | 18 | 131 | 16 | 212 | 8 | | | | | 26 | | 2 | 4 | 540 | 27 | 27 | 46 | 24 | 27 | 49 | 47 | 48 | 6 | 7 | 83 | 10 | 0.89 | 0.89 |
| YM T3-1-2 | 108 | 2 | 16 | 171 | 22 | 208 | 23 | | | | 1 | 12 | | 2 | 5 | 563 | 22 | 34 | 43 | 19 | 34 | 47 | 36 | 57 | 7 | 7 | 88 | 5 | 0.95 | 0.89 |

**Table3**

Table 3. Zircon U-Pb LA-ICPMS data*

| | $Pb^{207}/Pb^{206}$ | | $Pb^{207}/U^{235}$ | | $Pb^{206}/U^{238}$ | | $Pb^{207}/Pb^{206}$ | | $Pb^{207}/U^{235}$ | | $Pb^{206}/U^{238}$ | | Disc. | Best age estimate | |
|---|---|---|---|---|---|---|---|---|---|---|---|---|---|---|---|
| | Ratio | 1σ | Ratio | 1σ | Ratio | 1σ | Age | 1σ | Age | 1σ | Age | 1σ | % | Age(Ma) | 1σ |
| Sample F23 | | | | | | | | | | | | | | | |
| 1 | 0.1747 | 0.0021 | 11.9588 | 0.1430 | 0.4964 | 0.0052 | 2603 | 20 | 2601 | 11 | 2599 | 22 | 0.2 | 2603 | 20 |
| 2 | 0.0676 | 0.0010 | 1.3793 | 0.0200 | 0.1479 | 0.0016 | 858 | 30 | 880 | 9 | 889 | 9 | 3.6 | | |
| 3 | 0.0680 | 0.0010 | 1.3289 | 0.0197 | 0.1418 | 0.0015 | 868 | 31 | 858 | 9 | 855 | 9 | 1.5 | **855** | **9** |
| 4 | 0.0697 | 0.0016 | 1.4184 | 0.0322 | 0.1477 | 0.0017 | 918 | 47 | 897 | 14 | 888 | 10 | 3.4 | | |
| 5 | 0.1110 | 0.0014 | 5.1468 | 0.0633 | 0.3362 | 0.0035 | 1816 | 22 | 1844 | 10 | 1868 | 17 | 2.8 | 1816 | 22 |
| 6 | 0.0687 | 0.0011 | 1.3693 | 0.0212 | 0.1446 | 0.0016 | 889 | 32 | 876 | 9 | 871 | 9 | 2.1 | **871** | **9** |
| 7 | 0.1225 | 0.0017 | 6.1327 | 0.0837 | 0.3631 | 0.0039 | 1993 | 24 | 1995 | 12 | 1997 | 19 | 0.2 | 1993 | 24 |
| 8 | 0.0694 | 0.0010 | 1.4550 | 0.0214 | 0.1520 | 0.0016 | 911 | 30 | 912 | 9 | 912 | 9 | 0.1 | 912 | 9 |
| 9 | 0.0674 | 0.0010 | 1.3556 | 0.0208 | 0.1458 | 0.0016 | 851 | 32 | 870 | 9 | 877 | 9 | 3.0 | 877 | 9 |
| 10 | 0.0697 | 0.0015 | 1.4726 | 0.0321 | 0.1533 | 0.0018 | 918 | 45 | 919 | 13 | 920 | 10 | 0.2 | 920 | 10 |
| 11 | 0.0691 | 0.0016 | 1.3990 | 0.0327 | 0.1468 | 0.0017 | 903 | 48 | 889 | 14 | 883 | 10 | 2.2 | 883 | 10 |
| 12 | 0.0680 | 0.0009 | 1.3527 | 0.0180 | 0.1443 | 0.0015 | 869 | 27 | 869 | 8 | 869 | 9 | 0 | **869** | **9** |
| 13 | 0.0717 | 0.0010 | 1.5399 | 0.0205 | 0.1557 | 0.0016 | 978 | 27 | 947 | 8 | 933 | 9 | 4.7 | | |
| 14 | 0.0683 | 0.0012 | 1.3789 | 0.0232 | 0.1464 | 0.0016 | 879 | 35 | 880 | 10 | 881 | 9 | 0.2 | 881 | 9 |
| 15 | 0.1270 | 0.0017 | 6.9029 | 0.0925 | 0.3943 | 0.0042 | 2057 | 23 | 2099 | 12 | 2143 | 20 | 4.1 | | |
| 16 | 0.1796 | 0.0024 | 12.7856 | 0.1673 | 0.5163 | 0.0056 | 2649 | 22 | 2664 | 12 | 2684 | 24 | 1.3 | 2649 | 22 |
| 17 | 0.0683 | 0.0013 | 1.3726 | 0.0251 | 0.1458 | 0.0016 | 877 | 38 | 877 | 11 | 877 | 9 | 0 | 877 | 9 |
| 18 | 0.0690 | 0.0009 | 1.3639 | 0.0172 | 0.1434 | 0.0015 | 898 | 26 | 874 | 7 | 864 | 8 | 3.9 | | |
| 19 | 0.0688 | 0.0014 | 1.3452 | 0.0272 | 0.1419 | 0.0016 | 892 | 42 | 866 | 12 | 855 | 9 | 4.2 | | |
| 20 | 0.0701 | 0.0010 | 1.4866 | 0.0201 | 0.1538 | 0.0016 | 931 | 27 | 925 | 8 | 922 | 9 | 0.9 | 922 | 9 |
| 21 | 0.0676 | 0.0011 | 1.3185 | 0.0214 | 0.1416 | 0.0015 | 855 | 34 | 854 | 9 | 854 | 9 | 0.2 | **854** | **9** |
| 22 | 0.0723 | 0.0018 | 1.6481 | 0.0412 | 0.1653 | 0.0020 | 995 | 51 | 989 | 16 | 986 | 11 | 0.9 | 986 | 11 |
| 23 | 0.1219 | 0.0015 | 6.1732 | 0.0778 | 0.3672 | 0.0039 | 1984 | 22 | 2001 | 11 | 2016 | 18 | 1.6 | 1984 | 22 |
| 24 | 0.0690 | 0.0009 | 1.4192 | 0.0192 | 0.1492 | 0.0016 | 898 | 28 | 897 | 8 | 897 | 9 | 0.1 | 897 | 9 |
| 25 | 0.0676 | 0.0011 | 1.3131 | 0.0220 | 0.1408 | 0.0015 | 857 | 35 | 852 | 10 | 849 | 9 | 0.9 | **849** | **9** |
| 26 | 0.0696 | 0.0014 | 1.4648 | 0.0284 | 0.1526 | 0.0017 | 917 | 40 | 916 | 12 | 915 | 10 | 0.2 | 915 | 10 |
| 27 | 0.0686 | 0.0011 | 1.3947 | 0.0215 | 0.1475 | 0.0016 | 887 | 32 | 887 | 9 | 887 | 9 | 0 | 887 | 9 |
| 28 | 0.1265 | 0.0016 | 6.5102 | 0.0847 | 0.3734 | 0.0040 | 2049 | 23 | 2047 | 11 | 2045 | 19 | 0.2 | 2049 | 23 |
| 29 | 0.1239 | 0.0016 | 5.9332 | 0.0756 | 0.3474 | 0.0037 | 2013 | 22 | 1966 | 11 | 1922 | 18 | 4.6 | | |
| 30 | 0.1248 | 0.0016 | 6.2883 | 0.0815 | 0.3655 | 0.0039 | 2026 | 23 | 2017 | 11 | 2008 | 18 | 0.9 | 2026 | 23 |
| 31 | 0.0691 | 0.0012 | 1.4347 | 0.0254 | 0.1505 | 0.0017 | 903 | 36 | 904 | 11 | 904 | 9 | 0.1 | 904 | 9 |
| 32 | 0.1274 | 0.0016 | 6.6361 | 0.0858 | 0.3779 | 0.0040 | 2062 | 23 | 2064 | 11 | 2066 | 19 | 0.2 | 2062 | 23 |
| 33 | 0.0705 | 0.0011 | 1.5078 | 0.0223 | 0.1550 | 0.0017 | 944 | 30 | 934 | 9 | 929 | 9 | 1.6 | 929 | 9 |
| 34 | 0.0706 | 0.0015 | 1.4459 | 0.0307 | 0.1485 | 0.0017 | 947 | 44 | 908 | 13 | 892 | 10 | 5.9 | | |
| 35 | 0.0687 | 0.0016 | 1.3731 | 0.0305 | 0.1450 | 0.0017 | 890 | 46 | 878 | 13 | 873 | 9 | 1.9 | 873 | 9 |
| 36 | 0.1097 | 0.0015 | 4.8656 | 0.0656 | 0.3218 | 0.0034 | 1794 | 24 | 1796 | 11 | 1799 | 17 | 0.3 | 1794 | 24 |
| 37 | 0.0692 | 0.0010 | 1.4371 | 0.0202 | 0.1506 | 0.0016 | 905 | 29 | 905 | 8 | 904 | 9 | 0.1 | 904 | 9 |
| 38 | 0.1288 | 0.0019 | 6.7728 | 0.0988 | 0.3814 | 0.0042 | 2082 | 26 | 2082 | 13 | 2083 | 19 | 0.1 | 2082 | 26 |
| 39 | 0.0733 | 0.0028 | 1.7131 | 0.0631 | 0.1695 | 0.0025 | 1022 | 75 | 1013 | 24 | 1009 | 13 | 1.2 | 1022 | 75 |
| 40 | 0.0677 | 0.0011 | 1.3448 | 0.0219 | 0.1440 | 0.0016 | 860 | 34 | 865 | 9 | 868 | 9 | 0.9 | **868** | **9** |
| 41 | 0.1247 | 0.0018 | 6.3380 | 0.0890 | 0.3685 | 0.0040 | 2025 | 25 | 2024 | 12 | 2023 | 19 | 0.1 | 2025 | 25 |
| 42 | 0.1256 | 0.0018 | 6.4518 | 0.0920 | 0.3726 | 0.0040 | 2037 | 25 | 2039 | 13 | 2042 | 19 | 0.2 | 2037 | 25 |
| 43 | 0.0692 | 0.0013 | 1.3666 | 0.0253 | 0.1433 | 0.0016 | 903 | 38 | 875 | 11 | 864 | 9 | 4.5 | | |
| 44 | 0.0721 | 0.0012 | 1.5596 | 0.0252 | 0.1568 | 0.0017 | 990 | 33 | 954 | 10 | 939 | 10 | 5.2 | | |
| 45 | 0.1230 | 0.0017 | 6.1609 | 0.0840 | 0.3632 | 0.0039 | 2000 | 24 | 1999 | 12 | 1997 | 18 | 0.2 | 2000 | 24 |
| 46 | 0.0689 | 0.0011 | 1.4897 | 0.0240 | 0.1567 | 0.0017 | 897 | 33 | 926 | 10 | 939 | 10 | 4.6 | | |
| 47 | 0.0678 | 0.0011 | 1.3443 | 0.0222 | 0.1437 | 0.0016 | 863 | 34 | 865 | 10 | 866 | 9 | 0.3 | **866** | **9** |
| 48 | 0.0700 | 0.0013 | 1.4916 | 0.0282 | 0.1545 | 0.0017 | 929 | 39 | 927 | 11 | 926 | 10 | 0.3 | 926 | 10 |
| 49 | 0.0683 | 0.0017 | 1.3697 | 0.0326 | 0.1455 | 0.0017 | 877 | 49 | 876 | 14 | 876 | 10 | 0.2 | 876 | 10 |

*A total of 19 youngest concordant zircions used to define the maximum depostion age are shown in bold.

Table 3. Zircon U-Pb LA-ICPMS data (continued)

| | $Pb^{207}/Pb^{206}$ | | $Pb^{207}/U^{235}$ | | $Pb^{206}/U^{238}$ | | $Pb^{207}/Pb^{206}$ | | $Pb^{207}/U^{235}$ | | $Pb^{206}/U^{238}$ | | Disc. | Best age estimate | |
|---|---|---|---|---|---|---|---|---|---|---|---|---|---|---|---|
| | Ratio | 1σ | Ratio | 1σ | Ratio | 1σ | Age | 1σ | Age | 1σ | Age | 1σ | % | Age(Ma) | 1σ |
| 50 | 0.0687 | 0.0010 | 1.4077 | 0.0209 | 0.1485 | 0.0016 | 891 | 30 | 892 | 9 | 893 | 9 | 0.2 | 893 | 9 |
| 51 | 0.0712 | 0.0019 | 1.4592 | 0.0380 | 0.1487 | 0.0018 | 963 | 53 | 914 | 16 | 894 | 10 | 7.4 | | |
| 52 | 0.0685 | 0.0012 | 1.3267 | 0.0227 | 0.1405 | 0.0016 | 883 | 35 | 857 | 10 | 848 | 9 | 4.1 | | |
| 53 | 0.0697 | 0.0030 | 1.4771 | 0.0630 | 0.1537 | 0.0023 | 919 | 87 | 921 | 26 | 922 | 13 | 0.3 | 922 | 13 |
| 54 | 0.1659 | 0.0024 | 10.8526 | 0.1550 | 0.4743 | 0.0051 | 2517 | 24 | 2511 | 13 | 2503 | 22 | 0.6 | 2517 | 24 |
| 55 | 0.0687 | 0.0013 | 1.4217 | 0.0261 | 0.1500 | 0.0017 | 890 | 38 | 898 | 11 | 901 | 9 | 1.2 | 901 | 9 |
| 56 | 0.1237 | 0.0018 | 6.2384 | 0.0916 | 0.3657 | 0.0040 | 2010 | 26 | 2010 | 13 | 2009 | 19 | 0 | 2010 | 26 |
| 57 | 0.2149 | 0.0031 | 17.1552 | 0.2512 | 0.5791 | 0.0063 | 2943 | 23 | 2944 | 14 | 2945 | 26 | 0.1 | 2943 | 23 |
| 58 | 0.0703 | 0.0012 | 1.4722 | 0.0241 | 0.1518 | 0.0017 | 938 | 33 | 919 | 10 | 911 | 9 | 2.9 | 911 | 9 |
| 59 | 0.0699 | 0.0012 | 1.4070 | 0.0233 | 0.1459 | 0.0016 | 926 | 34 | 892 | 10 | 878 | 9 | 5.3 | | |
| 60 | 0.0697 | 0.0014 | 1.4298 | 0.0276 | 0.1487 | 0.0017 | 920 | 40 | 902 | 12 | 894 | 9 | 2.9 | 894 | 9 |
| Sample F26 | | | | | | | | | | | | | | | |
| 1 | 0.0713 | 0.0010 | 1.4611 | 0.0203 | 0.1486 | 0.0016 | 966 | 28 | 915 | 8 | 893 | 9 | 7.8 | | |
| 2 | 0.0700 | 0.0010 | 1.3875 | 0.0191 | 0.1439 | 0.0015 | 927 | 28 | 884 | 8 | 867 | 9 | 6.7 | | |
| 3 | 0.0724 | 0.0010 | 1.5491 | 0.0211 | 0.1553 | 0.0016 | 996 | 28 | 950 | 8 | 930 | 9 | 6.8 | | |
| 4 | 0.0708 | 0.0010 | 1.5402 | 0.0218 | 0.1578 | 0.0017 | 951 | 29 | 947 | 9 | 945 | 9 | 0.6 | 945 | 9 |
| 5 | 0.0704 | 0.0011 | 1.5070 | 0.0231 | 0.1553 | 0.0017 | 939 | 31 | 933 | 9 | 931 | 9 | 0.9 | 931 | 9 |
| 6 | 0.0688 | 0.0010 | 1.4104 | 0.0206 | 0.1486 | 0.0016 | 894 | 30 | 893 | 9 | 893 | 9 | 0 | 893 | 9 |
| 7 | 0.0720 | 0.0011 | 1.6095 | 0.0250 | 0.1622 | 0.0017 | 985 | 32 | 974 | 10 | 969 | 10 | 1.6 | **969** | **10** |
| 8 | 0.0712 | 0.0020 | 1.5768 | 0.0428 | 0.1607 | 0.0020 | 963 | 56 | 961 | 17 | 960 | 11 | 0.2 | 960 | 11 |
| 9 | 0.0689 | 0.0018 | 1.4175 | 0.0371 | 0.1492 | 0.0018 | 896 | 54 | 896 | 16 | 896 | 10 | 0 | 896 | 10 |
| 10 | 0.0681 | 0.0012 | 1.3846 | 0.0244 | 0.1476 | 0.0016 | 870 | 37 | 882 | 10 | 887 | 9 | 1.9 | 887 | 9 |
| 11 | 0.0716 | 0.0010 | 1.4686 | 0.0210 | 0.1488 | 0.0016 | 975 | 29 | 918 | 9 | 894 | 9 | 8.6 | | |
| 12 | 0.1492 | 0.0031 | 3.4552 | 0.0696 | 0.1680 | 0.0021 | 2337 | 35 | 1517 | 16 | 1001 | 11 | 80 | | |
| 13 | 0.0689 | 0.0014 | 1.4114 | 0.0288 | 0.1486 | 0.0017 | 895 | 42 | 894 | 12 | 893 | 9 | 0.2 | 893 | 9 |
| 14 | 0.0695 | 0.0010 | 1.3420 | 0.0196 | 0.1401 | 0.0015 | 913 | 30 | 864 | 9 | 845 | 8 | 7.8 | | |
| 15 | 0.0664 | 0.0023 | 1.1731 | 0.0389 | 0.1282 | 0.0017 | 818 | 69 | 788 | 18 | 778 | 10 | 5.0 | | |
| 16 | 0.0693 | 0.0010 | 1.3423 | 0.0189 | 0.1404 | 0.0015 | 908 | 29 | 864 | 8 | 847 | 8 | 6.9 | | |
| 17 | 0.0781 | 0.0020 | 1.6387 | 0.0407 | 0.1521 | 0.0019 | 1151 | 50 | 985 | 16 | 913 | 10 | 23 | | |
| 18 | 0.0691 | 0.0018 | 1.4277 | 0.0354 | 0.1500 | 0.0018 | 900 | 51 | 901 | 15 | 901 | 10 | 0 | 901 | 10 |
| 19 | 0.0696 | 0.0010 | 1.4677 | 0.0216 | 0.1529 | 0.0016 | 917 | 30 | 917 | 9 | 917 | 9 | 0 | 917 | 9 |
| 20 | 0.0712 | 0.0011 | 1.4712 | 0.0229 | 0.1498 | 0.0016 | 964 | 32 | 919 | 9 | 900 | 9 | 6.9 | | |
| 21 | 0.0703 | 0.0011 | 1.5170 | 0.0233 | 0.1566 | 0.0017 | 936 | 31 | 937 | 9 | 938 | 9 | 0.2 | 938 | 9 |
| 22 | 0.0686 | 0.0009 | 1.3949 | 0.0189 | 0.1475 | 0.0016 | 886 | 28 | 887 | 8 | 887 | 9 | 0.1 | 887 | 9 |
| 23 | 0.0689 | 0.0016 | 1.4034 | 0.0322 | 0.1478 | 0.0017 | 895 | 47 | 890 | 14 | 889 | 10 | 0.7 | 889 | 10 |
| 24 | 0.0693 | 0.0013 | 1.4428 | 0.0260 | 0.1510 | 0.0017 | 907 | 37 | 907 | 11 | 907 | 9 | 0 | 907 | 9 |
| 25 | 0.0712 | 0.0011 | 1.5062 | 0.0237 | 0.1535 | 0.0017 | 962 | 32 | 933 | 10 | 921 | 9 | 4 | | |
| 26 | 0.0730 | 0.0016 | 1.5189 | 0.0325 | 0.1509 | 0.0017 | 1015 | 43 | 938 | 13 | 906 | 10 | 11 | | |
| 27 | 0.0696 | 0.0012 | 1.4573 | 0.0254 | 0.1518 | 0.0017 | 917 | 36 | 913 | 11 | 911 | 9 | 0.6 | 911 | 9 |
| 28 | 0.0718 | 0.0013 | 1.5011 | 0.0262 | 0.1517 | 0.0017 | 980 | 36 | 931 | 11 | 910 | 9 | 7.3 | | |
| 29 | 0.0702 | 0.0011 | 1.5093 | 0.0237 | 0.1559 | 0.0017 | 935 | 32 | 934 | 10 | 934 | 9 | 0.1 | 934 | 9 |
| 30 | 0.0733 | 0.0033 | 1.7038 | 0.0739 | 0.1687 | 0.0027 | 1021 | 88 | 1010 | 28 | 1005 | 15 | 1.6 | 1005 | 15 |
| 31 | 0.0687 | 0.0011 | 1.4049 | 0.0223 | 0.1482 | 0.0016 | 891 | 33 | 891 | 9 | 891 | 9 | 0 | 891 | 9 |
| 32 | 0.0697 | 0.0011 | 1.4450 | 0.0231 | 0.1503 | 0.0016 | 920 | 33 | 908 | 10 | 903 | 9 | 1.9 | 903 | 9 |
| 33 | 0.0702 | 0.0011 | 1.5067 | 0.0239 | 0.1558 | 0.0017 | 933 | 33 | 933 | 10 | 933 | 9 | 0.1 | 933 | 9 |
| 34 | 0.0683 | 0.0010 | 1.3717 | 0.0197 | 0.1456 | 0.0016 | 878 | 30 | 877 | 8 | 877 | 9 | 0.2 | 877 | 9 |
| 35 | 0.0703 | 0.0011 | 1.4870 | 0.0235 | 0.1535 | 0.0017 | 937 | 32 | 925 | 10 | 920 | 9 | 1.8 | 920 | 9 |
| 36 | 0.0727 | 0.0012 | 1.5204 | 0.0242 | 0.1516 | 0.0016 | 1006 | 32 | 939 | 10 | 910 | 9 | 10 | | |
| 37 | 0.0712 | 0.0014 | 1.4255 | 0.0273 | 0.1452 | 0.0016 | 964 | 39 | 900 | 11 | 874 | 9 | 9.8 | | |
| 38 | 0.0725 | 0.0013 | 1.3722 | 0.0234 | 0.1373 | 0.0015 | 999 | 35 | 877 | 10 | 830 | 9 | 19 | | |

Table 3. Zircon U-Pb LA-ICPMS data (continued)

| | $Pb^{207}/Pb^{206}$ | | $Pb^{207}/U^{235}$ | | $Pb^{206}/U^{238}$ | | $Pb^{207}/Pb^{206}$ | | $Pb^{207}/U^{235}$ | | $Pb^{206}/U^{238}$ | | Disc. | Best age estimate | |
|---|---|---|---|---|---|---|---|---|---|---|---|---|---|---|---|
| | Ratio | 1σ | Ratio | 1σ | Ratio | 1σ | Age | 1σ | Age | 1σ | Age | 1σ | % | Age(Ma) | 1σ |
| 39 | 0.0716 | 0.0025 | 1.5722 | 0.0543 | 0.1592 | 0.0022 | 976 | 71 | 959 | 21 | 952 | 12 | 2.4 | 952 | 12 |
| 40 | 0.0706 | 0.0011 | 1.5263 | 0.0241 | 0.1567 | 0.0017 | 947 | 32 | 941 | 10 | 939 | 9 | 0.8 | 939 | 9 |
| 41 | 0.0705 | 0.0017 | 1.5075 | 0.0348 | 0.1551 | 0.0018 | 943 | 47 | 933 | 14 | 929 | 10 | 1.5 | 929 | 10 |
| 42 | 0.0702 | 0.0012 | 1.4962 | 0.0255 | 0.1547 | 0.0017 | 933 | 35 | 929 | 10 | 927 | 9 | 0.6 | 927 | 9 |
| 43 | 0.0699 | 0.0018 | 1.4769 | 0.0365 | 0.1534 | 0.0018 | 924 | 51 | 921 | 15 | 920 | 10 | 0.4 | 920 | 10 |
| 44 | 0.0699 | 0.0012 | 1.4815 | 0.0248 | 0.1538 | 0.0017 | 924 | 34 | 923 | 10 | 922 | 9 | 0.2 | 922 | 9 |
| 45 | 0.0698 | 0.0015 | 1.4757 | 0.0305 | 0.1533 | 0.0018 | 924 | 43 | 920 | 12 | 919 | 10 | 0.5 | 919 | 10 |
| 46 | 0.0700 | 0.0013 | 1.4972 | 0.0265 | 0.1550 | 0.0017 | 930 | 36 | 929 | 11 | 929 | 10 | 0.1 | 929 | 10 |
| 47 | 0.0683 | 0.0019 | 1.3724 | 0.0373 | 0.1457 | 0.0018 | 878 | 56 | 877 | 16 | 877 | 10 | 0.1 | 877 | 10 |
| 48 | 0.0683 | 0.0015 | 1.3725 | 0.0298 | 0.1457 | 0.0017 | 879 | 45 | 877 | 13 | 877 | 9 | 0.2 | 877 | 9 |
| 49 | 0.0709 | 0.0018 | 1.5599 | 0.0378 | 0.1596 | 0.0019 | 955 | 50 | 954 | 15 | 954 | 11 | 0.1 | 954 | 11 |
| 50 | 0.0693 | 0.0012 | 1.3932 | 0.0229 | 0.1459 | 0.0016 | 907 | 34 | 886 | 10 | 878 | 9 | 3.2 | | |
| 51 | 0.0686 | 0.0014 | 1.3947 | 0.0284 | 0.1474 | 0.0017 | 887 | 42 | 887 | 12 | 886 | 9 | 0.1 | 886 | 9 |
| 52 | 0.0689 | 0.0012 | 1.4111 | 0.0246 | 0.1486 | 0.0016 | 895 | 36 | 894 | 10 | 893 | 9 | 0.2 | 893 | 9 |
| 53 | 0.0678 | 0.0015 | 1.3268 | 0.0295 | 0.1420 | 0.0017 | 861 | 46 | 858 | 13 | 856 | 9 | 0.6 | 856 | 9 |
| 54 | 0.0685 | 0.0013 | 1.3894 | 0.0255 | 0.1470 | 0.0016 | 885 | 38 | 884 | 11 | 884 | 9 | 0 | 884 | 9 |
| 55 | 0.0702 | 0.0013 | 1.4982 | 0.0264 | 0.1548 | 0.0017 | 934 | 36 | 930 | 11 | 928 | 10 | 0.6 | 928 | 10 |
| 56 | 0.0699 | 0.0012 | 1.5011 | 0.0244 | 0.1557 | 0.0017 | 926 | 33 | 931 | 10 | 933 | 9 | 0.8 | 933 | 9 |
| 57 | 0.0691 | 0.0023 | 1.4252 | 0.0454 | 0.1496 | 0.0020 | 902 | 66 | 900 | 19 | 899 | 11 | 0.3 | 899 | 11 |
| 58 | 0.0687 | 0.0012 | 1.3986 | 0.0244 | 0.1476 | 0.0016 | 890 | 36 | 888 | 10 | 888 | 9 | 0.3 | 888 | 9 |
| 59 | 0.0696 | 0.0012 | 1.4631 | 0.0247 | 0.1525 | 0.0017 | 916 | 35 | 915 | 10 | 915 | 9 | 0 | 915 | 9 |
| 60 | 0.0699 | 0.0012 | 1.4857 | 0.0253 | 0.1542 | 0.0017 | 925 | 35 | 925 | 10 | 925 | 9 | 0 | 925 | 9 |
| Sample F4 | | | | | | | | | | | | | | | |
| 1 | 0.1817 | 0.0022 | 12.7955 | 0.1577 | 0.5107 | 0.0055 | 2669 | 20 | 2665 | 12 | 2660 | 23 | 0.3 | 2669 | 20 |
| 2 | 0.0682 | 0.0010 | 1.3674 | 0.0204 | 0.1454 | 0.0016 | 874 | 30 | 875 | 9 | 875 | 9 | 0.1 | 875 | 9 |
| 3 | 0.1707 | 0.0020 | 8.4354 | 0.1027 | 0.3584 | 0.0038 | 2565 | 20 | 2279 | 11 | 1975 | 18 | 26 | | |
| 4 | 0.0690 | 0.0014 | 1.4184 | 0.0290 | 0.1490 | 0.0017 | 900 | 42 | 897 | 12 | 895 | 10 | 0.5 | 895 | 10 |
| 5 | 0.0703 | 0.0013 | 1.5193 | 0.0270 | 0.1568 | 0.0018 | 937 | 36 | 938 | 11 | 939 | 10 | 0.3 | 939 | 10 |
| 6 | 0.0696 | 0.0010 | 1.4647 | 0.0217 | 0.1526 | 0.0017 | 917 | 30 | 916 | 9 | 916 | 9 | 0.1 | 916 | 9 |
| 7 | 0.0690 | 0.0011 | 1.4226 | 0.0219 | 0.1496 | 0.0016 | 898 | 31 | 898 | 9 | 899 | 9 | 0.1 | 899 | 9 |
| 8 | 0.1196 | 0.0015 | 2.3069 | 0.0286 | 0.1400 | 0.0015 | 1949 | 22 | 1214 | 9 | 844 | 8 | 79 | | |
| 9 | 0.1737 | 0.0021 | 10.7804 | 0.1330 | 0.4500 | 0.0048 | 2594 | 20 | 2504 | 11 | 2395 | 21 | 8.0 | | |
| 10 | 0.0702 | 0.0019 | 1.5102 | 0.0391 | 0.1559 | 0.0019 | 935 | 53 | 935 | 16 | 934 | 11 | 0.1 | 934 | 11 |
| 11 | 0.0683 | 0.0009 | 1.3712 | 0.0185 | 0.1457 | 0.0016 | 877 | 27 | 877 | 8 | 877 | 9 | 0 | 877 | 9 |
| 12 | 0.0713 | 0.0012 | 1.5836 | 0.0272 | 0.1611 | 0.0018 | 965 | 35 | 964 | 11 | 963 | 10 | 0.2 | 963 | 10 |
| 13 | 0.0680 | 0.0009 | 1.3502 | 0.0186 | 0.1441 | 0.0016 | 867 | 28 | 868 | 8 | 868 | 9 | 0.1 | 868 | 9 |
| 14 | 0.0700 | 0.0010 | 1.4886 | 0.0219 | 0.1543 | 0.0017 | 927 | 30 | 926 | 9 | 925 | 9 | 0.2 | 925 | 9 |
| 15 | 0.0699 | 0.0010 | 1.4880 | 0.0217 | 0.1545 | 0.0017 | 924 | 29 | 926 | 9 | 926 | 9 | 0.2 | 926 | 9 |
| 16 | 0.0689 | 0.0009 | 1.4145 | 0.0194 | 0.1490 | 0.0016 | 894 | 28 | 895 | 8 | 895 | 9 | 0.1 | 895 | 9 |
| 17 | 0.0695 | 0.0011 | 1.4606 | 0.0231 | 0.1524 | 0.0017 | 913 | 32 | 914 | 10 | 915 | 9 | 0.1 | 915 | 9 |
| 18 | 0.0690 | 0.0011 | 1.4214 | 0.0219 | 0.1493 | 0.0016 | 900 | 31 | 898 | 9 | 897 | 9 | 0.3 | 897 | 9 |
| 19 | 0.0690 | 0.0011 | 1.4190 | 0.0222 | 0.1492 | 0.0017 | 898 | 32 | 897 | 9 | 897 | 9 | 0.2 | 897 | 9 |
| 20 | 0.0694 | 0.0008 | 1.2403 | 0.0139 | 0.1296 | 0.0014 | 911 | 22 | 819 | 6 | 785 | 8 | 15 | | |
| 21 | 0.1626 | 0.0021 | 7.9200 | 0.1046 | 0.3533 | 0.0038 | 2483 | 22 | 2222 | 12 | 1950 | 18 | 24 | | |
| 22 | 0.1580 | 0.0020 | 7.8123 | 0.1003 | 0.3586 | 0.0039 | 2434 | 21 | 2210 | 12 | 1976 | 18 | 21 | | |
| 23 | 0.1380 | 0.0018 | 7.7464 | 0.1048 | 0.4070 | 0.0045 | 2203 | 23 | 2202 | 12 | 2201 | 20 | 0.1 | 2203 | 23 |
| 24 | 0.0695 | 0.0012 | 1.4544 | 0.0247 | 0.1517 | 0.0017 | 914 | 35 | 912 | 10 | 911 | 10 | 0.4 | 911 | 10 |
| 25 | 0.0700 | 0.0016 | 1.5050 | 0.0329 | 0.1558 | 0.0019 | 930 | 45 | 932 | 13 | 934 | 10 | 0.4 | 934 | 10 |
| 26 | 0.0674 | 0.0011 | 1.3110 | 0.0209 | 0.1410 | 0.0016 | 851 | 33 | 851 | 9 | 850 | 9 | 0.1 | **850** | **9** |
| 27 | 0.0689 | 0.0011 | 1.4126 | 0.0223 | 0.1487 | 0.0017 | 895 | 32 | 894 | 9 | 894 | 9 | 0.1 | 894 | 9 |

Table 3. Zircon U-Pb LA-ICPMS data (continued)

| | $Pb^{207}/Pb^{206}$ | | $Pb^{207}/U^{235}$ | | $Pb^{206}/U^{238}$ | | $Pb^{207}/Pb^{206}$ | | $Pb^{207}/U^{235}$ | | $Pb^{206}/U^{238}$ | | Disc. | Best age estimate | |
|---|---|---|---|---|---|---|---|---|---|---|---|---|---|---|---|
| | Ratio | 1σ | Ratio | 1σ | Ratio | 1σ | Age | 1σ | Age | 1σ | Age | 1σ | % | Age(Ma) | 1σ |
| 28 | 0.0690 | 0.0010 | 1.4247 | 0.0204 | 0.1498 | 0.0016 | 898 | 29 | 899 | 9 | 900 | 9 | 0.2 | 900 | 9 |
| 29 | 0.0674 | 0.0009 | 1.3115 | 0.0178 | 0.1411 | 0.0015 | 850 | 27 | 851 | 8 | 851 | 9 | 0 | **851** | **9** |
| 30 | 0.0713 | 0.0013 | 1.5832 | 0.0295 | 0.1610 | 0.0019 | 966 | 38 | 964 | 12 | 963 | 10 | 0.3 | 963 | 10 |
| 31 | 0.0694 | 0.0020 | 1.4406 | 0.0410 | 0.1506 | 0.0019 | 909 | 59 | 906 | 17 | 905 | 11 | 0.5 | 905 | 11 |
| 32 | 0.0684 | 0.0009 | 1.3797 | 0.0194 | 0.1463 | 0.0016 | 880 | 28 | 880 | 8 | 880 | 9 | 0 | 880 | 9 |
| 33 | 0.0681 | 0.0009 | 1.3574 | 0.0191 | 0.1447 | 0.0016 | 870 | 28 | 871 | 8 | 871 | 9 | 0.1 | **871** | **9** |
| 34 | 0.0691 | 0.0010 | 1.4249 | 0.0202 | 0.1496 | 0.0016 | 900 | 29 | 899 | 8 | 899 | 9 | 0.2 | 899 | 9 |
| 35 | 0.1830 | 0.0025 | 13.0071 | 0.1780 | 0.5154 | 0.0056 | 2680 | 22 | 2680 | 13 | 2680 | 24 | 0 | 2680 | 24 |
| 36 | 0.0697 | 0.0010 | 1.4692 | 0.0219 | 0.1529 | 0.0017 | 919 | 30 | 918 | 9 | 917 | 9 | 0.1 | 917 | 9 |
| 37 | 0.0698 | 0.0014 | 1.4828 | 0.0300 | 0.1541 | 0.0018 | 923 | 41 | 923 | 12 | 924 | 10 | 0.1 | 924 | 10 |
| 38 | 0.0699 | 0.0011 | 1.4789 | 0.0242 | 0.1535 | 0.0017 | 925 | 33 | 922 | 10 | 921 | 10 | 0.4 | 921 | 10 |
| 39 | 0.0695 | 0.0016 | 1.4546 | 0.0331 | 0.1519 | 0.0018 | 912 | 47 | 912 | 14 | 911 | 10 | 0.1 | 911 | 10 |
| 40 | 0.0676 | 0.0011 | 1.3163 | 0.0223 | 0.1413 | 0.0016 | 855 | 35 | 853 | 10 | 852 | 9 | 0.3 | 852 | 9 |
| 41 | 0.0697 | 0.0011 | 1.4749 | 0.0236 | 0.1534 | 0.0017 | 921 | 32 | 920 | 10 | 920 | 10 | 0.1 | 920 | 10 |
| 42 | 0.0708 | 0.0011 | 1.5573 | 0.0242 | 0.1595 | 0.0018 | 952 | 31 | 953 | 10 | 954 | 10 | 0.2 | 954 | 10 |
| 43 | 0.0705 | 0.0015 | 1.5334 | 0.0315 | 0.1577 | 0.0019 | 944 | 42 | 944 | 13 | 944 | 10 | 0 | 944 | 10 |
| 44 | 0.0685 | 0.0016 | 1.3877 | 0.0327 | 0.1469 | 0.0018 | 883 | 48 | 884 | 14 | 884 | 10 | 0 | 884 | 10 |
| 45 | 0.0682 | 0.0010 | 1.5182 | 0.0222 | 0.1613 | 0.0018 | 876 | 29 | 938 | 9 | 964 | 10 | 9.6 | | |
| 46 | 0.0850 | 0.0019 | 2.0445 | 0.0460 | 0.1744 | 0.0021 | 1316 | 44 | 1131 | 15 | 1036 | 12 | 24 | | |
| 47 | 0.0699 | 0.0011 | 1.4864 | 0.0236 | 0.1542 | 0.0017 | 926 | 32 | 925 | 10 | 924 | 10 | 0.2 | 924 | 10 |
| 48 | 0.0667 | 0.0011 | 1.0473 | 0.0172 | 0.1139 | 0.0013 | 827 | 34 | 728 | 9 | 696 | 7 | 17 | | |
| 49 | 0.0696 | 0.0011 | 1.4653 | 0.0236 | 0.1527 | 0.0017 | 916 | 32 | 916 | 10 | 916 | 10 | 0 | 916 | 10 |
| 50 | 0.0725 | 0.0012 | 1.6761 | 0.0284 | 0.1677 | 0.0019 | 999 | 34 | 1000 | 11 | 1000 | 11 | 0.1 | 1000 | 11 |
| 51 | 0.1884 | 0.0028 | 9.3023 | 0.1394 | 0.3581 | 0.0040 | 2728 | 24 | 2368 | 14 | 1973 | 19 | 32 | | |
| 52 | 0.0689 | 0.0012 | 1.4161 | 0.0246 | 0.1490 | 0.0017 | 896 | 35 | 896 | 10 | 896 | 10 | 0 | 896 | 10 |
| 53 | 0.1401 | 0.0021 | 7.5719 | 0.1155 | 0.3918 | 0.0044 | 2229 | 26 | 2182 | 14 | 2131 | 20 | 4.5 | | |
| 54 | 0.0696 | 0.0012 | 1.4702 | 0.0252 | 0.1531 | 0.0017 | 918 | 35 | 918 | 10 | 918 | 10 | 0.1 | 918 | 10 |
| 55 | 0.0675 | 0.0011 | 1.3140 | 0.0210 | 0.1413 | 0.0016 | 852 | 32 | 852 | 9 | 852 | 9 | 0 | **852** | **9** |
| 56 | 0.0698 | 0.0012 | 1.4766 | 0.0250 | 0.1535 | 0.0017 | 922 | 34 | 921 | 10 | 920 | 10 | 0.2 | 920 | 10 |
| 57 | 0.0687 | 0.0012 | 1.4093 | 0.0246 | 0.1487 | 0.0017 | 890 | 35 | 893 | 10 | 894 | 10 | 0.4 | 894 | 10 |
| 58 | 0.0672 | 0.0011 | 1.4552 | 0.0233 | 0.1571 | 0.0018 | 843 | 32 | 912 | 10 | 941 | 10 | 11 | | |
| 59 | 0.0701 | 0.0013 | 1.4986 | 0.0283 | 0.1551 | 0.0018 | 931 | 38 | 930 | 11 | 929 | 10 | 0.2 | 929 | 10 |
| 60 | 0.0696 | 0.0013 | 1.4711 | 0.0268 | 0.1532 | 0.0018 | 918 | 37 | 919 | 11 | 919 | 10 | 0.1 | 919 | 10 |
| Sample F3 | | | | | | | | | | | | | | | |
| 1 | 0.0695 | 0.0010 | 1.4595 | 0.0206 | 0.1524 | 0.0016 | 913 | 29 | 914 | 9 | 914 | 9 | 0.2 | 914 | 9 |
| 2 | 0.0707 | 0.0010 | 1.5490 | 0.0219 | 0.1588 | 0.0017 | 950 | 29 | 950 | 9 | 950 | 9 | 0 | 950 | 9 |
| 3 | 0.0692 | 0.0009 | 1.5022 | 0.0184 | 0.1574 | 0.0016 | 906 | 25 | 931 | 7 | 942 | 9 | 4.0 | 942 | 9 |
| 4 | 0.0680 | 0.0012 | 1.3491 | 0.0227 | 0.1439 | 0.0016 | 868 | 35 | 867 | 10 | 867 | 9 | 0.2 | **867** | **9** |
| 5 | 0.0696 | 0.0009 | 1.4639 | 0.0196 | 0.1526 | 0.0016 | 916 | 28 | 916 | 8 | 915 | 9 | 0.1 | 915 | 9 |
| 6 | 0.0711 | 0.0012 | 1.5710 | 0.0263 | 0.1602 | 0.0017 | 961 | 34 | 959 | 10 | 958 | 10 | 0.3 | 958 | 10 |
| 7 | 0.0686 | 0.0011 | 1.3903 | 0.0219 | 0.1471 | 0.0016 | 885 | 33 | 885 | 9 | 885 | 9 | 0 | 885 | 9 |
| 8 | 0.0691 | 0.0010 | 1.4291 | 0.0198 | 0.1499 | 0.0016 | 903 | 28 | 901 | 8 | 901 | 9 | 0.2 | 901 | 9 |
| 9 | 0.0724 | 0.0010 | 1.6640 | 0.0232 | 0.1668 | 0.0018 | 996 | 28 | 995 | 9 | 995 | 10 | 0.1 | 995 | 10 |
| 10 | 0.0685 | 0.0009 | 1.3850 | 0.0181 | 0.1467 | 0.0015 | 883 | 27 | 883 | 8 | 883 | 9 | 0 | 883 | 9 |
| 11 | 0.0682 | 0.0012 | 1.3712 | 0.0237 | 0.1457 | 0.0016 | 876 | 36 | 877 | 10 | 877 | 9 | 0.1 | 877 | 9 |
| 12 | 0.0697 | 0.0009 | 1.4707 | 0.0194 | 0.1531 | 0.0016 | 919 | 27 | 918 | 8 | 918 | 9 | 0.1 | 918 | 9 |
| 13 | 0.0692 | 0.0012 | 1.4355 | 0.0247 | 0.1505 | 0.0016 | 904 | 36 | 904 | 10 | 904 | 9 | 0 | 904 | 9 |
| 14 | 0.0688 | 0.0013 | 1.4070 | 0.0257 | 0.1482 | 0.0016 | 894 | 38 | 892 | 11 | 891 | 9 | 0.3 | 891 | 9 |
| 15 | 0.0806 | 0.0010 | 1.6356 | 0.0207 | 0.1472 | 0.0015 | 1211 | 25 | 984 | 8 | 885 | 9 | 31 | | |
| 16 | 0.0691 | 0.0013 | 1.3720 | 0.0245 | 0.1441 | 0.0016 | 901 | 37 | 877 | 11 | 868 | 9 | 3.8 | **868** | **9** |
| 17 | 0.0918 | 0.0012 | 1.3533 | 0.0172 | 0.1069 | 0.0011 | 1464 | 24 | 869 | 7 | 655 | 6 | 76 | | |

Table 3. Zircon U-Pb LA-ICPMS data (continued)

| | $Pb^{207}/Pb^{206}$ Ratio | $1\sigma$ | $Pb^{207}/U^{235}$ Ratio | $1\sigma$ | $Pb^{206}/U^{238}$ Ratio | $1\sigma$ | $Pb^{207}/Pb^{206}$ Age | $1\sigma$ | $Pb^{207}/U^{235}$ Age | $1\sigma$ | $Pb^{206}/U^{238}$ Age | $1\sigma$ | Disc. % | Best age estimate Age(Ma) | $1\sigma$ |
|---|---|---|---|---|---|---|---|---|---|---|---|---|---|---|---|
| 18 | 0.0695 | 0.0009 | 1.4625 | 0.0191 | 0.1526 | 0.0016 | 913 | 27 | 915 | 8 | 916 | 9 | 0.3 | 916 | 9 |
| 19 | 0.0688 | 0.0011 | 1.4038 | 0.0214 | 0.1480 | 0.0016 | 892 | 31 | 891 | 9 | 890 | 9 | 0.3 | 890 | 9 |
| 20 | 0.0698 | 0.0009 | 1.4841 | 0.0188 | 0.1541 | 0.0016 | 924 | 26 | 924 | 8 | 924 | 9 | 0 | 924 | 9 |
| 21 | 0.0828 | 0.0014 | 1.6643 | 0.0273 | 0.1457 | 0.0016 | 1266 | 32 | 995 | 10 | 877 | 9 | 36 | | |
| 22 | 0.0714 | 0.0011 | 1.5864 | 0.0243 | 0.1611 | 0.0017 | 969 | 31 | 965 | 10 | 963 | 10 | 0.6 | 963 | 10 |
| 23 | 0.0850 | 0.0015 | 1.8289 | 0.0322 | 0.1560 | 0.0017 | 1316 | 34 | 1056 | 12 | 934 | 10 | 34 | | |
| 24 | 0.0685 | 0.0011 | 1.3891 | 0.0212 | 0.1470 | 0.0016 | 885 | 31 | 884 | 9 | 884 | 9 | 0.1 | 884 | 9 |
| 25 | 0.0688 | 0.0009 | 1.4106 | 0.0186 | 0.1488 | 0.0016 | 892 | 27 | 893 | 8 | 894 | 9 | 0.2 | 894 | 9 |
| 26 | 0.1196 | 0.0019 | 5.7505 | 0.0903 | 0.3486 | 0.0038 | 1951 | 28 | 1939 | 14 | 1928 | 18 | 1.2 | 1951 | 28 |
| 27 | 0.0690 | 0.0010 | 1.4279 | 0.0207 | 0.1500 | 0.0016 | 900 | 30 | 901 | 9 | 901 | 9 | 0.1 | 901 | 9 |
| 28 | 0.0694 | 0.0010 | 1.4474 | 0.0214 | 0.1514 | 0.0016 | 909 | 30 | 909 | 9 | 909 | 9 | 0.1 | 909 | 9 |
| 29 | 0.0733 | 0.0010 | 1.6188 | 0.0218 | 0.1602 | 0.0017 | 1022 | 27 | 978 | 8 | 958 | 9 | 6.5 | | |
| 30 | 0.0702 | 0.0012 | 1.5064 | 0.0243 | 0.1556 | 0.0017 | 935 | 33 | 933 | 10 | 932 | 9 | 0.3 | 932 | 9 |
| 31 | 0.0699 | 0.0013 | 1.4860 | 0.0274 | 0.1542 | 0.0017 | 926 | 38 | 925 | 11 | 924 | 9 | 0.1 | 924 | 9 |
| 32 | 0.0698 | 0.0010 | 1.4762 | 0.0209 | 0.1535 | 0.0016 | 921 | 29 | 921 | 9 | 921 | 9 | 0.1 | 921 | 9 |
| 33 | 0.0760 | 0.0010 | 1.5237 | 0.0201 | 0.1454 | 0.0015 | 1096 | 26 | 940 | 8 | 875 | 9 | 22 | | |
| 34 | 0.0706 | 0.0009 | 1.5371 | 0.0204 | 0.1579 | 0.0017 | 946 | 27 | 945 | 8 | 945 | 9 | 0.1 | 945 | 9 |
| 35 | 0.0722 | 0.0011 | 1.6521 | 0.0240 | 0.1660 | 0.0018 | 991 | 29 | 990 | 9 | 990 | 10 | 0 | 990 | 10 |
| 36 | 0.0706 | 0.0012 | 1.5393 | 0.0255 | 0.1581 | 0.0017 | 947 | 34 | 946 | 10 | 946 | 10 | 0.1 | 946 | 10 |
| 37 | 0.0699 | 0.0010 | 1.4841 | 0.0217 | 0.1540 | 0.0016 | 925 | 30 | 924 | 9 | 924 | 9 | 0.1 | 924 | 9 |
| 38 | 0.0775 | 0.0015 | 1.5968 | 0.0297 | 0.1495 | 0.0017 | 1133 | 37 | 969 | 12 | 898 | 9 | 23 | | |
| 39 | 0.0695 | 0.0010 | 1.4613 | 0.0202 | 0.1525 | 0.0016 | 914 | 28 | 915 | 8 | 915 | 9 | 0.1 | 915 | 9 |
| 40 | 0.0724 | 0.0011 | 1.4769 | 0.0217 | 0.1480 | 0.0016 | 997 | 30 | 921 | 9 | 890 | 9 | 11.4 | | |
| 41 | 0.0687 | 0.0010 | 1.3970 | 0.0204 | 0.1476 | 0.0016 | 889 | 30 | 888 | 9 | 887 | 9 | 0.1 | 887 | 9 |
| 42 | 0.0747 | 0.0012 | 1.5199 | 0.0250 | 0.1476 | 0.0016 | 1060 | 33 | 938 | 10 | 888 | 9 | 18 | | |
| 43 | 0.0695 | 0.0011 | 1.4589 | 0.0226 | 0.1523 | 0.0016 | 914 | 32 | 914 | 9 | 914 | 9 | 0 | 914 | 9 |
| 44 | 0.0712 | 0.0013 | 1.5834 | 0.0277 | 0.1613 | 0.0018 | 964 | 36 | 964 | 11 | 964 | 10 | 0 | **964** | **10** |
| 45 | 0.0680 | 0.0012 | 1.3501 | 0.0239 | 0.1440 | 0.0016 | 868 | 37 | 868 | 10 | 868 | 9 | 0 | **868** | **9** |
| 46 | 0.0693 | 0.0011 | 1.4420 | 0.0222 | 0.1510 | 0.0016 | 907 | 32 | 907 | 9 | 906 | 9 | 0.1 | 906 | 9 |
| 47 | 0.0699 | 0.0011 | 1.4924 | 0.0229 | 0.1548 | 0.0017 | 926 | 31 | 927 | 9 | 928 | 9 | 0.2 | 928 | 9 |
| 48 | 0.0706 | 0.0010 | 1.4622 | 0.0212 | 0.1502 | 0.0016 | 946 | 30 | 915 | 9 | 902 | 9 | 4.8 | 902 | 9 |
| 49 | 0.0700 | 0.0012 | 1.4973 | 0.0243 | 0.1550 | 0.0017 | 930 | 33 | 929 | 10 | 929 | 9 | 0 | 929 | 9 |
| 50 | 0.0834 | 0.0013 | 1.3573 | 0.0209 | 0.1181 | 0.0013 | 1277 | 30 | 871 | 9 | 720 | 7 | 56 | | |
| 51 | 0.0709 | 0.0017 | 1.5551 | 0.0359 | 0.1592 | 0.0019 | 953 | 47 | 953 | 14 | 952 | 10 | 0.1 | 952 | 10 |
| 52 | 0.0691 | 0.0012 | 1.4347 | 0.0251 | 0.1505 | 0.0016 | 903 | 36 | 904 | 10 | 904 | 9 | 0.1 | 904 | 9 |
| 53 | 0.0700 | 0.0012 | 1.4975 | 0.0262 | 0.1551 | 0.0017 | 928 | 36 | 929 | 11 | 930 | 9 | 0.1 | 930 | 9 |
| 54 | 0.0740 | 0.0011 | 1.5527 | 0.0232 | 0.1522 | 0.0016 | 1041 | 30 | 952 | 9 | 913 | 9 | 13 | | |
| 55 | 0.0712 | 0.0013 | 1.4545 | 0.0253 | 0.1482 | 0.0016 | 963 | 35 | 912 | 10 | 891 | 9 | 7.8 | | |
| 56 | 0.0701 | 0.0011 | 1.5066 | 0.0242 | 0.1558 | 0.0017 | 932 | 33 | 933 | 10 | 934 | 9 | 0.2 | 934 | 9 |
| 57 | 0.0786 | 0.0013 | 1.5576 | 0.0252 | 0.1437 | 0.0016 | 1162 | 32 | 954 | 10 | 866 | 9 | 29 | | |
| 58 | 0.0710 | 0.0018 | 1.5655 | 0.0384 | 0.1600 | 0.0019 | 957 | 50 | 957 | 15 | 957 | 11 | 0 | 957 | 11 |
| Sample F38 | | | | | | | | | | | | | | | |
| 1 | 0.0691 | 0.0008 | 1.4284 | 0.0169 | 0.1500 | 0.0015 | 901 | 24 | 901 | 7 | 901 | 9 | 0 | 901 | 9 |
| 2 | 0.0719 | 0.0026 | 1.4467 | 0.0503 | 0.1460 | 0.0020 | 983 | 71 | 909 | 21 | 878 | 11 | 12 | | |
| 3 | 0.0689 | 0.0009 | 1.3850 | 0.0175 | 0.1459 | 0.0015 | 895 | 26 | 883 | 7 | 878 | 8 | 1.9 | 878 | 8 |
| 4 | 0.0692 | 0.0011 | 1.4367 | 0.0226 | 0.1506 | 0.0016 | 905 | 33 | 904 | 9 | 904 | 9 | 0.1 | 904 | 9 |
| 5 | 0.0688 | 0.0011 | 1.4100 | 0.0222 | 0.1487 | 0.0016 | 893 | 33 | 893 | 9 | 893 | 9 | 0.1 | 893 | 9 |
| 6 | 0.0688 | 0.0008 | 1.4194 | 0.0156 | 0.1497 | 0.0015 | 892 | 23 | 897 | 7 | 899 | 9 | 0.8 | 899 | 9 |
| 7 | 0.0688 | 0.0009 | 1.4073 | 0.0184 | 0.1484 | 0.0015 | 892 | 27 | 892 | 8 | 892 | 9 | 0.1 | 892 | 9 |
| 8 | 0.0697 | 0.0009 | 1.4699 | 0.0188 | 0.1531 | 0.0016 | 918 | 26 | 918 | 8 | 918 | 9 | 0 | 918 | 9 |
| 9 | 0.0685 | 0.0008 | 1.3890 | 0.0161 | 0.1471 | 0.0015 | 884 | 24 | 884 | 7 | 885 | 8 | 0.1 | 885 | 8 |

Table 3. Zircon U-Pb LA-ICPMS data (continued)

| | $Pb^{207}/Pb^{206}$ | | $Pb^{207}/U^{235}$ | | $Pb^{206}/U^{238}$ | | $Pb^{207}/Pb^{206}$ | | $Pb^{207}/U^{235}$ | | $Pb^{206}/U^{238}$ | | Disc. | Best age estimate | |
|---|---|---|---|---|---|---|---|---|---|---|---|---|---|---|---|
| | Ratio | 1σ | Ratio | 1σ | Ratio | 1σ | Age | 1σ | Age | 1σ | Age | 1σ | % | Age(Ma) | 1σ |
| 10 | 0.0729 | 0.0035 | 1.6331 | 0.0753 | 0.1625 | 0.0027 | 1011 | 93 | 983 | 29 | 971 | 15 | 4.2 | | |
| 11 | 0.0704 | 0.0014 | 1.5216 | 0.0301 | 0.1568 | 0.0017 | 939 | 41 | 939 | 12 | 939 | 10 | 0 | 939 | 10 |
| 12 | 0.0687 | 0.0014 | 1.4061 | 0.0276 | 0.1484 | 0.0016 | 891 | 41 | 892 | 12 | 892 | 9 | 0.1 | 892 | 9 |
| 13 | 0.0700 | 0.0013 | 1.4675 | 0.0261 | 0.1520 | 0.0017 | 929 | 37 | 917 | 11 | 912 | 9 | 1.9 | 912 | 9 |
| 14 | 0.0689 | 0.0012 | 1.4168 | 0.0247 | 0.1491 | 0.0016 | 896 | 36 | 896 | 10 | 896 | 9 | 0 | 896 | 9 |
| 15 | 0.0695 | 0.0008 | 1.4608 | 0.0157 | 0.1524 | 0.0015 | 914 | 22 | 914 | 6 | 914 | 9 | 0 | 914 | 9 |
| 16 | 0.0689 | 0.0011 | 1.4201 | 0.0228 | 0.1494 | 0.0016 | 897 | 33 | 897 | 10 | 898 | 9 | 0.1 | 898 | 9 |
| 17 | 0.0696 | 0.0008 | 1.4667 | 0.0164 | 0.1528 | 0.0016 | 917 | 23 | 917 | 7 | 917 | 9 | 0 | 917 | 9 |
| 18 | 0.0704 | 0.0013 | 1.5248 | 0.0278 | 0.1571 | 0.0017 | 940 | 38 | 940 | 11 | 941 | 10 | 0.1 | 941 | 10 |
| 19 | 0.0695 | 0.0008 | 1.4611 | 0.0160 | 0.1524 | 0.0015 | 915 | 22 | 915 | 7 | 915 | 9 | 0 | 915 | 9 |
| 20 | 0.0702 | 0.0009 | 1.5146 | 0.0198 | 0.1564 | 0.0016 | 935 | 27 | 936 | 8 | 937 | 9 | 0.2 | 937 | 9 |
| 21 | 0.0745 | 0.0013 | 1.5630 | 0.0265 | 0.1521 | 0.0017 | 1056 | 34.4 | 955.6 | 11 | 913 | 9 | 16 | | |
| 22 | 0.0692 | 0.0011 | 1.4496 | 0.0236 | 0.1519 | 0.0016 | 905 | 34 | 910 | 10 | 912 | 9 | 0.7 | 912 | 9 |
| 23 | 0.0698 | 0.0010 | 1.4809 | 0.0199 | 0.1539 | 0.0016 | 923 | 28 | 923 | 8 | 923 | 9 | 0 | 923 | 9 |
| 24 | 0.0690 | 0.0010 | 1.4227 | 0.0200 | 0.1496 | 0.0016 | 898 | 29 | 899 | 8 | 899 | 9 | 0.1 | 899 | 9 |
| 25 | 0.0696 | 0.0008 | 1.4658 | 0.0173 | 0.1527 | 0.0016 | 917 | 24 | 916 | 7 | 916 | 9 | 0.1 | 916 | 9 |
| 26 | 0.0695 | 0.0010 | 1.4563 | 0.0200 | 0.1521 | 0.0016 | 913 | 28 | 913 | 8 | 912 | 9 | 0 | 912 | 9 |
| 27 | 0.0710 | 0.0013 | 1.5680 | 0.0290 | 0.1601 | 0.0018 | 958 | 38 | 958 | 11 | 957 | 10 | 0.1 | 957 | 10 |
| 28 | 0.0697 | 0.0012 | 1.4720 | 0.0247 | 0.1532 | 0.0016 | 920 | 35 | 919 | 10 | 919 | 9 | 0.1 | 919 | 9 |
| 29 | 0.0710 | 0.0012 | 1.5627 | 0.0268 | 0.1597 | 0.0017 | 957 | 35 | 956 | 11 | 955 | 10 | 0.1 | 955 | 10 |
| 30 | 0.0705 | 0.0008 | 1.5292 | 0.0175 | 0.1574 | 0.0016 | 941 | 23 | 942 | 7 | 943 | 9 | 0.1 | 943 | 9 |
| 31 | 0.0716 | 0.0018 | 1.6105 | 0.0385 | 0.1633 | 0.0019 | 973 | 49 | 974 | 15 | 975 | 11 | 0.2 | 975 | 11 |
| 32 | 0.0703 | 0.0013 | 1.5188 | 0.0277 | 0.1566 | 0.0017 | 938 | 38 | 938 | 11 | 938 | 10 | 0 | 938 | 10 |
| 33 | 0.0709 | 0.0012 | 1.5566 | 0.0269 | 0.1593 | 0.0017 | 953 | 35 | 953 | 11 | 953 | 10 | 0 | 953 | 10 |
| 34 | 0.0679 | 0.0041 | 1.3543 | 0.0792 | 0.1446 | 0.0027 | 867 | 120 | 869 | 34 | 871 | 15 | 0.4 | **871** | **15** |
| 35 | 0.0698 | 0.0012 | 1.4766 | 0.0242 | 0.1535 | 0.0016 | 921 | 34 | 921 | 10 | 921 | 9 | 0.1 | 921 | 9 |
| 36 | 0.0687 | 0.0018 | 1.3998 | 0.0353 | 0.1478 | 0.0018 | 890 | 52 | 889 | 15 | 889 | 10 | 0.1 | 889 | 10 |
| 37 | 0.0670 | 0.0015 | 1.2385 | 0.0267 | 0.1341 | 0.0015 | 837 | 45 | 818 | 12 | 811 | 9 | 3.2 | | |
| 38 | 0.0685 | 0.0007 | 1.3834 | 0.0150 | 0.1466 | 0.0015 | 883 | 22 | 882 | 6 | 882 | 8 | 0.1 | 882 | 8 |
| 39 | 0.0700 | 0.0009 | 1.4932 | 0.0195 | 0.1547 | 0.0016 | 929 | 27 | 928 | 8 | 927 | 9 | 0.2 | 927 | 9 |
| 40 | 0.0694 | 0.0012 | 1.4509 | 0.0241 | 0.1517 | 0.0016 | 910 | 34 | 910 | 10 | 910 | 9 | 0 | 910 | 9 |
| 41 | 0.0696 | 0.0012 | 1.4661 | 0.0249 | 0.1528 | 0.0016 | 916 | 35 | 917 | 10 | 917 | 9 | 0.1 | 917 | 9 |
| 42 | 0.0702 | 0.0015 | 1.5076 | 0.0315 | 0.1557 | 0.0017 | 935 | 43 | 934 | 13 | 933 | 10 | 0.2 | 933 | 10 |
| 43 | 0.0700 | 0.0011 | 1.4933 | 0.0230 | 0.1548 | 0.0016 | 927 | 32 | 928 | 9 | 928 | 9 | 0.1 | 928 | 9 |
| 44 | 0.0693 | 0.0008 | 1.4454 | 0.0163 | 0.1512 | 0.0015 | 908 | 23 | 908 | 7 | 908 | 9 | 0 | 908 | 9 |
| 45 | 0.0707 | 0.0015 | 1.5425 | 0.0310 | 0.1583 | 0.0018 | 948 | 41 | 948 | 12 | 947 | 10 | 0.1 | 947 | 10 |
| 46 | 0.0685 | 0.0012 | 1.3849 | 0.0230 | 0.1467 | 0.0016 | 882 | 34 | 883 | 10 | 883 | 9 | 0.1 | 883 | 9 |
| 47 | 0.0709 | 0.0017 | 1.5593 | 0.0364 | 0.1595 | 0.0019 | 954 | 48 | 954 | 14 | 954 | 10 | 0 | 954 | 10 |
| 48 | 0.0678 | 0.0014 | 1.3427 | 0.0271 | 0.1436 | 0.0016 | 863 | 42 | 864 | 12 | 865 | 9 | 0.2 | **865** | **9** |
| 49 | 0.0699 | 0.0011 | 1.4892 | 0.0238 | 0.1545 | 0.0016 | 926 | 33 | 926 | 10 | 926 | 9 | 0 | 926 | 9 |
| 50 | 0.0691 | 0.0013 | 1.4266 | 0.0260 | 0.1498 | 0.0016 | 901 | 38 | 900 | 11 | 900 | 9 | 0.1 | 900 | 9 |
| 51 | 0.0703 | 0.0018 | 1.5147 | 0.0377 | 0.1564 | 0.0018 | 936 | 51 | 936 | 15 | 937 | 10 | 0.1 | 937 | 10 |
| 52 | 0.0699 | 0.0008 | 1.4896 | 0.0174 | 0.1545 | 0.0016 | 926 | 24 | 926 | 7 | 926 | 9 | 0 | 926 | 9 |
| 53 | 0.0703 | 0.0012 | 1.5111 | 0.0262 | 0.1559 | 0.0017 | 937 | 36 | 935 | 11 | 934 | 9 | 0.3 | 934 | 9 |
| 54 | 0.0705 | 0.0020 | 1.5338 | 0.0421 | 0.1577 | 0.0019 | 944 | 57 | 944 | 17 | 944 | 11 | 0 | 944 | 11 |
| 55 | 0.0701 | 0.0008 | 1.4976 | 0.0161 | 0.1551 | 0.0016 | 930 | 22 | 929 | 7 | 929 | 9 | 0.1 | 929 | 9 |
| 56 | 0.0701 | 0.0008 | 1.4999 | 0.0166 | 0.1552 | 0.0016 | 931 | 22 | 930 | 7 | 930 | 9 | 0.1 | 930 | 9 |
| 57 | 0.0696 | 0.0013 | 1.4614 | 0.0262 | 0.1524 | 0.0017 | 915 | 37 | 915 | 11 | 914 | 9 | 0.1 | 914 | 9 |
| 58 | 0.0700 | 0.0008 | 1.4927 | 0.0161 | 0.1547 | 0.0016 | 928 | 22 | 927 | 7 | 927 | 9 | 0.1 | 927 | 9 |
| 59 | 0.0690 | 0.0012 | 1.4206 | 0.0238 | 0.1493 | 0.0016 | 899 | 35 | 898 | 10 | 897 | 9 | 0.2 | 897 | 9 |
| 60 | 0.0700 | 0.0010 | 1.4989 | 0.0211 | 0.1553 | 0.0016 | 929 | 29 | 930 | 9 | 930 | 9 | 0.2 | 930 | 9 |

**Table4**

Table 4 Chemical compostion of the Yanbian rocks in the western margin of the Yangtze Block.

| | Yumen Formation | | | | | | | | | | | | |
|---|---|---|---|---|---|---|---|---|---|---|---|---|---|
| | Sandstone | | | | | | | Mudstone | | | | | |
| | F38 | T3-1-2 | T3-2 | T-1 | T-3 | Z3 | Average | st11 | st12 | st13 | st14 | st15 | st16 | Average |
| Major Oxides (wt%) | | | | | | | | | | | | | |
| $SiO_2$ | 69.7 | 79.8 | 65.2 | 64.1 | 80.1 | 67.7 | 71.1 | 65.7 | 62.1 | 64.1 | 65.7 | 65.3 | 73.4 | 66.0 |
| $TiO_2$ | 0.99 | 0.48 | 0.81 | 1.02 | 0.30 | 0.79 | 0.73 | 0.89 | 0.85 | 0.76 | 0.93 | 0.98 | 0.84 | 0.88 |
| $Al_2O_3$ | 12.7 | 10.4 | 15.5 | 15.7 | 10.9 | 13.9 | 13.2 | 14.0 | 16.3 | 14.7 | 13.3 | 17.8 | 14.3 | 15.1 |
| $Fe_2O_3$ | 6.62 | 1.13 | 5.92 | 7.87 | 0.87 | 7.21 | 4.94 | 7.42 | 7.30 | 7.70 | 6.74 | 2.62 | 1.69 | 5.58 |
| MnO | 0.05 | 0.03 | 0.07 | 0.10 | 0.01 | 0.03 | 0.05 | 0.07 | 0.04 | 0.03 | 0.03 | 0.01 | 0.02 | 0.03 |
| MgO | 1.94 | 0.23 | 1.07 | 2.17 | 0.20 | 1.91 | 1.25 | 2.12 | 1.97 | 1.81 | 2.27 | 1.32 | 1.01 | 1.75 |
| CaO | 0.31 | 0.22 | 0.91 | 0.30 | 0.25 | 0.34 | 0.39 | 0.28 | 0.20 | 0.22 | 0.69 | 0.05 | 0.05 | 0.25 |
| $Na_2O$ | 3.66 | 5.05 | 4.97 | 1.70 | 5.14 | 2.43 | 3.82 | 2.91 | 2.06 | 2.82 | 3.41 | 0.87 | 1.01 | 2.18 |
| $K_2O$ | 1.11 | 0.50 | 2.23 | 2.45 | 0.43 | 1.50 | 1.37 | 1.71 | 2.57 | 1.95 | 1.34 | 3.55 | 3.76 | 2.48 |
| $P_2O_5$ | 0.16 | 0.00 | 0.09 | 0.10 | 0.00 | 0.16 | 0.09 | 0.14 | 0.10 | 0.16 | 0.21 | 0.00 | 0.00 | 0.10 |
| LOI | 2.64 | 1.67 | 3.07 | 3.65 | 1.06 | 3.12 | 2.54 | 4.67 | 5.70 | 5.10 | 5.06 | 6.23 | 3.85 | 5.10 |
| Total | 99.9 | 99.6 | 99.8 | 99.2 | 99.3 | 99.1 | 99.5 | 99.9 | 99.2 | 99.3 | 99.7 | 98.7 | 100.0 | 99.5 |
| CIA | 63 | 53 | 56 | 73 | 54 | 70 | 61 | 67 | 72 | 68 | 63 | 77 | 71 | 70 |
| Trace elements (ppm) | | | | | | | | | | | | | |
| Sc | 11.8 | 7.85 | 12.8 | 17.5 | 6.29 | 17.1 | 12.2 | 16.0 | 19.3 | 15.9 | 17.2 | 19.1 | 19.7 | 17.8 |
| V | 89 | 17.7 | 46 | 127 | 20 | 115 | 69 | 108 | 137 | 114 | 134 | 257 | 206 | 159 |
| Cr | 260 | 14.9 | 37 | 74 | 19.0 | 152 | 93 | 186 | 182 | 170 | 261 | 148 | 81 | 171 |
| Co | 3.46 | 1.72 | 2.29 | 18.3 | 0.98 | 9.33 | 6.01 | 10.1 | 8.89 | 4.25 | 7.03 | 2.76 | 0.59 | 5.61 |
| Ni | 45.3 | 9.4 | 9.2 | 38.6 | 2.7 | 32.7 | 23.0 | 48.9 | 55.7 | 48.2 | 69.9 | 41.3 | 10.4 | 45.7 |
| Rb | 30.5 | 7.4 | 36.2 | 90.7 | 9.3 | 70.8 | 40.8 | 69.7 | 114 | 80.8 | 54.3 | 137 | 134 | 98 |
| Sr | 48 | 153 | 213 | 80 | 266 | 60 | 137 | 62 | 61 | 88 | 138 | 29 | 18 | 66 |
| Y | 19.7 | 6.0 | 28.0 | 21.6 | 10.1 | 21.7 | 17.8 | 18.7 | 24.6 | 35.6 | 20.1 | 26.1 | 25.9 | 25.1 |
| Zr | 125 | 89 | 214 | 193 | 119 | 162 | 150 | 122 | 135 | 119 | 129 | 153 | 170 | 138 |
| Nb | 5.14 | 5.23 | 9.59 | 11.40 | 6.21 | 6.18 | 7.29 | 6.41 | 10.04 | 7.94 | 6.20 | 10.52 | 13.24 | 9.06 |
| Cs | 1.98 | 0.38 | 2.52 | 3.85 | 0.43 | 3.47 | 2.10 | 3.39 | 5.71 | 5.07 | 2.82 | 8.03 | 7.62 | 5.44 |
| Ba | 170 | 125 | 352 | 324 | 132 | 255 | 226 | 271 | 419 | 296 | 295 | 417 | 618 | 386 |
| La | 22.2 | 8.5 | 15.0 | 22.3 | 17.4 | 21.9 | 17.89 | 20.6 | 29.5 | 32.0 | 13.1 | 41.5 | 29.9 | 27.8 |
| Ce | 45.8 | 15.5 | 28.8 | 44.3 | 28.9 | 51.7 | 35.83 | 46.0 | 61.9 | 81.8 | 26.8 | 83.6 | 57.0 | 59.5 |
| Pr | 6.00 | 1.94 | 3.91 | 4.95 | 3.82 | 6.14 | 4.46 | 5.19 | 6.75 | 9.12 | 3.49 | 9.45 | 6.37 | 6.73 |
| Nd | 27.4 | 8.15 | 17.3 | 19.4 | 14.1 | 26.6 | 18.82 | 21.9 | 26.1 | 38.1 | 15.7 | 40.5 | 26.2 | 28.1 |
| Sm | 6.43 | 1.68 | 4.14 | 4.07 | 2.62 | 6.20 | 4.19 | 4.61 | 5.21 | 8.48 | 3.62 | 8.16 | 4.73 | 5.80 |
| Eu | 0.94 | 0.28 | 1.01 | 0.96 | 0.56 | 1.48 | 0.87 | 1.16 | 1.32 | 2.33 | 0.89 | 1.72 | 0.90 | 1.39 |
| Gd | 5.29 | 1.69 | 3.94 | 3.60 | 2.01 | 5.20 | 3.62 | 4.66 | 5.05 | 9.21 | 3.71 | 6.75 | 4.55 | 5.66 |
| Tb | 0.94 | 0.28 | 0.70 | 0.62 | 0.34 | 0.89 | 0.63 | 0.58 | 0.76 | 1.29 | 0.55 | 0.96 | 0.67 | 0.80 |
| Dy | 5.71 | 1.70 | 4.79 | 3.63 | 1.82 | 4.44 | 3.68 | 3.54 | 4.24 | 6.91 | 3.43 | 5.30 | 4.50 | 4.65 |
| Ho | 1.12 | 0.32 | 1.14 | 0.78 | 0.40 | 0.87 | 0.77 | 0.71 | 1.02 | 1.35 | 0.78 | 1.08 | 0.99 | 0.99 |
| Er | 2.83 | 0.84 | 3.30 | 2.36 | 1.21 | 2.32 | 2.14 | 1.96 | 2.80 | 3.28 | 2.11 | 3.07 | 3.08 | 2.72 |
| Tm | 0.38 | 0.13 | 0.49 | 0.34 | 0.18 | 0.31 | 0.31 | 0.30 | 0.41 | 0.44 | 0.32 | 0.49 | 0.48 | 0.41 |
| Yb | 2.36 | 0.83 | 3.08 | 2.38 | 1.30 | 2.13 | 2.01 | 1.80 | 2.85 | 2.70 | 2.00 | 2.89 | 3.10 | 2.56 |
| Lu | 0.36 | 0.14 | 0.51 | 0.35 | 0.22 | 0.30 | 0.31 | 0.29 | 0.43 | 0.39 | 0.29 | 0.44 | 0.49 | 0.39 |
| Hf | 4.14 | 3.06 | 6.75 | 4.84 | 3.01 | 4.10 | 4.32 | 3.74 | 4.30 | 3.57 | 3.99 | 4.65 | 5.22 | 4.25 |
| Ta | 0.27 | 0.20 | 0.43 | 0.73 | 0.41 | 0.40 | 0.41 | 0.36 | 0.60 | 0.47 | 0.36 | 0.68 | 0.90 | 0.56 |
| Pb | 9.83 | 5.96 | 7.95 | 3.48 | 4.32 | 5.06 | 6.10 | 5.88 | 7.96 | 11.3 | 17.4 | 13.7 | 47.4 | 17.3 |
| Th | 4.57 | 2.99 | 6.03 | 7.68 | 3.64 | 5.45 | 5.06 | 5.19 | 8.66 | 6.58 | 4.72 | 8.94 | 14.50 | 8.10 |
| U | 1.31 | 0.93 | 1.72 | 1.50 | 0.69 | 1.16 | 1.22 | 1.53 | 2.12 | 1.65 | 1.42 | 3.26 | 3.95 | 2.32 |
| Eu/Eu* | 0.49 | 0.51 | 0.76 | 0.77 | 0.75 | 0.80 | 0.68 | 0.76 | 0.79 | 0.81 | 0.74 | 0.71 | 0.59 | 0.73 |
| REE | 128 | 42 | 88 | 110 | 75 | 130 | 96 | 113 | 148 | 197 | 77 | 206 | 143 | 147 |
| $La/Yb_N$ | 6.33 | 6.92 | 3.28 | 6.31 | 9.01 | 6.92 | 6.46 | 7.69 | 6.95 | 7.98 | 4.41 | 9.65 | 6.49 | 7.20 |
| La/Yb | 9.40 | 10.29 | 4.87 | 9.37 | 13.38 | 10.28 | 9.60 | 11.43 | 10.33 | 11.86 | 6.56 | 14.34 | 9.65 | 10.7 |
| Cr/Th | 56.8 | 5.0 | 6.1 | 9.7 | 5.2 | 27.9 | 18.45 | 35.8 | 21.0 | 25.9 | 55.3 | 16.5 | 5.6 | 26.7 |

Table 4 (continued)

| | Xiaoping Formation | | | | | | | | | | | | | | | | |
| | Sandstone | | | | | | | | | | | | | | | | |
| | F3 | F4-1 | F4-2 | F5 | F6 | F7 | F8 | F9 | F10 | F11 | F12 | F13 | F14 | F15 | F16 | F17 | F18 |
| Major Oxides (wt%) | | | | | | | | | | | | | | | | | |
| $SiO_2$ | 67.5 | 69.0 | 69.8 | 66.5 | 66.4 | 59.6 | 58.8 | 66.3 | 71.1 | 71.1 | 62.3 | 53.3 | 54.9 | 55.1 | 54.7 | 60.8 | 59.59 |
| $TiO_2$ | 1.00 | 0.65 | 0.69 | 0.81 | 0.78 | 1.01 | 1.18 | 0.79 | 0.54 | 0.73 | 1.02 | 1.74 | 1.23 | 1.14 | 1.14 | 1.25 | 1.20 |
| $Al_2O_3$ | 13.8 | 13.2 | 13.5 | 14.3 | 14.1 | 16.6 | 16.3 | 15.5 | 14.7 | 14.6 | 16.2 | 16.2 | 17.9 | 16.9 | 17.7 | 16.2 | 17.51 |
| $Fe_2O_3$ | 5.97 | 4.86 | 5.09 | 5.97 | 5.86 | 8.11 | 8.43 | 6.52 | 2.12 | 1.91 | 6.17 | 10.71 | 9.50 | 6.94 | 8.84 | 6.49 | 7.17 |
| MnO | 0.08 | 0.09 | 0.06 | 0.07 | 0.08 | 0.11 | 0.13 | 0.05 | 0.02 | 0.03 | 0.11 | 0.26 | 0.23 | 0.18 | 0.22 | 0.14 | 0.14 |
| MgO | 1.63 | 1.22 | 1.15 | 1.51 | 1.84 | 2.85 | 3.12 | 1.60 | 0.75 | 0.47 | 1.82 | 3.24 | 2.63 | 1.97 | 2.62 | 1.86 | 1.72 |
| CaO | 0.29 | 1.64 | 0.35 | 0.98 | 0.35 | 0.82 | 1.07 | 0.16 | 0.31 | 0.32 | 2.26 | 4.67 | 3.52 | 5.33 | 3.39 | 2.88 | 1.22 |
| $Na_2O$ | 2.80 | 4.05 | 4.31 | 3.02 | 5.07 | 6.21 | 6.04 | 2.73 | 3.76 | 5.82 | 4.58 | 3.63 | 3.65 | 4.78 | 3.45 | 5.54 | 4.09 |
| $K_2O$ | 1.95 | 1.49 | 1.50 | 2.22 | 2.10 | 0.61 | 0.56 | 1.71 | 3.99 | 2.33 | 2.25 | 1.55 | 2.43 | 1.93 | 2.84 | 1.57 | 3.11 |
| $P_2O_5$ | 0.13 | 0.08 | 0.07 | 0.07 | 0.10 | 0.15 | 0.17 | 0.08 | 0.06 | 0.02 | 0.16 | 0.27 | 0.25 | 0.28 | 0.24 | 0.18 | 0.18 |
| LOI | 3.51 | 3.22 | 2.97 | 3.01 | 2.71 | 3.05 | 3.17 | 3.78 | 2.18 | 1.90 | 2.55 | 4.21 | 3.50 | 5.22 | 3.60 | 2.83 | 3.39 |
| Total | 98.6 | 99.5 | 99.5 | 98.4 | 99.4 | 99.1 | 98.9 | 99.2 | 99.6 | 99.3 | 99.4 | 99.7 | 99.8 | 99.8 | 98.8 | 99.8 | 99.3 |
| CIA | 66 | 54 | 59 | 61 | 56 | 58 | 57 | 71 | 57 | 54 | 54 | 54 | 55 | 49 | 55 | 51 | 60 |
| Trace elements (ppm) | | | | | | | | | | | | | | | | | |
| Sc | 12.5 | 11.6 | 10.4 | 10.2 | 12.6 | 13.5 | 14.5 | 11.5 | 13.4 | 14.4 | 14.6 | 18.4 | 14.5 | 15.9 | 14.0 | 10.8 | 14.9 |
| V | 93 | 64 | 60 | 70 | 94 | 130 | 158 | 102 | 36 | 33 | 93 | 228 | 147 | 105 | 125 | 38 | 117 |
| Cr | 72 | 56 | 53 | 72 | 74 | 51 | 60 | 78 | 28 | 33 | 47 | 147 | 77 | 47 | 70 | 30 | 62 |
| Co | 12.1 | 9.9 | 9.1 | 11.2 | 12.8 | 17.1 | 16.4 | 4.2 | 9.5 | 1.0 | 11.5 | 22.4 | 15.5 | 15.0 | 14.9 | 7.0 | 19.1 |
| Ni | 40.0 | 23.9 | 22.4 | 25.2 | 37.6 | 29.5 | 24.2 | 18.9 | 22.1 | 4.3 | 25.8 | 53.9 | 36.1 | 27.3 | 34.5 | 13.7 | 37.7 |
| Rb | 55.0 | 33.1 | 30.1 | 53.4 | 45.4 | 11.4 | 9.9 | 42.7 | 55.4 | 30.2 | 34.9 | 16.6 | 32.2 | 29.9 | 39.4 | 17.7 | 42.9 |
| Sr | 73 | 141 | 152 | 160 | 99 | 255 | 244 | 103 | 204 | 178 | 325 | 339 | 377 | 310 | 330 | 218 | 194 |
| Y | 17.8 | 16.0 | 18.2 | 17.0 | 16.0 | 18.1 | 15.8 | 66.7 | 49.7 | 15.8 | 25.4 | 24.7 | 21.6 | 24.9 | 22.1 | 21.7 | 29.0 |
| Zr | 202 | 119 | 99 | 140 | 117 | 101 | 104 | 123 | 146 | 164 | 171 | 158 | 154 | 147 | 160 | 47 | 174 |
| Nb | 12.0 | 6.21 | 5.64 | 7.99 | 5.59 | 4.91 | 5.12 | 5.99 | 8.12 | 8.38 | 9.89 | 9.31 | 8.94 | 8.27 | 8.95 | 2.93 | 10.14 |
| Cs | 2.97 | 1.32 | 1.44 | 2.93 | 2.29 | 0.76 | 1.23 | 1.46 | 2.43 | 1.32 | 1.46 | 1.24 | 2.32 | 1.84 | 2.63 | 0.88 | 1.65 |
| Ba | 308 | 278 | 284 | 355 | 303 | 195 | 179 | 316 | 943 | 424 | 480 | 407 | 650 | 589 | 568 | 341 | 1125 |
| La | 27.1 | 15.3 | 22.1 | 24.6 | 20.2 | 14.5 | 16.0 | 51.8 | 34.9 | 25.0 | 24.4 | 25.6 | 25.1 | 26.0 | 24.9 | 20.4 | 23.6 |
| Ce | 48.9 | 34.2 | 37.8 | 44.4 | 38.0 | 28.5 | 31.1 | 104 | 67.2 | 45.6 | 48.0 | 45.6 | 44.8 | 45.2 | 46.6 | 36.1 | 47.8 |
| Pr | 5.40 | 3.82 | 5.06 | 5.34 | 4.33 | 3.43 | 3.72 | 15 | 8.47 | 5.06 | 5.79 | 5.79 | 5.65 | 5.71 | 6.13 | 4.46 | 6.47 |
| Nd | 21.1 | 16.2 | 21.1 | 22.4 | 17.0 | 15.0 | 16.0 | 69.3 | 37.1 | 19.9 | 25.0 | 25.7 | 23.6 | 24.5 | 26.1 | 20.1 | 28.8 |
| Sm | 3.83 | 3.45 | 4.42 | 4.39 | 3.43 | 3.25 | 3.46 | 16 | 8.04 | 3.76 | 5.28 | 5.32 | 4.99 | 4.98 | 5.33 | 4.12 | 6.37 |
| Eu | 0.71 | 0.71 | 0.76 | 0.92 | 0.75 | 0.73 | 0.77 | 2.88 | 1.81 | 1.07 | 1.18 | 1.26 | 1.37 | 1.24 | 1.31 | 0.97 | 1.73 |
| Gd | 4.44 | 3.16 | 4.27 | 4.36 | 3.52 | 2.83 | 3.20 | 17 | 7.50 | 4.18 | 4.99 | 4.93 | 4.83 | 4.91 | 5.18 | 4.03 | 5.64 |
| Tb | 0.67 | 0.55 | 0.72 | 0.72 | 0.57 | 0.52 | 0.56 | 2.49 | 1.40 | 0.63 | 0.84 | 0.86 | 0.81 | 0.84 | 0.87 | 0.70 | 1.02 |
| Dy | 4.22 | 3.47 | 4.48 | 4.58 | 3.56 | 3.46 | 3.50 | 16 | 9.02 | 3.95 | 5.44 | 5.47 | 5.01 | 5.27 | 5.55 | 4.46 | 6.66 |
| Ho | 0.80 | 0.68 | 0.92 | 0.85 | 0.76 | 0.72 | 0.68 | 2.60 | 1.78 | 0.76 | 1.06 | 1.04 | 0.96 | 1.10 | 1.12 | 0.89 | 1.37 |
| Er | 2.27 | 1.84 | 2.57 | 2.36 | 2.09 | 2.05 | 2.01 | 6.05 | 4.62 | 2.14 | 2.87 | 2.82 | 2.43 | 3.02 | 3.09 | 2.51 | 3.61 |
| Tm | 0.34 | 0.29 | 0.36 | 0.32 | 0.30 | 0.30 | 0.28 | 0.85 | 0.60 | 0.30 | 0.42 | 0.40 | 0.36 | 0.45 | 0.44 | 0.36 | 0.51 |
| Yb | 2.19 | 1.80 | 2.22 | 2.10 | 1.92 | 1.88 | 1.77 | 5.04 | 3.53 | 1.91 | 2.72 | 2.54 | 2.32 | 2.72 | 2.70 | 2.32 | 3.25 |
| Lu | 0.36 | 0.27 | 0.34 | 0.32 | 0.30 | 0.29 | 0.28 | 0.74 | 0.55 | 0.32 | 0.41 | 0.40 | 0.37 | 0.43 | 0.42 | 0.38 | 0.5 |
| Hf | 5.90 | 3.61 | 3.44 | 4.43 | 3.76 | 3.15 | 3.25 | 4.26 | 4.78 | 4.89 | 5.10 | 4.80 | 4.74 | 4.58 | 5.03 | 1.72 | 5.45 |
| Ta | 0.38 | 0.23 | 0.22 | 0.29 | 0.24 | 0.20 | 0.22 | 0.27 | 0.30 | 0.32 | 0.33 | 0.31 | 0.31 | 0.30 | 0.32 | 0.11 | 0.4 |
| Pb | 17.2 | 15.6 | 15.0 | 15.6 | 18.6 | 5.78 | 8.56 | 22.7 | 10.1 | 8.46 | 9.90 | 5.44 | 4.74 | 8.99 | 6.77 | 4.68 | 10.2 |
| Th | 10.7 | 4.27 | 4.15 | 5.50 | 5.35 | 2.71 | 2.57 | 5.28 | 5.48 | 5.13 | 4.72 | 3.29 | 3.98 | 3.76 | 3.98 | 2.86 | 3.77 |
| U | 2.44 | 1.03 | 1.02 | 1.31 | 1.24 | 0.80 | 0.83 | 1.24 | 1.51 | 1.48 | 1.42 | 1.00 | 1.16 | 1.09 | 1.16 | 0.54 | 1.08 |
| Eu/Eu* | 0.53 | 0.66 | 0.53 | 0.64 | 0.66 | 0.74 | 0.71 | 0.54 | 0.71 | 0.82 | 0.70 | 0.75 | 0.85 | 0.77 | 0.76 | 0.73 | 0.88 |
| REE | 122 | 86 | 107 | 118 | 97 | 77 | 83 | 309 | 187 | 115 | 128 | 128 | 123 | 126 | 130 | 102 | 137 |
| $La/Yb_N$ | 8.32 | 5.74 | 6.70 | 7.89 | 7.08 | 5.18 | 6.06 | 6.92 | 6.66 | 8.80 | 6.03 | 6.79 | 7.28 | 6.43 | 6.21 | 5.93 | 4.89 |
| La/Yb | 12.4 | 8.52 | 9.95 | 11.7 | 10.52 | 7.70 | 9.01 | 10 | 9.90 | 13.07 | 8.96 | 10.09 | 10.82 | 9.55 | 9.22 | 8.81 | 7.26 |
| Cr/Th | 6.7 | 13.1 | 12.8 | 13.1 | 13.9 | 19.0 | 23.5 | 14.7 | 5.1 | 6.4 | 9.9 | 44.6 | 19.4 | 12.6 | 17.5 | 10.4 | 16.3 |

Table 4 (continued)

| | F19 | F20 | F21 | F24 | F25 | F26 | F27 | F28 | F29 | F30 | F31 | F32 | F33 | F34 | Z4 | Z5 | Average |
|---|---|---|---|---|---|---|---|---|---|---|---|---|---|---|---|---|---|
| | | | | | | | | Xiaoping Formation | | | | | | | | | |
| | | | | | | | | Sandstone | | | | | | | | | |
| **Major Oxides (wt%)** | | | | | | | | | | | | | | | | | |
| $SiO_2$ | 64.2 | 62.7 | 62.7 | 61.9 | 60.3 | 62.1 | 60.9 | 62.3 | 68.6 | 72.1 | 66.9 | 62.0 | 68.9 | 72.5 | 66.2 | 63.4 | 63.8 |
| $TiO_2$ | 1.09 | 1.14 | 1.04 | 1.21 | 1.21 | 1.14 | 1.20 | 1.25 | 1.06 | 0.83 | 0.87 | 0.92 | 0.75 | 0.66 | 0.72 | 0.92 | 1.00 |
| $Al_2O_3$ | 15.8 | 15.0 | 15.0 | 15.3 | 15.5 | 15.3 | 16.1 | 15.1 | 13.8 | 12.2 | 14.6 | 15.0 | 14.1 | 12.5 | 13.8 | 14.4 | 15.11 |
| $Fe_2O_3$ | 5.49 | 7.82 | 7.38 | 7.77 | 8.97 | 8.64 | 8.32 | 8.00 | 4.94 | 4.31 | 6.34 | 7.39 | 4.64 | 3.49 | 7.04 | 8.64 | 6.66 |
| MnO | 0.10 | 0.11 | 0.09 | 0.08 | 0.07 | 0.06 | 0.04 | 0.05 | 0.06 | 0.20 | 0.03 | 0.09 | 0.10 | 0.08 | 0.05 | 0.05 | 0.10 |
| MgO | 1.40 | 3.02 | 2.95 | 2.87 | 3.24 | 2.93 | 2.75 | 2.93 | 1.62 | 1.54 | 1.42 | 1.86 | 1.14 | 0.83 | 2.75 | 2.17 | 2.04 |
| CaO | 0.99 | 0.56 | 0.59 | 0.40 | 0.50 | 0.50 | 0.45 | 0.36 | 0.10 | 0.11 | 0.26 | 0.13 | 0.63 | 0.63 | 0.35 | 0.79 | 1.12 |
| $Na_2O$ | 4.28 | 4.36 | 3.93 | 3.82 | 3.45 | 2.96 | 2.97 | 3.48 | 3.64 | 3.35 | 3.01 | 2.00 | 5.48 | 5.63 | 2.46 | 2.32 | 3.96 |
| $K_2O$ | 3.03 | 1.87 | 2.09 | 2.08 | 1.95 | 2.18 | 2.24 | 1.92 | 1.64 | 1.19 | 1.93 | 2.01 | 1.44 | 1.08 | 2.24 | 1.85 | 1.97 |
| $P_2O_5$ | 0.18 | 0.20 | 0.22 | 0.21 | 0.30 | 0.27 | 0.20 | 0.23 | 0.06 | 0.03 | 0.09 | 0.13 | 0.05 | 0.04 | 0.12 | 0.27 | 0.15 |
| LOI | 2.71 | 3.18 | 3.29 | 3.56 | 3.75 | 3.33 | 4.09 | 3.82 | 3.90 | 3.18 | 4.14 | 6.86 | 2.28 | 1.67 | 3.07 | 4.12 | 3.39 |
| Total | 99.2 | 100.0 | 99.3 | 99.2 | 99.2 | 99.4 | 99.2 | 99.5 | 99.4 | 99.0 | 99.6 | 98.4 | 99.6 | 99.1 | 98.8 | 98.9 | 99.3 |
| CIA | 57 | 61 | 62 | 64 | 66 | 67 | 68 | 66 | 64 | 64 | 67 | 73 | 55 | 52 | 67 | 68 | 59 |
| **Trace elements (ppm)** | | | | | | | | | | | | | | | | | |
| Sc | 15.4 | 13.8 | 12.9 | 14.1 | 13.7 | 12.0 | 13.3 | 13.6 | 12.5 | 10.2 | 11.8 | 10.3 | 13.4 | 11.6 | 14.2 | 16.7 | 13.2 |
| V | 94 | 110 | 104 | 130 | 128 | 129 | 137 | 133 | 98 | 82 | 98 | 106 | 62 | 48 | 106 | 143 | 103 |
| Cr | 52 | 46 | 42 | 69 | 71 | 79 | 70 | 75 | 67 | 84 | 177 | 67 | 55 | 45 | 38 | 41 | 65 |
| Co | 15.3 | 12.1 | 12.4 | 11.5 | 13.4 | 11.6 | 10.4 | 10.1 | 6.8 | 2.6 | 7.8 | 4.5 | 7.0 | 8.4 | 11.3 | 22.1 | 11.4 |
| Ni | 24.1 | 28.2 | 31.0 | 30.0 | 34.0 | 37.1 | 30.6 | 28.5 | 22.2 | 16.5 | 37.9 | 21.3 | 16.9 | 18.3 | 16.8 | 22.2 | 27.0 |
| Rb | 39.7 | 42.3 | 47.6 | 52.2 | 49.6 | 53.8 | 51.7 | 41.8 | 41.8 | 31.7 | 53.4 | 42.8 | 27.8 | 16.3 | 59.4 | 63.7 | 39.3 |
| Sr | 189 | 60 | 54 | 57 | 56 | 48 | 49 | 51 | 63 | 80 | 75 | 51 | 107 | 112 | 75 | 83 | 149 |
| Y | 36.5 | 25.7 | 25.1 | 24.1 | 29.6 | 27.0 | 36.2 | 26.2 | 16.5 | 13.1 | 14.6 | 24.5 | 16.3 | 13.0 | 28.4 | 26.4 | 24.4 |
| Zr | 154 | 116 | 114 | 128 | 118 | 113 | 124 | 113 | 125 | 89 | 122 | 128 | 135 | 105 | 133 | 132 | 130 |
| Nb | 8.81 | 5.69 | 5.42 | 6.25 | 5.91 | 5.69 | 5.89 | 5.57 | 7.22 | 5.44 | 7.12 | 7.51 | 6.86 | 5.93 | 7.18 | 5.44 | 6.98 |
| Cs | 1.26 | 2.32 | 2.58 | 2.46 | 2.32 | 3.06 | 2.74 | 2.15 | 3.17 | 2.37 | 4.14 | 2.77 | 1.22 | 0.71 | 2.00 | 3.07 | 2.08 |
| Ba | 1215 | 336 | 349 | 337 | 320 | 349 | 427 | 351 | 283 | 223 | 235 | 275 | 317 | 259 | 523 | 408 | 423 |
| La | 26.6 | 15.2 | 15.1 | 16.6 | 18.1 | 16.1 | 24.1 | 15.9 | 15.8 | 18.9 | 24.1 | 20.3 | 15.4 | 11.0 | 22.8 | 14.1 | 21.6 |
| Ce | 51.6 | 34.2 | 34.7 | 34.7 | 40.9 | 34.9 | 43.8 | 35.4 | 32.0 | 32.7 | 48.1 | 37.7 | 32.6 | 20.2 | 45.0 | 33.4 | 42.0 |
| Pr | 6.72 | 4.01 | 4.41 | 4.19 | 5.19 | 4.49 | 6.59 | 4.62 | 3.74 | 4.17 | 5.46 | 4.77 | 3.86 | 2.38 | 5.30 | 4.10 | 5.26 |
| Nd | 29.3 | 18.8 | 20.3 | 18.9 | 24.1 | 20.2 | 30.7 | 21.5 | 15.0 | 15.9 | 22.9 | 20.2 | 16.2 | 9.7 | 21.7 | 18.3 | 22.8 |
| Sm | 6.22 | 4.37 | 4.79 | 4.22 | 5.59 | 5.04 | 7.23 | 5.27 | 3.16 | 3.15 | 4.63 | 4.21 | 3.50 | 2.04 | 4.87 | 4.27 | 4.93 |
| Eu | 1.69 | 0.91 | 0.93 | 0.81 | 0.93 | 1.04 | 1.49 | 1.05 | 0.64 | 0.55 | 0.78 | 0.83 | 0.73 | 0.59 | 1.23 | 1.21 | 1.08 |
| Gd | 5.97 | 4.23 | 4.59 | 3.49 | 4.44 | 4.09 | 5.71 | 4.17 | 3.14 | 3.42 | 4.56 | 4.06 | 3.22 | 2.03 | 4.76 | 4.31 | 4.70 |
| Tb | 1.06 | 0.74 | 0.76 | 0.67 | 0.89 | 0.80 | 1.10 | 0.83 | 0.54 | 0.50 | 0.73 | 0.73 | 0.57 | 0.34 | 0.85 | 0.76 | 0.81 |
| Dy | 6.94 | 4.74 | 5.10 | 4.61 | 5.96 | 5.37 | 7.32 | 5.60 | 3.56 | 3.14 | 4.45 | 4.80 | 3.77 | 2.34 | 5.00 | 4.70 | 5.18 |
| Ho | 1.44 | 1.05 | 1.07 | 1.05 | 1.28 | 1.16 | 1.51 | 1.19 | 0.75 | 0.59 | 0.90 | 1.05 | 0.78 | 0.54 | 1.03 | 1.03 | 1.05 |
| Er | 4.10 | 3.04 | 3.01 | 3.04 | 3.71 | 3.39 | 4.23 | 3.49 | 2.19 | 1.55 | 2.32 | 3.01 | 2.22 | 1.67 | 2.73 | 2.83 | 2.88 |
| Tm | 0.58 | 0.43 | 0.42 | 0.45 | 0.55 | 0.50 | 0.64 | 0.51 | 0.34 | 0.23 | 0.32 | 0.46 | 0.34 | 0.26 | 0.37 | 0.41 | 0.42 |
| Yb | 3.62 | 2.70 | 2.66 | 2.80 | 3.32 | 3.20 | 3.94 | 3.21 | 2.12 | 1.48 | 2.02 | 2.93 | 2.19 | 1.65 | 2.41 | 2.74 | 2.60 |
| Lu | 0.59 | 0.43 | 0.40 | 0.43 | 0.51 | 0.48 | 0.58 | 0.48 | 0.35 | 0.24 | 0.30 | 0.47 | 0.35 | 0.27 | 0.34 | 0.40 | 0.40 |
| Hf | 4.99 | 3.80 | 3.62 | 4.08 | 4.00 | 3.93 | 4.20 | 3.90 | 4.21 | 2.92 | 3.85 | 4.32 | 4.32 | 3.62 | 3.60 | 3.51 | 4.11 |
| Ta | 0.32 | 0.24 | 0.24 | 0.26 | 0.26 | 0.25 | 0.27 | 0.25 | 0.27 | 0.19 | 0.24 | 0.28 | 0.28 | 0.23 | 0.45 | 0.35 | 0.28 |
| Pb | 8.61 | 9.86 | 8.14 | 5.67 | 11.3 | 10.9 | 5.66 | 6.01 | 7.78 | 16.8 | 11.5 | 4.61 | 10.2 | 14.1 | 5.92 | 7.46 | 10.1 |
| Th | 3.34 | 3.04 | 3.12 | 3.66 | 3.30 | 3.27 | 3.48 | 3.06 | 5.40 | 4.01 | 5.30 | 6.03 | 4.83 | 4.31 | 5.49 | 2.93 | 4.31 |
| U | 1.08 | 0.78 | 0.81 | 0.95 | 0.90 | 0.87 | 0.92 | 0.80 | 1.34 | 1.07 | 1.39 | 1.45 | 1.26 | 1.10 | 0.88 | 0.42 | 1.10 |
| Eu/Eu* | 0.85 | 0.65 | 0.61 | 0.65 | 0.57 | 0.70 | 0.71 | 0.68 | 0.62 | 0.51 | 0.52 | 0.61 | 0.66 | 0.89 | 0.78 | 0.86 | 0.69 |
| REE | 146 | 95 | 98 | 96 | 115 | 101 | 139 | 103 | 83 | 87 | 121 | 105 | 86 | 55 | 118 | 93 | 116 |
| La/Yb$_N$ | 4.95 | 3.78 | 3.83 | 3.99 | 3.66 | 3.39 | 4.12 | 3.33 | 5.01 | 8.59 | 8.02 | 4.65 | 4.72 | 4.47 | 6.37 | 3.46 | 5.7 |
| La/Yb | 7.35 | 5.61 | 5.69 | 5.93 | 5.44 | 5.04 | 6.13 | 4.94 | 7.45 | 12.8 | 11.9 | 6.91 | 7.02 | 6.64 | 9.46 | 5.15 | 8.5 |
| Cr/Th | 15.7 | 15.2 | 13.6 | 18.8 | 21.4 | 24.1 | 20.0 | 24.5 | 12.4 | 20.9 | 33.5 | 11.2 | 11.4 | 10.4 | 6.9 | 13.9 | 16.1 |

Table 4 (continued)

| | st2 | st4 | st5 | st6 | st7 | st8 | st17 | st18 | st19 | st20 | st21 | st22 | St23 | St24 | St25 | St26 | Average |
|---|---|---|---|---|---|---|---|---|---|---|---|---|---|---|---|---|---|
| | | | | | | Xiaoping Formation | | | | | | | | | | | |
| | | | | | | Mudstone | | | | | | | | | | | |
| **Major Oxides (wt%)** | | | | | | | | | | | | | | | | | |
| $SiO_2$ | 59.0 | 70.6 | 65.2 | 68.8 | 62.2 | 59.4 | 63.3 | 58.4 | 61.2 | 59.5 | 58.5 | 60.9 | 57.9 | 63.5 | 58.1 | 59.1 | 61.6 |
| $TiO_2$ | 0.74 | 0.98 | 0.95 | 0.83 | 0.83 | 0.87 | 0.98 | 0.75 | 0.78 | 0.74 | 0.82 | 0.92 | 0.88 | 0.78 | 0.97 | 0.80 | 0.9 |
| $Al_2O_3$ | 15.2 | 15.4 | 15.3 | 13.6 | 15.5 | 15.9 | 17.0 | 19.6 | 16.8 | 17.3 | 16.1 | 16.9 | 18.5 | 15.5 | 19.5 | 17.7 | 16.6 |
| $Fe_2O_3$ | 6.55 | 2.70 | 5.42 | 5.22 | 7.67 | 8.68 | 3.94 | 8.11 | 7.30 | 8.59 | 9.51 | 6.99 | 7.45 | 5.68 | 5.15 | 7.59 | 6.7 |
| MnO | 0.13 | 0.04 | 0.04 | 0.02 | 0.15 | 0.07 | 0.04 | 0.04 | 0.15 | 0.05 | 0.10 | 0.06 | 0.03 | 0.12 | 0.04 | 0.03 | 0.1 |
| MgO | 3.21 | 1.37 | 1.92 | 1.31 | 2.50 | 2.16 | 1.77 | 1.26 | 2.20 | 1.99 | 2.90 | 2.39 | 1.99 | 1.77 | 1.72 | 1.89 | 2.0 |
| CaO | 2.54 | 0.06 | 0.09 | 0.31 | 0.37 | 0.40 | 0.09 | 0.06 | 0.24 | 0.08 | 0.57 | 0.99 | 0.26 | 0.88 | 1.29 | 0.13 | 0.5 |
| $Na_2O$ | 2.34 | 0.14 | 2.97 | 2.90 | 1.70 | 1.66 | 0.35 | 0.17 | 0.93 | 0.54 | 2.16 | 2.51 | 0.57 | 2.76 | 1.41 | 0.69 | 1.5 |
| $K_2O$ | 3.59 | 3.60 | 2.23 | 1.91 | 2.43 | 2.20 | 3.28 | 3.22 | 2.91 | 2.93 | 2.43 | 2.72 | 2.98 | 3.77 | 4.67 | 2.91 | 3.0 |
| $P_2O_5$ | 0.13 | 0.02 | 0.06 | 0.09 | 0.13 | 0.18 | 0.01 | 0.11 | 0.06 | 0.10 | 0.32 | 0.18 | 0.10 | 0.06 | 0.21 | 0.12 | 0.1 |
| LOI | 5.82 | 4.77 | 5.02 | 4.14 | 5.96 | 7.52 | 8.06 | 7.84 | 6.37 | 7.34 | 5.44 | 4.45 | 7.99 | 4.50 | 5.62 | 7.91 | 6.2 |
| Total | 99.2 | 99.7 | 99.2 | 99.2 | 99.4 | 99.1 | 98.9 | 99.5 | 99.0 | 99.1 | 98.9 | 99.0 | 98.6 | 99.3 | 98.7 | 98.9 | 99.1 |
| CIA | 57 | 79 | 68 | 65 | 73 | 75 | 80 | 84 | 77 | 81 | 71 | 67 | 81 | 61 | 68 | 81 | 72 |
| **Trace elements (ppm)** | | | | | | | | | | | | | | | | | |
| Sc | 19.5 | 22.3 | 19.8 | 15.4 | 19.2 | 18.8 | 20.9 | 19.5 | 20.5 | 17.4 | 19.2 | 22.2 | 9.3 | 14.6 | 13.9 | 9.6 | 17.6 |
| V | 133 | 241 | 145 | 110 | 143 | 140 | 238 | 141 | 133 | 125 | 132 | 142 | 136 | 80 | 106 | 124 | 142 |
| Cr | 57 | 119 | 61 | 157 | 111 | 78 | 102 | 96 | 112 | 100 | 91 | 89 | 99 | 57 | 38 | 83 | 91 |
| Co | 27.0 | 8.9 | 11.7 | 13.4 | 17.8 | 13.1 | 1.6 | 7.4 | 11.4 | 5.0 | 10.4 | 6.7 | 4.3 | 8.5 | 3.5 | 6.1 | 9.8 |
| Ni | 11.8 | 0 | 0 | 10.4 | 28.7 | 19.2 | 32.6 | 44.2 | 59.4 | 32.5 | 77.1 | 36.0 | 31.0 | 25.8 | 15.1 | 39.0 | 28.9 |
| Rb | 128 | 140 | 73.9 | 74.0 | 90.5 | 79.0 | 114 | 114 | 105 | 96.1 | 74.8 | 83.0 | 75.1 | 80.3 | 112 | 69.1 | 94.3 |
| Sr | 90 | 23 | 95 | 102 | 53 | 65 | 48 | 11 | 103 | 14 | 114 | 171 | 13 | 78 | 59 | 27 | 67 |
| Y | 25.6 | 22.0 | 20.4 | 17.8 | 23.2 | 27.6 | 33.9 | 28.3 | 28.8 | 28.0 | 23.8 | 31.1 | 24.6 | 20.4 | 42.1 | 43.5 | 27.6 |
| Zr | 158 | 178 | 150 | 147 | 158 | 164 | 176 | 166 | 158 | 161 | 135 | 147 | 147 | 166 | 206 | 125 | 159 |
| Nb | 10 | 13 | 8.55 | 8.13 | 9.96 | 9.16 | 12.0 | 12.1 | 10.9 | 10.6 | 8.87 | 9.11 | 9.61 | 10.01 | 12.6 | 7.97 | 10.15 |
| Cs | 7.08 | 8.42 | 4.63 | 4.61 | 4.97 | 3.24 | 5.39 | 6.33 | 4.65 | 3.70 | 3.12 | 4.16 | 4.06 | 6.83 | 6.16 | 2.79 | 5.01 |
| Ba | 519 | 554 | 472 | 283 | 413 | 340 | 602 | 576 | 652 | 530 | 393 | 579 | 491 | 725 | 966 | 531 | 539 |
| La | 27.9 | 36.3 | 22.4 | 25.1 | 31.8 | 24.3 | 38.8 | 39.9 | 38.9 | 16.4 | 13.3 | 24.8 | 27.4 | 26.4 | 14.9 | 43.5 | 28.3 |
| Ce | 53.9 | 72.4 | 46.7 | 53.8 | 60.7 | 43.6 | 72.7 | 78.7 | 75.0 | 19.1 | 29.2 | 55.2 | 50.9 | 47.2 | 35.6 | 51.7 | 52.9 |
| Pr | 5.79 | 7.44 | 5.18 | 6.06 | 6.86 | 5.60 | 9.58 | 9.19 | 8.19 | 4.07 | 4.34 | 6.77 | 7.28 | 5.72 | 5.68 | 11.0 | 6.80 |
| Nd | 21.9 | 27.2 | 19.8 | 24.2 | 26.7 | 23.4 | 37.9 | 37.8 | 31.8 | 18.5 | 19.7 | 28.4 | 31.7 | 22.9 | 27.3 | 47.6 | 27.9 |
| Sm | 4.67 | 4.81 | 4.23 | 5.37 | 5.42 | 5.73 | 7.29 | 7.26 | 5.50 | 3.99 | 4.66 | 6.12 | 7.10 | 4.53 | 7.51 | 10.5 | 5.92 |
| Eu | 1.03 | 1.04 | 0.98 | 1.21 | 1.20 | 1.30 | 1.76 | 1.69 | 1.36 | 1.12 | 1.11 | 1.90 | 1.32 | 1.03 | 1.43 | 1.86 | 1.33 |
| Gd | 4.54 | 4.28 | 3.76 | 4.79 | 5.02 | 5.78 | 7.12 | 5.80 | 5.22 | 4.64 | 4.70 | 6.06 | 6.31 | 4.76 | 6.63 | 9.06 | 5.53 |
| Tb | 0.79 | 0.66 | 0.61 | 0.69 | 0.75 | 0.87 | 0.93 | 0.83 | 0.74 | 0.67 | 0.67 | 0.91 | 1.08 | 0.74 | 1.15 | 1.67 | 0.86 |
| Dy | 4.61 | 3.91 | 3.63 | 3.71 | 4.31 | 4.82 | 5.92 | 4.97 | 5.12 | 4.47 | 4.07 | 5.78 | 6.72 | 4.85 | 7.94 | 10.6 | 5.34 |
| Ho | 0.95 | 0.82 | 0.82 | 0.73 | 0.90 | 1.01 | 1.29 | 1.10 | 1.11 | 1.01 | 0.94 | 1.23 | 1.32 | 0.95 | 1.71 | 2.10 | 1.12 |
| Er | 2.80 | 2.64 | 2.38 | 2.07 | 2.70 | 2.79 | 3.73 | 3.14 | 3.14 | 3.15 | 2.66 | 3.56 | 3.52 | 2.71 | 4.73 | 5.34 | 3.19 |
| Tm | 0.46 | 0.43 | 0.41 | 0.31 | 0.41 | 0.43 | 0.58 | 0.53 | 0.49 | 0.51 | 0.46 | 0.55 | 0.50 | 0.42 | 0.64 | 0.71 | 0.49 |
| Yb | 2.99 | 3.07 | 2.76 | 2.18 | 2.67 | 2.85 | 3.80 | 3.43 | 3.34 | 3.17 | 2.64 | 3.57 | 3.21 | 2.69 | 4.13 | 4.39 | 3.18 |
| Lu | 0.46 | 0.48 | 0.40 | 0.33 | 0.40 | 0.44 | 0.59 | 0.50 | 0.53 | 0.48 | 0.41 | 0.52 | 0.51 | 0.44 | 0.66 | 0.65 | 0.49 |
| Hf | 4.41 | 4.90 | 4.06 | 3.76 | 4.34 | 4.37 | 5.41 | 5.19 | 4.72 | 4.89 | 4.20 | 5.03 | 5.03 | 5.44 | 7.45 | 4.65 | 4.87 |
| Ta | 0.88 | 0.82 | 0.56 | 0.49 | 0.65 | 0.60 | 0.67 | 0.77 | 0.73 | 0.67 | 0.52 | 0.59 | 0.33 | 0.35 | 0.47 | 0.30 | 0.59 |
| Pb | 6.30 | 31.1 | 9.55 | 8.87 | 12.7 | 6.79 | 17.9 | 6.27 | 8.22 | 11.4 | 8.15 | 7.87 | 12.0 | 17.4 | 4.10 | 6.65 | 11.0 |
| Th | 11 | 10 | 5.79 | 5.34 | 8.52 | 6.21 | 10.41 | 10.40 | 12.2 | 8.27 | 7.59 | 7.75 | 7.14 | 7.06 | 7.76 | 6.92 | 8.27 |
| U | 1.63 | 2.30 | 1.52 | 1.47 | 1.64 | 1.38 | 4.74 | 2.30 | 2.31 | 1.73 | 1.72 | 1.75 | 1.89 | 2.31 | 1.81 | 1.53 | 2.00 |
| Eu/Eu* | 0.68 | 0.70 | 0.75 | 0.73 | 0.71 | 0.69 | 0.75 | 0.80 | 0.78 | 0.80 | 0.72 | 0.95 | 0.60 | 0.68 | 0.62 | 0.58 | 0.72 |
| REE | 133 | 166 | 114 | 131 | 150 | 123 | 192 | 195 | 180 | 81 | 89 | 145 | 149 | 125 | 120 | 201 | 143 |
| La/Yb$_N$ | 6.28 | 7.95 | 5.45 | 7.75 | 8.04 | 5.74 | 6.88 | 7.83 | 7.84 | 3.48 | 3.38 | 4.67 | 5.75 | 6.61 | 2.42 | 6.66 | 6.0 |
| La/Yb | 9.33 | 11.8 | 8.10 | 11.51 | 11.95 | 8.53 | 10.22 | 11.63 | 11.6 | 5.17 | 5.02 | 6.94 | 8.54 | 9.83 | 3.60 | 9.90 | 9.0 |
| Cr/Th | 5.4 | 11.4 | 10.6 | 29.5 | 13.0 | 12.5 | 9.8 | 9.2 | 9.2 | 12.1 | 12.0 | 11.4 | 13.8 | 8.1 | 5.0 | 12.0 | 11.6 |

Table 4 (continued)

| | Zagu | | | | | | |
| | Sandstone | | | | Mudstone | | |
| | F22 | F23 | Z1 | Average | st1 | st9 | st10 | Average |
|---|---|---|---|---|---|---|---|---|
| Major Oxides (wt%) | | | | | | | | |
| $SiO_2$ | 63.1 | 65.4 | 66.8 | 65.1 | 61.5 | 58.9 | 67.1 | 62.5 |
| $TiO_2$ | 1.03 | 0.89 | 0.70 | 0.9 | 0.85 | 0.81 | 0.55 | 0.7 |
| $Al_2O_3$ | 15.2 | 14.0 | 13.8 | 14.3 | 16.1 | 20.0 | 14.9 | 17.0 |
| $Fe_2O_3$ | 7.44 | 6.63 | 6.32 | 6.8 | 8.04 | 7.26 | 5.84 | 7.0 |
| MnO | 0.05 | 0.05 | 0.05 | 0.0 | 0.14 | 0.02 | 0.05 | 0.1 |
| MgO | 3.15 | 2.80 | 2.50 | 2.8 | 3.28 | 2.02 | 1.91 | 2.4 |
| CaO | 0.37 | 0.31 | 0.49 | 0.4 | 0.27 | 0.08 | 0.30 | 0.2 |
| $Na_2O$ | 3.45 | 3.34 | 2.40 | 3.1 | 2.52 | 0.26 | 1.73 | 1.5 |
| $K_2O$ | 2.70 | 2.24 | 2.33 | 2.4 | 2.65 | 3.48 | 2.23 | 2.8 |
| $P_2O_5$ | 0.15 | 0.13 | 0.19 | 0.2 | 0.14 | 0.11 | 0.05 | 0.1 |
| LOI | 2.98 | 3.39 | 3.13 | 3.2 | 4.27 | 6.21 | 4.69 | 5.1 |
| Total | 99.7 | 99.2 | 98.7 | 99.2 | 99.8 | 99.1 | 99.3 | 99.4 |
| CIA | 63 | 63 | 67 | 64 | 69 | 83 | 72 | 75 |
| Trace elements (ppm) | | | | | | | | |
| Sc | 12.7 | 11.7 | 14.3 | 12.9 | 20.1 | 20.4 | 12.8 | 17.8 |
| V | 116 | 96 | 103 | 105 | 126 | 160 | 72 | 119 |
| Cr | 58 | 49 | 34 | 47 | 56 | 90 | 40 | 62 |
| Co | 11.8 | 6.7 | 10.5 | 9.7 | 18.5 | 10.2 | 10.1 | 12.9 |
| Ni | 26.0 | 21.1 | 16.7 | 21.3 | 5.96 | 25.9 | 0.00 | 10.6 |
| Rb | 52.3 | 44.8 | 63.6 | 53.6 | 85.9 | 122.9 | 78.3 | 95.7 |
| Sr | 70 | 68 | 85 | 74 | 51 | 16 | 75 | 47 |
| Y | 21.1 | 21.4 | 33.5 | 25.3 | 28.9 | 36.5 | 32.3 | 32.6 |
| Zr | 138 | 111 | 135 | 128 | 167 | 204 | 181 | 184 |
| Nb | 8.73 | 7.01 | 7.40 | 7.71 | 10.05 | 13.40 | 10.68 | 11.37 |
| Cs | 1.88 | 1.60 | 2.10 | 1.86 | 3.88 | 4.86 | 6.54 | 5.09 |
| Ba | 553 | 464 | 563 | 527 | 319 | 733 | 853 | 635 |
| La | 20.2 | 18.1 | 22.5 | 20.3 | 30.2 | 48.2 | 34.7 | 37.7 |
| Ce | 39.7 | 36.6 | 44.7 | 40.3 | 61.2 | 84.6 | 47.7 | 64.5 |
| Pr | 4.35 | 4.02 | 5.59 | 4.65 | 6.83 | 11.31 | 8.61 | 8.92 |
| Nd | 18.0 | 16.8 | 23.8 | 19.5 | 26.6 | 44.6 | 34.8 | 35.3 |
| Sm | 3.77 | 3.74 | 5.90 | 4.47 | 6.15 | 9.41 | 8.49 | 8.02 |
| Eu | 0.89 | 0.85 | 1.75 | 1.16 | 1.09 | 2.03 | 1.57 | 1.56 |
| Gd | 3.75 | 3.56 | 6.23 | 4.51 | 5.60 | 8.39 | 7.62 | 7.21 |
| Tb | 0.63 | 0.64 | 1.14 | 0.80 | 0.93 | 1.25 | 1.27 | 1.15 |
| Dy | 4.24 | 4.27 | 6.51 | 5.01 | 5.30 | 7.03 | 6.66 | 6.33 |
| Ho | 0.91 | 0.94 | 1.29 | 1.05 | 1.13 | 1.41 | 1.26 | 1.27 |
| Er | 2.58 | 2.74 | 3.23 | 2.85 | 3.31 | 3.98 | 3.59 | 3.63 |
| Tm | 0.41 | 0.39 | 0.43 | 0.41 | 0.53 | 0.60 | 0.56 | 0.56 |
| Yb | 2.57 | 2.44 | 2.69 | 2.57 | 3.75 | 3.95 | 3.67 | 3.79 |
| Lu | 0.43 | 0.39 | 0.37 | 0.40 | 0.53 | 0.58 | 0.54 | 0.55 |
| Hf | 4.64 | 3.70 | 3.68 | 4.01 | 4.61 | 5.74 | 5.08 | 5.14 |
| Ta | 0.30 | 0.24 | 0.46 | 0.33 | 0.65 | 0.95 | 0.80 | 0.80 |
| Pb | 10.2 | 6.68 | 6.27 | 7.72 | 1.58 | 15.8 | 3.88 | 7.09 |
| Th | 7.66 | 5.50 | 5.82 | 6.33 | 8.47 | 11.13 | 8.05 | 9.21 |
| U | 1.77 | 1.28 | 0.92 | 1.32 | 1.51 | 2.35 | 1.60 | 1.82 |
| Eu/Eu* | 0.72 | 0.71 | 0.88 | 0.77 | 0.57 | 0.70 | 0.60 | 0.62 |
| REE | 102 | 95 | 126 | 108 | 153 | 227 | 161 | 180 |
| La/Yb$_N$ | 5.30 | 5.00 | 5.63 | 5.3 | 5.42 | 8.21 | 6.35 | 6.7 |
| La/Yb | 7.87 | 7.43 | 8.36 | 7.9 | 8.05 | 12.20 | 9.44 | 9.9 |
| Cr/Th | 7.6 | 9.0 | 5.8 | 7.5 | 6.6 | 8.1 | 4.9 | 6.5 |

**Table 5**

Table 5 Discriminating  REE elements and ratios for the Yanbian sandstones (after Bhatia,1983)

| Tectonic settings | La | Ce | $\sum$REE | La/Yb | La/Yb$_N$ | $\sum$LREE/$\sum$HREE | Eu/Eu* |
|---|---|---|---|---|---|---|---|
| Oceanic island arc | 8±1.7 | 19±3.7 | 58±10 | 4.2±1.3 | 2.8±0.9 | 3.8±0.9 | 1.04±0.11 |
| Andean-type continetnal margin | 37 | 78 | 186 | 12.5 | 8.5 | 9.1 | 0.6 |
| Passive margins | 39 | 85 | 210 | 15.9 | 10.8 | 8.5 | 0.56 |
| Continental island arc | 27±4.5 | 59±8.2 | 146±20 | 11±3.6 | 7.5±2.5 | 7.7±1.7 | 0.79±0.13 |
| Yanbian Group* | 22 | 42 | 116 | 8.5 | 5.7 | 5.6 | 0.69 |

*Values are adopted from the mean values of the 33 sandstones in the Xiaoping Formation.
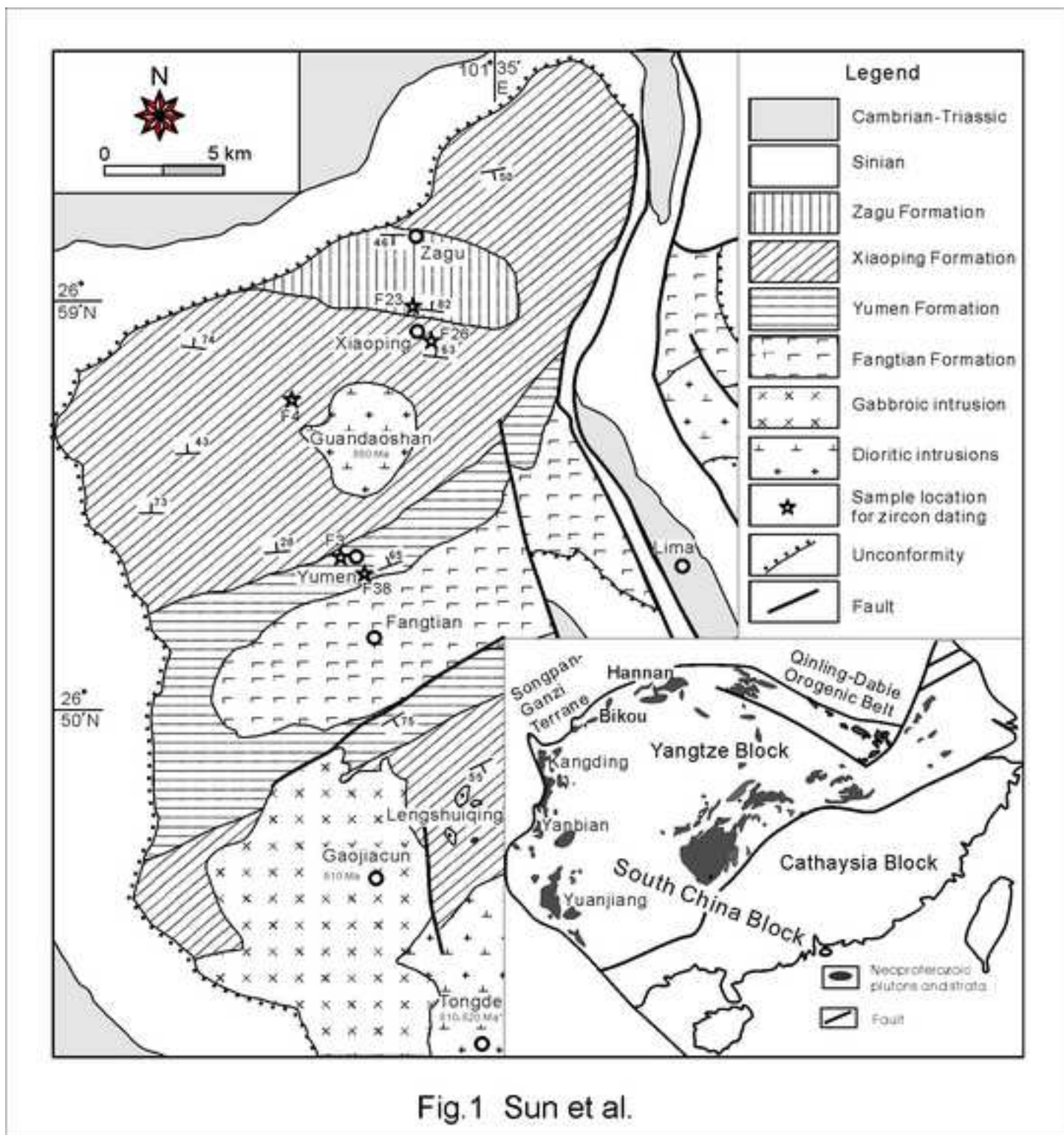
Fig.1  Sun et al.

| Formations | Lithological log | Lithologies description | Sedimentary structure |
|---|---|---|---|
| Lieguliu (Sinian) | 5250 m | Shale and sandstone with a ~30 m layer of conglomerate of glacial-interglacial origin. | |
| Zagu Formation | 4870 m | Dolomitic slate, dolomitic limestone and gray siliceous slate. | parallel bedding |
| Zagu Formation | | Dark gray slates with minor black cabonaceous slate and sandstone interbeds. | parallel bedding, grading, Bouma sequence. |
| Zagu Formation | F23 3980 m | At the base there is a layer of conglomerate and pebbly sandstone (~10 m thick). | |
| Xiaoping Formation | F26 2680 m | Dark gray slate and black cabonaceous slate with minor sandstone interbeds. At the top, the sandstone beds increase. | parallel bedding, grading, Bouma sequence, scour and filling, load and flame textures. |
| Xiaoping Formation | F4 | In the upper part, there are black and gray slates with minor sandstone interbeds. | |
| Xiaoping Formation | | In the lower part, there are dark gray or black cabonaceous slates with minor sandstone interbeds. Locally limestone lenses are present. | parallel bedding, grading, Bouma sequence, scour, slump, ferruginous nodules. |
| Xiaoping Formation | 1720 m | At the base, there are thick pebbly and coarse sandstones where Bouma sequences are well observed. | |
| Yumen Formation | F3 | Dark gray, or black carbonaceous slate and gray slate with minor sandstone interbeds. | parallel bedding, grading, and Bouma sequence. |
| Yumen Formation | 370 m F38 0 m | Dark gray, black carbonaceous and siliceous slate with isolated lenses of limestone and minor sandstone interbeds. It conformabaly overlies the Fangtian Formation. | parallel bedding, grading and slumps. |
| Fangtian Formation | | A volcanic sequence, >1500 m thick, is composed of massive basalt, pillow basalt, and volcanic breccia, with minor interbedded chert and siliceous or pelitic slate. | pillow, vesicular, and amygdaloidal textures. |

Fig. 2  Sun et al.
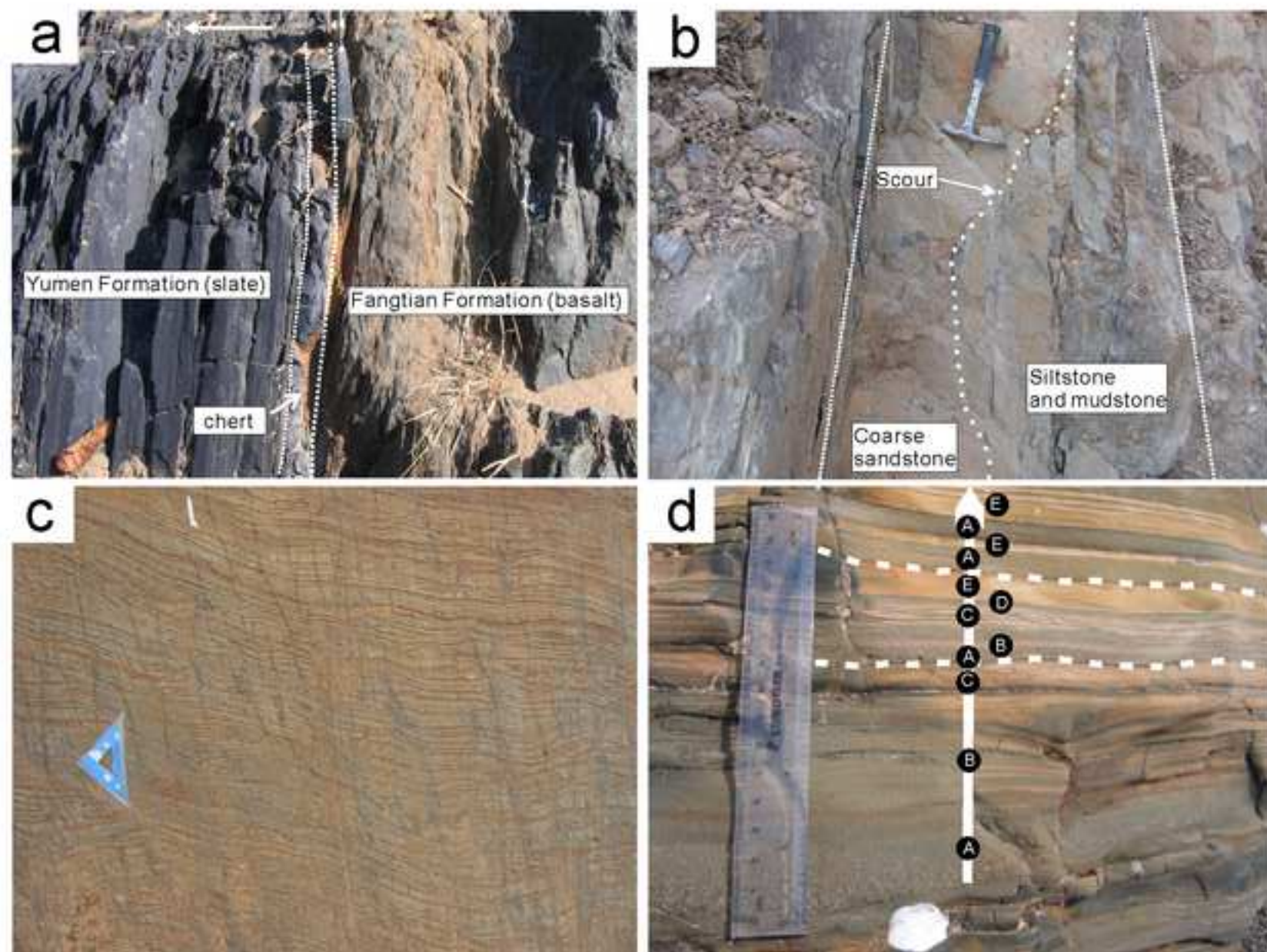
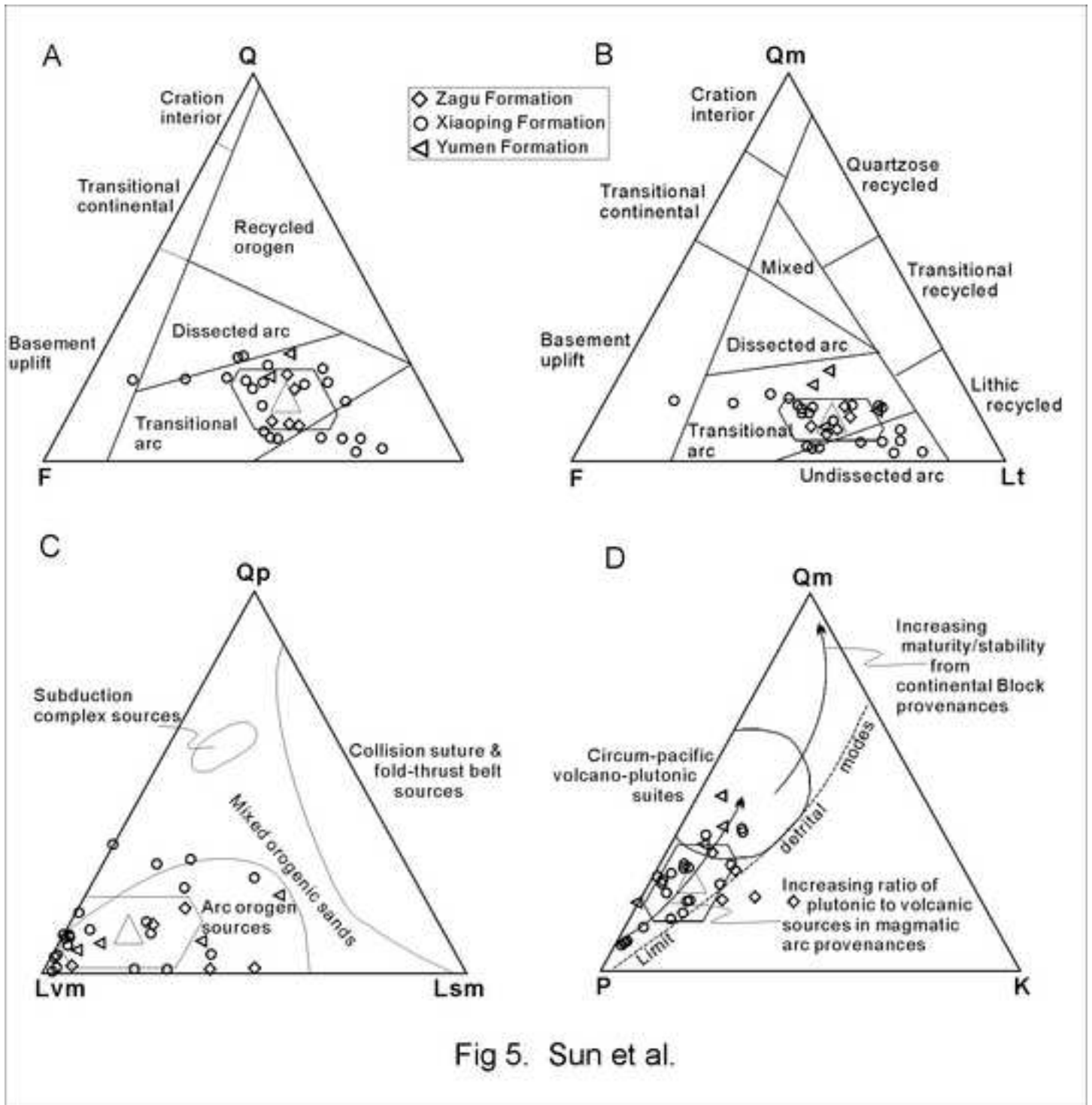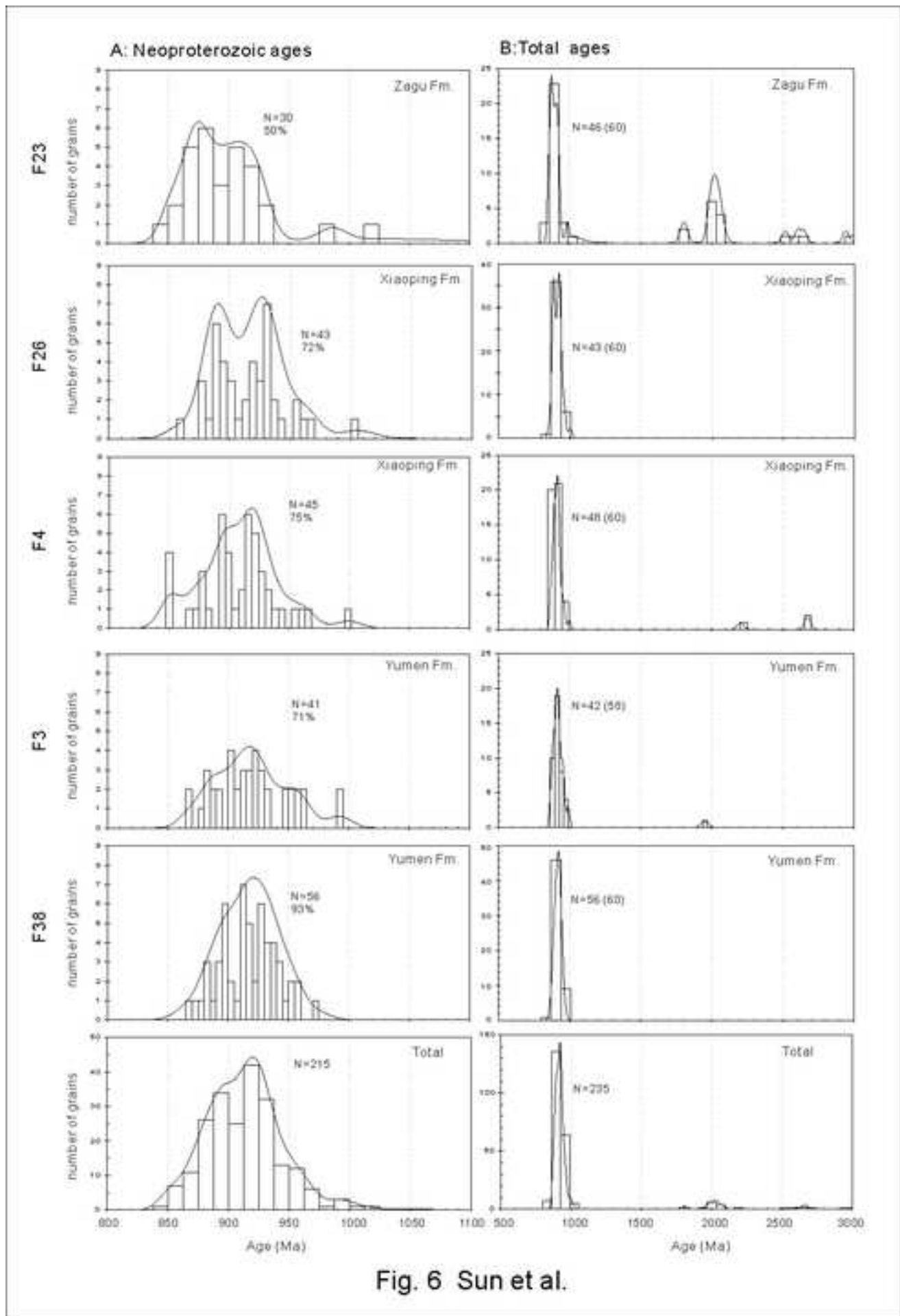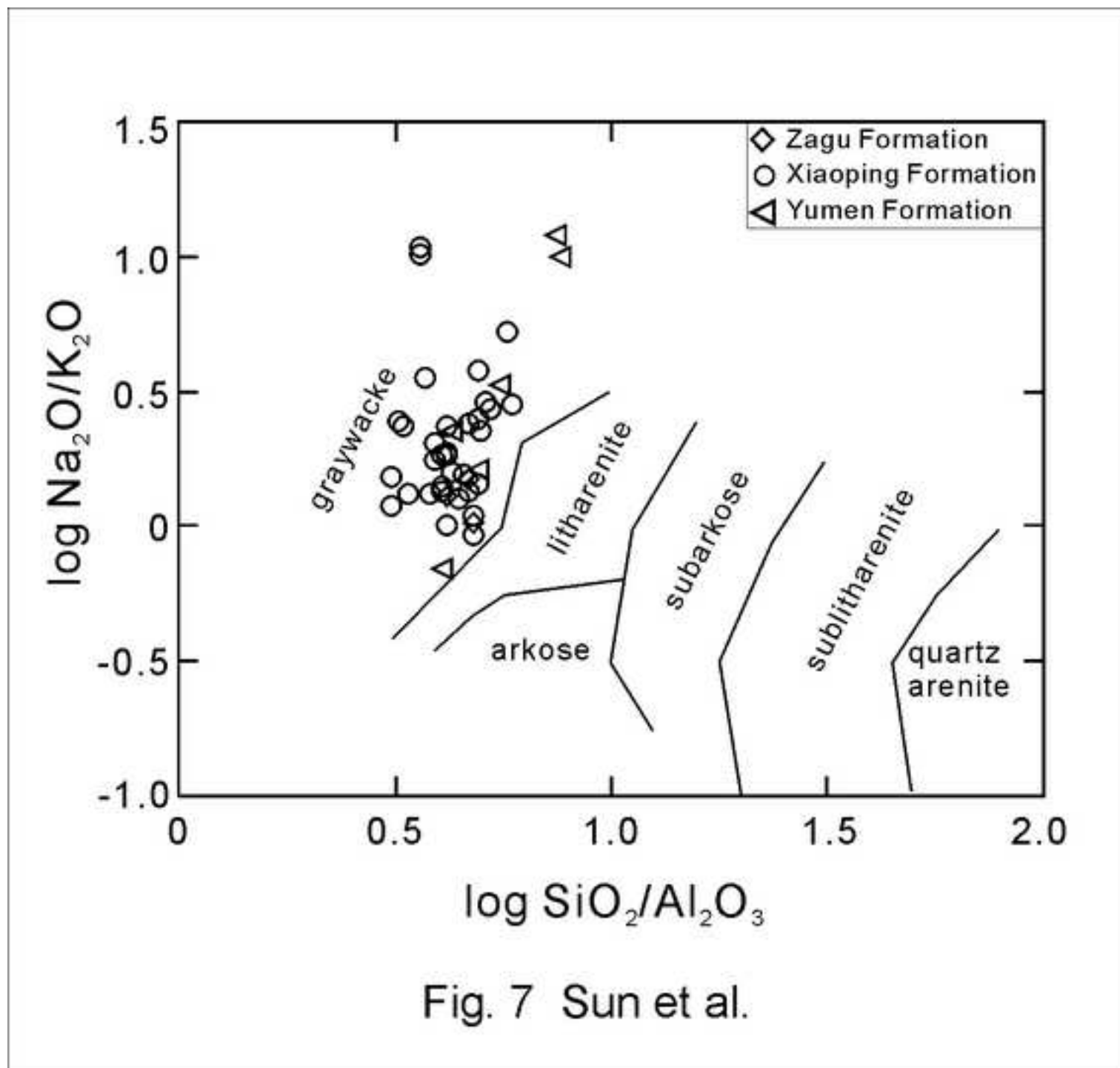Fig. 3  Sun et al.
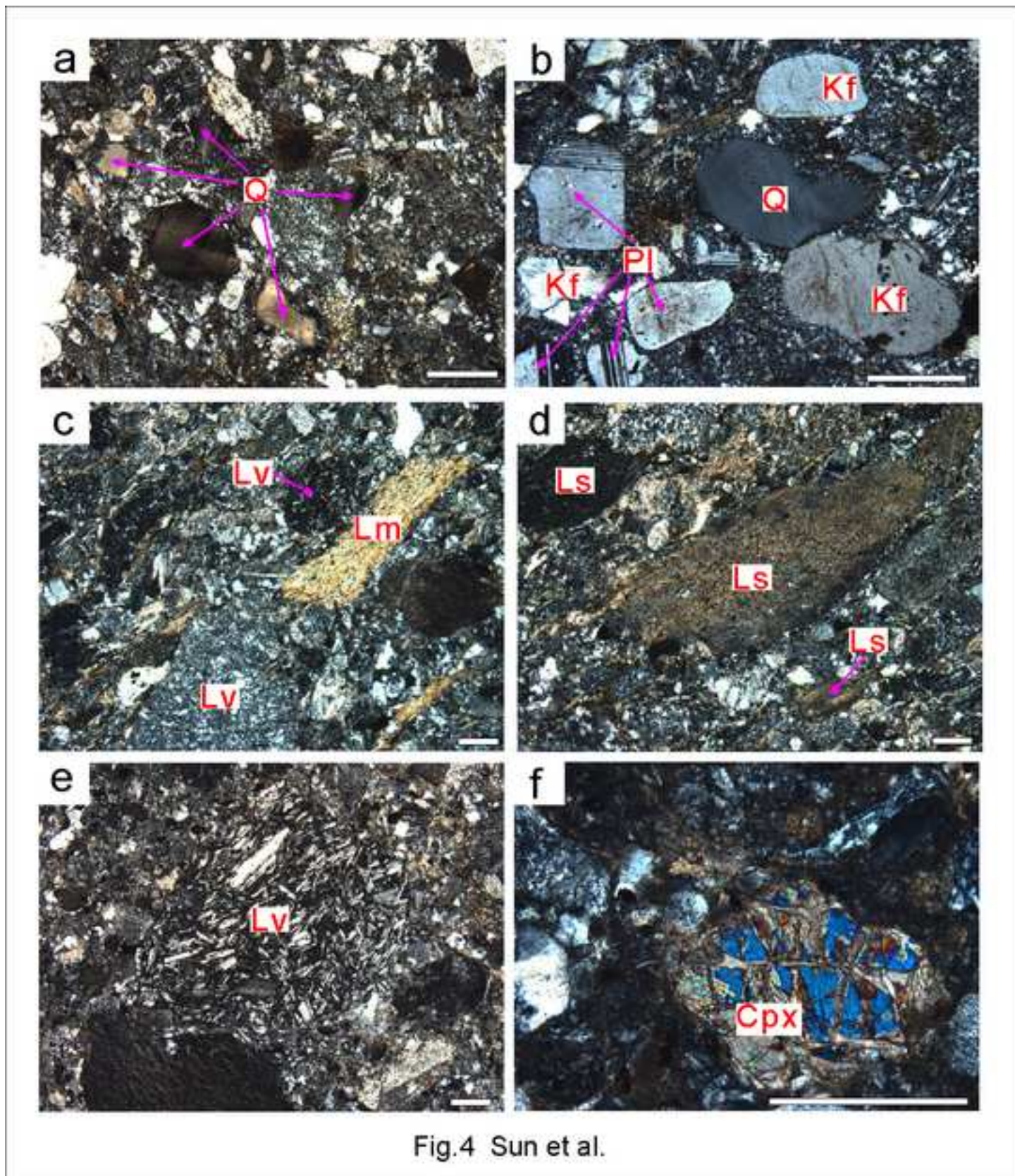
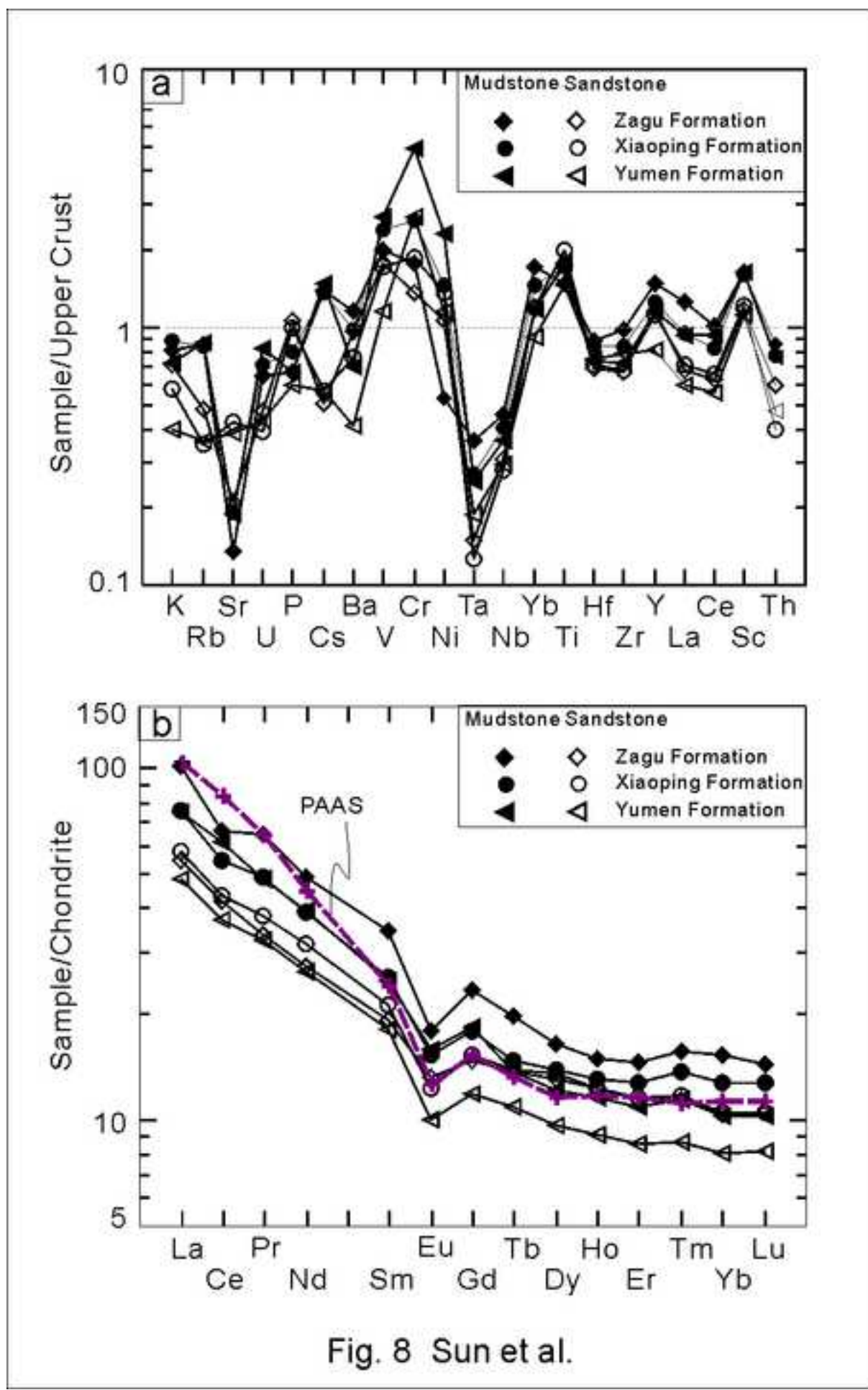Fig.4 Sun et al.

Fig 5. Sun et al.

Fig. 6  Sun et al.

Fig. 7  Sun et al.

Fig. 8  Sun et al.
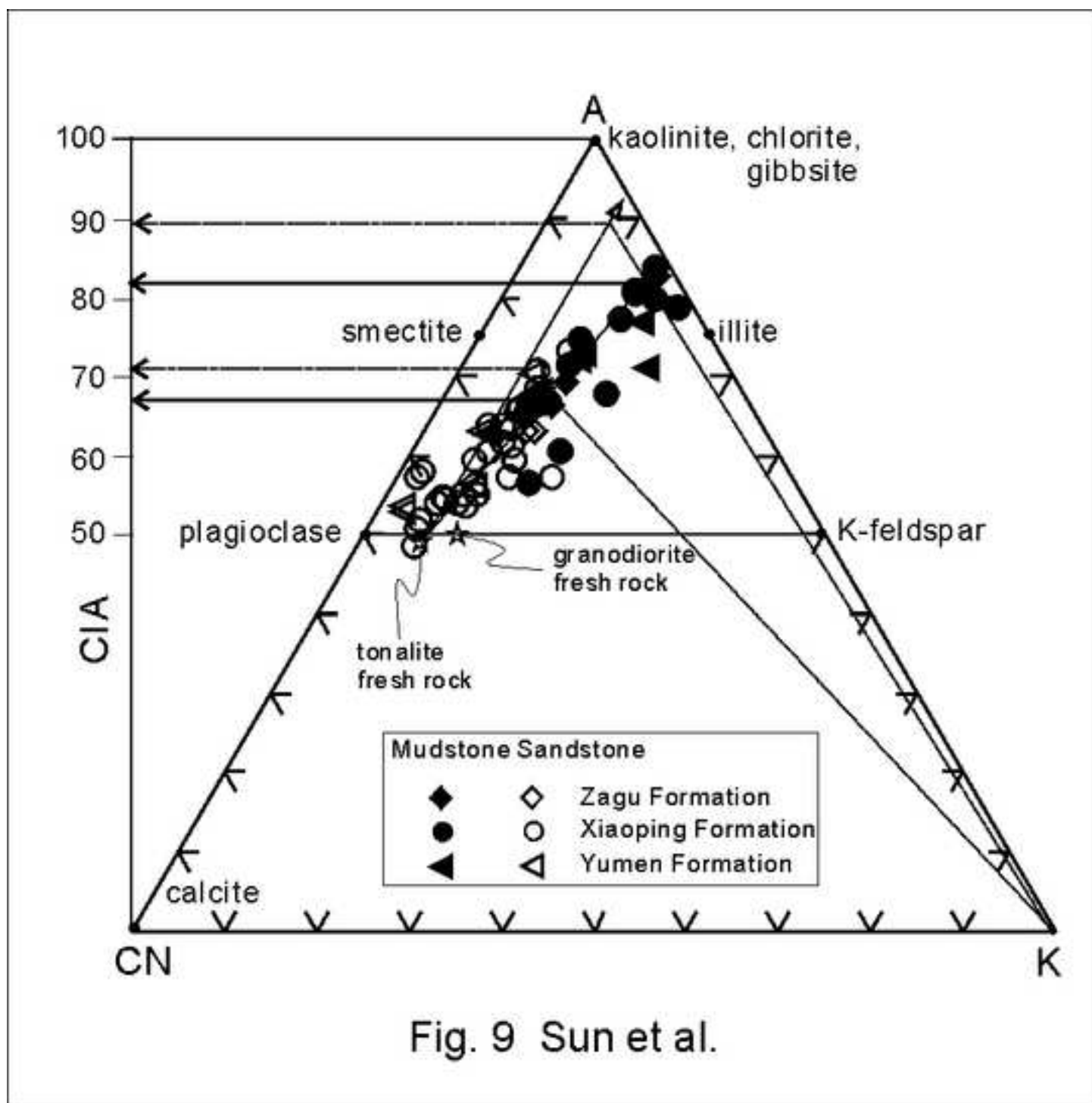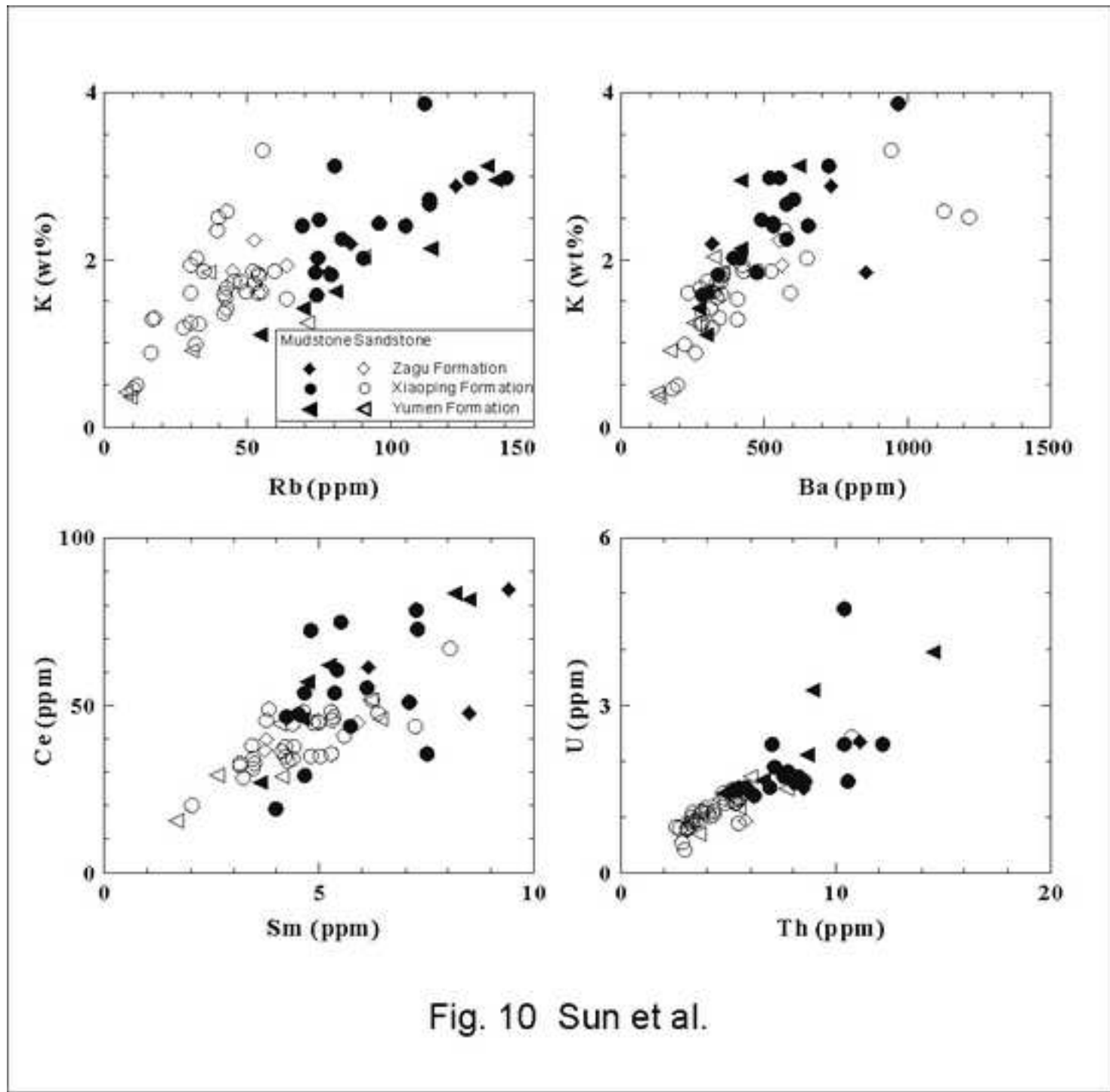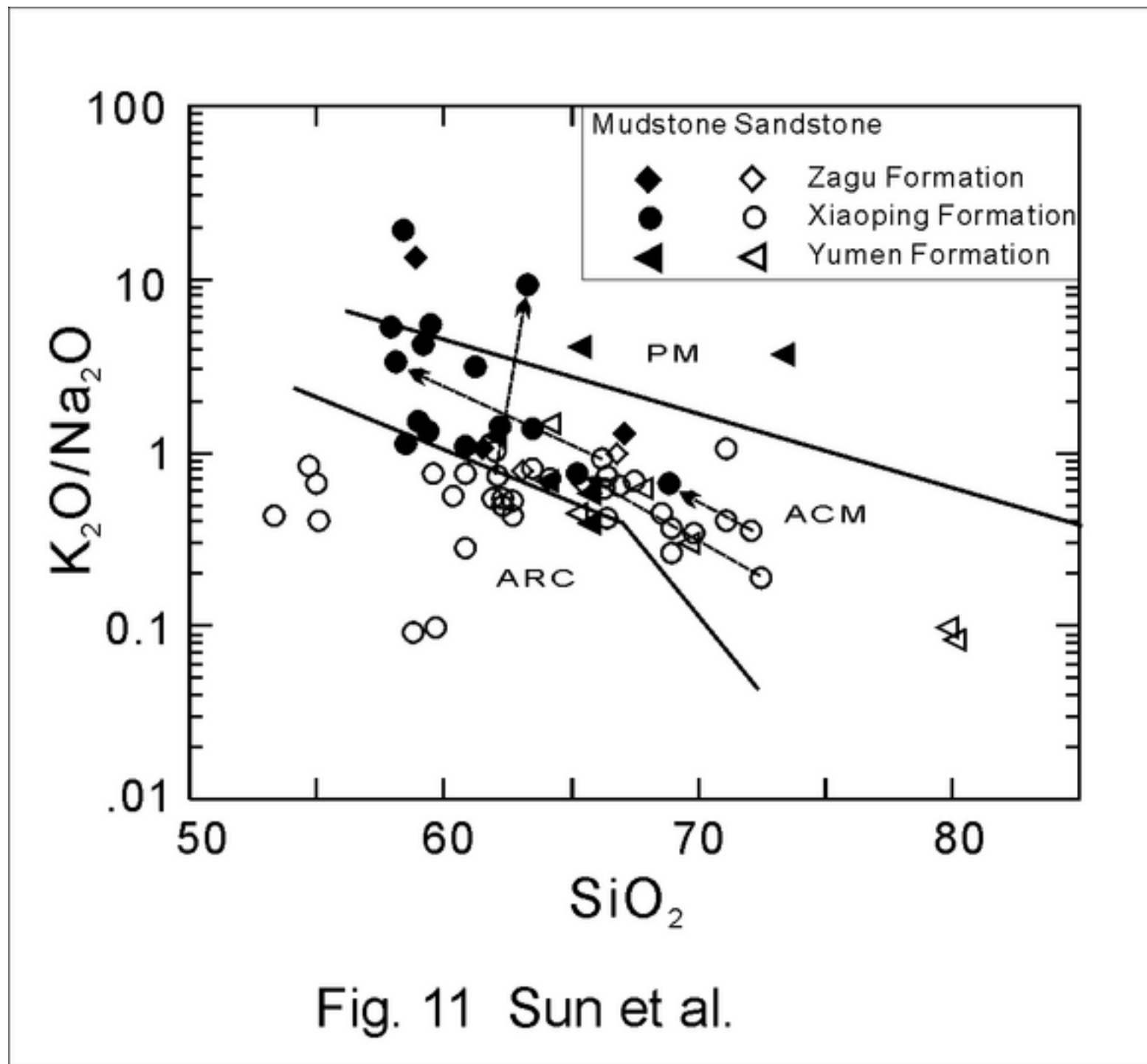
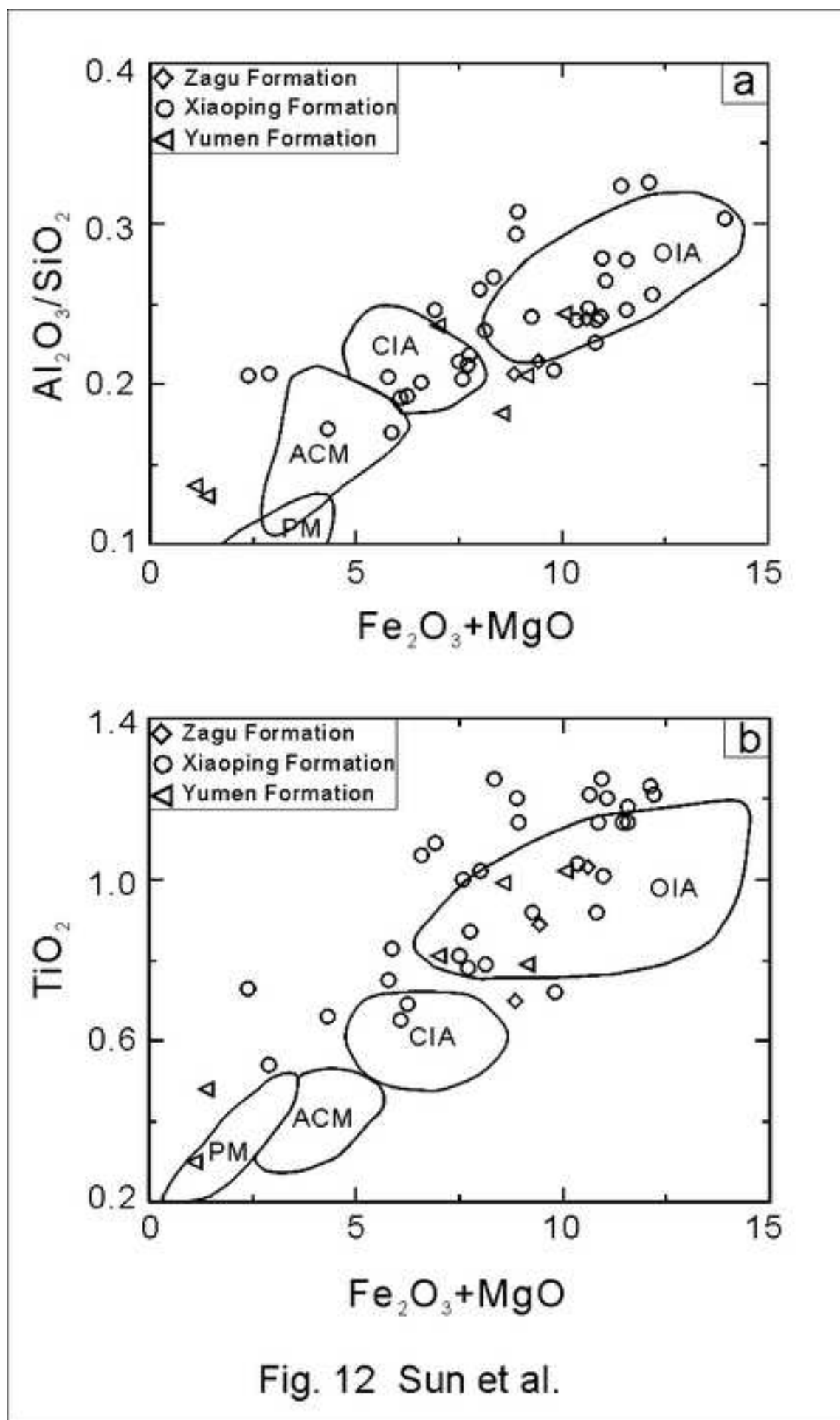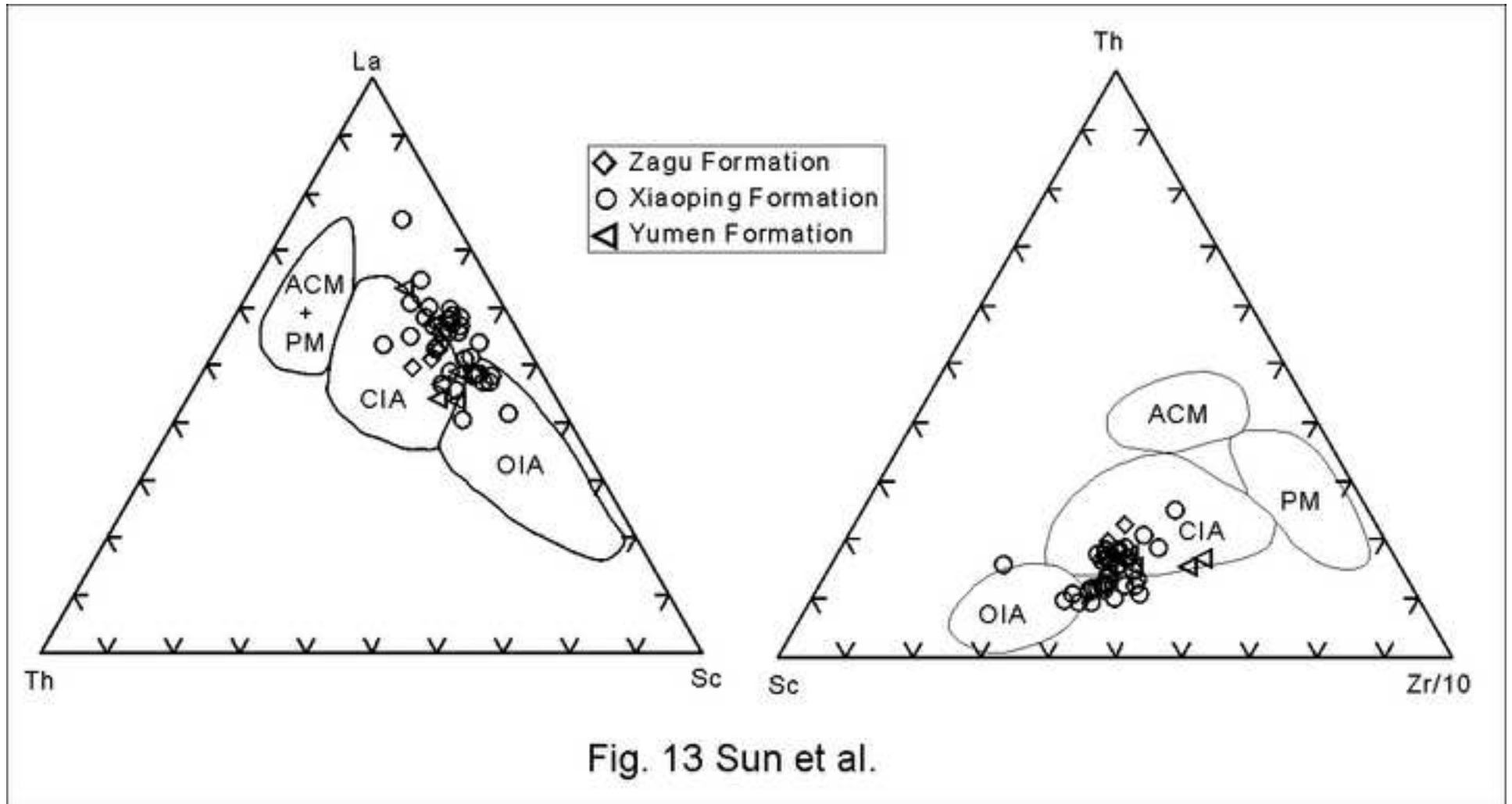Fig. 9  Sun et al.

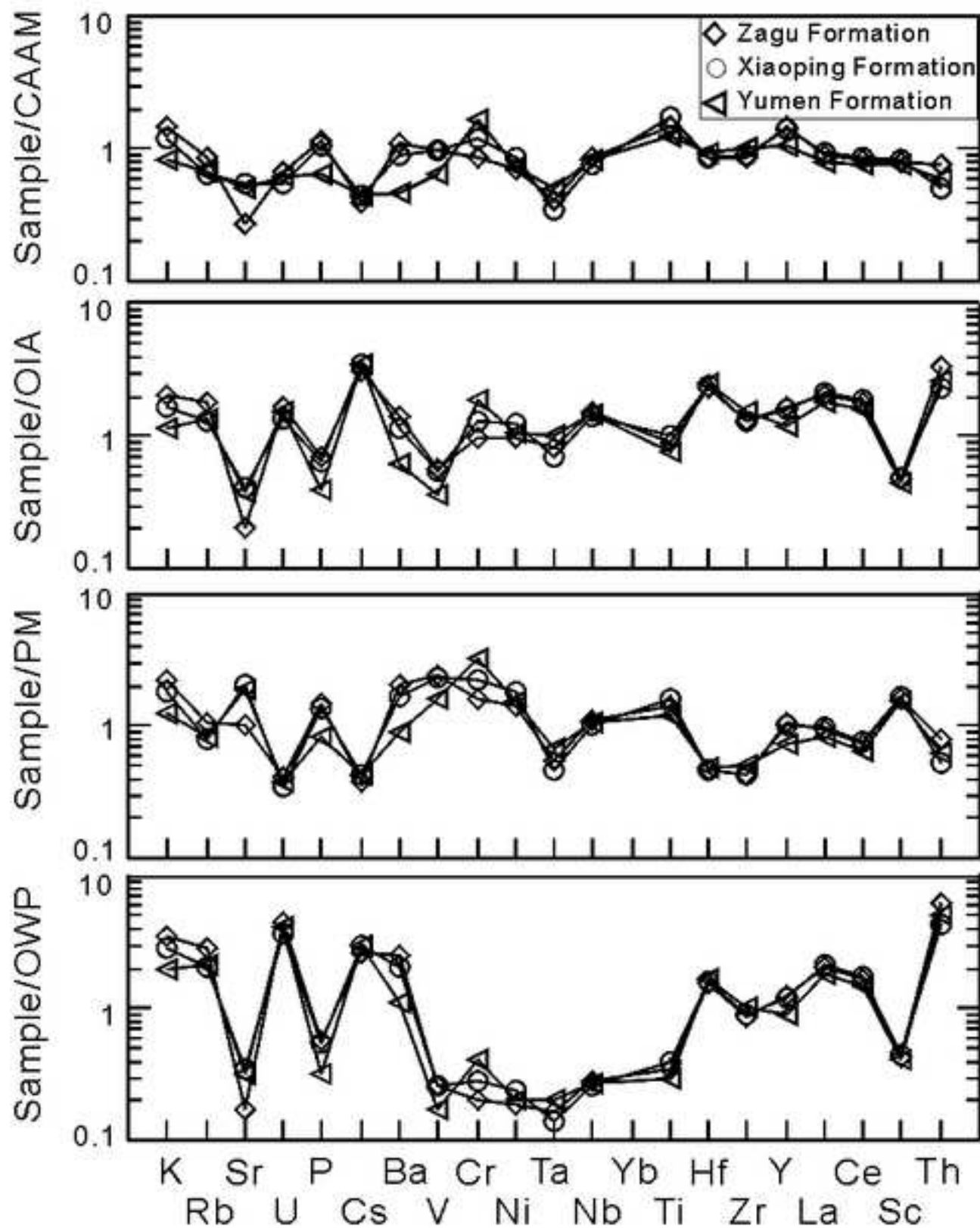Fig. 10  Sun et al.

Fig. 11 Sun et al.
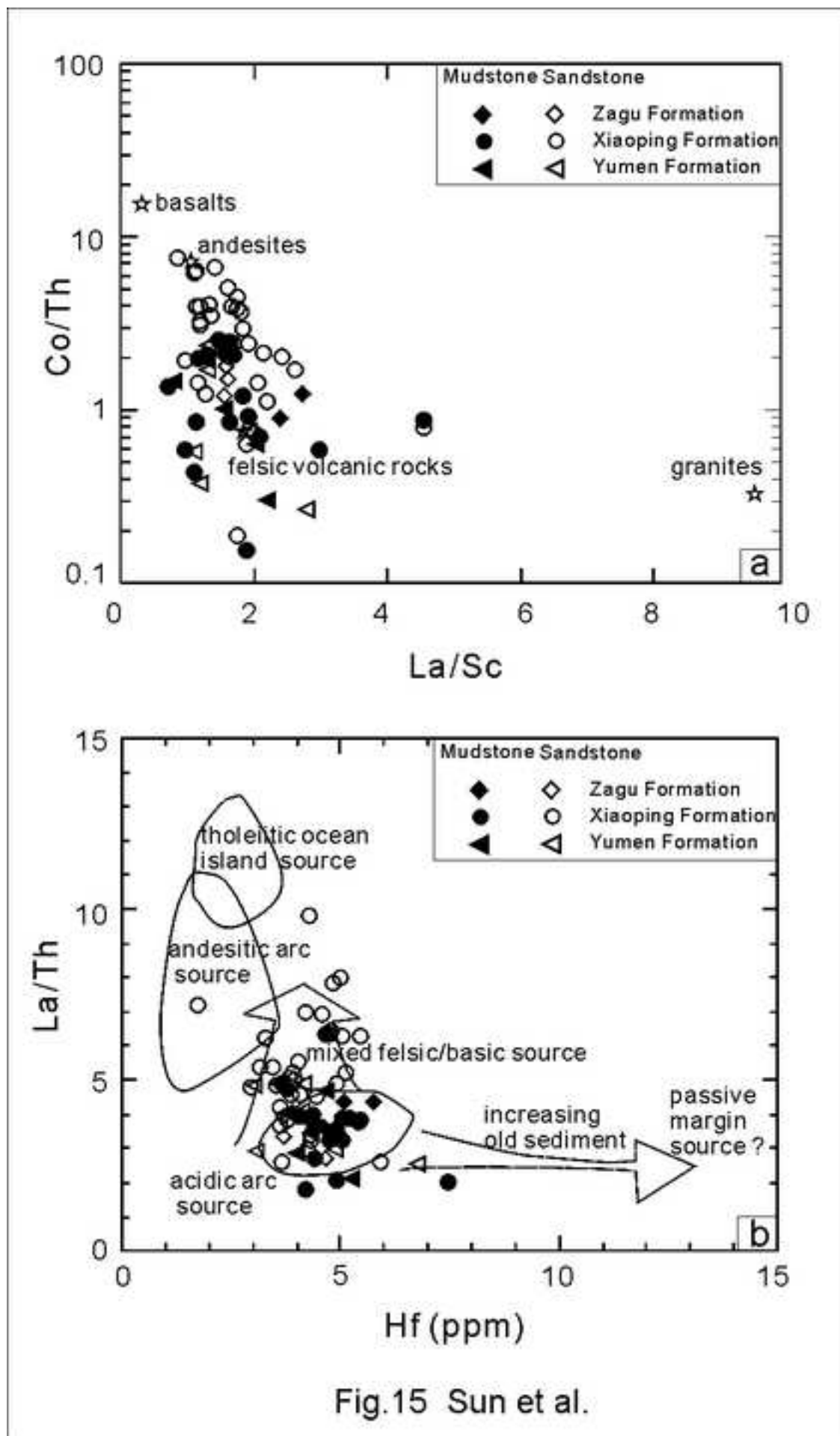
Fig. 12  Sun et al.
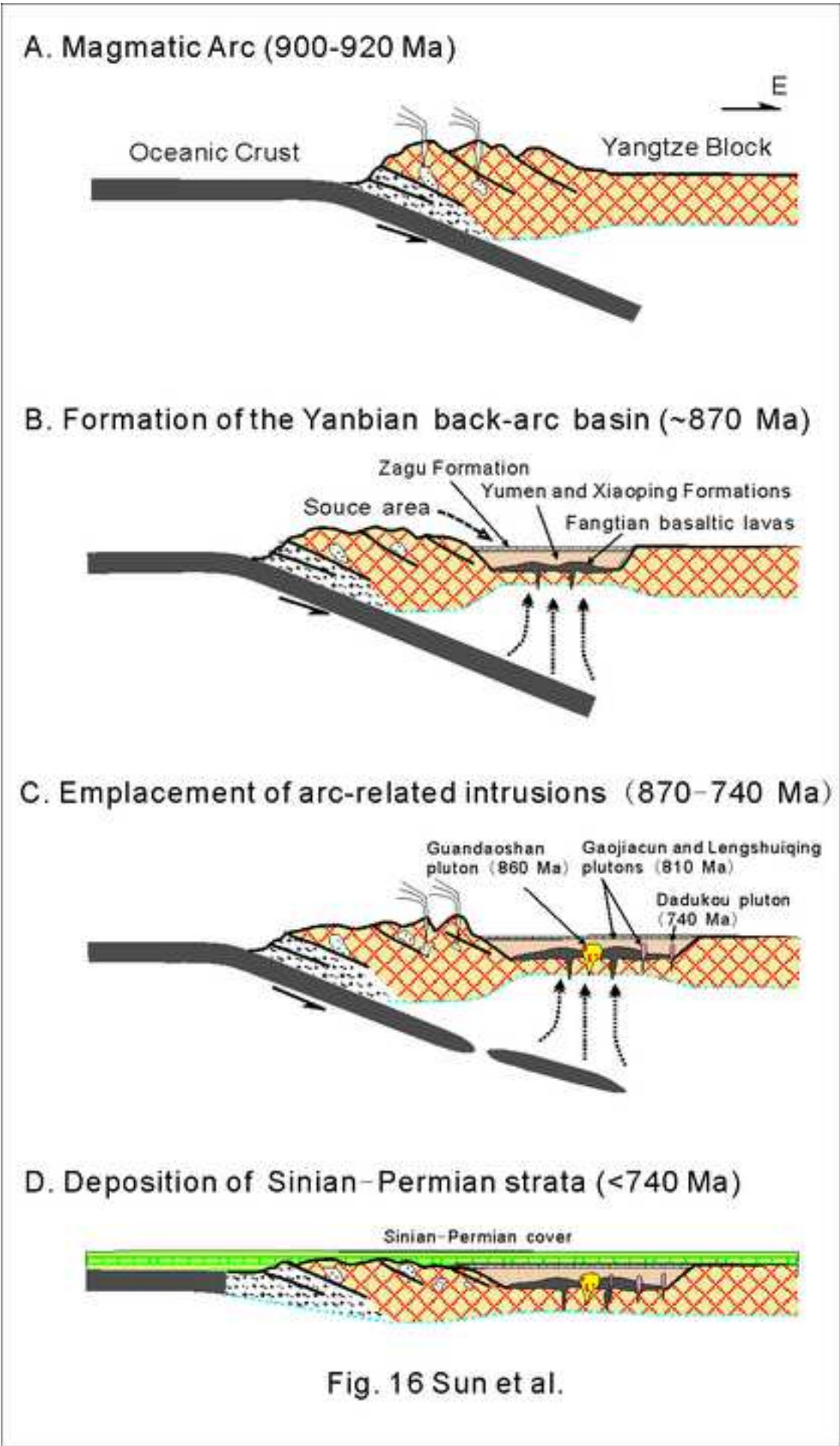
Fig. 13 Sun et al.

Fig. 14  Sun et al.

Fig.15  Sun et al.

A. Magmatic Arc (900-920 Ma)

Oceanic Crust
Yangtze Block
E

B. Formation of the Yanbian back-arc basin (~870 Ma)

Zagu Formation
Souce area
Yumen and Xiaoping Formations
Fangtian basaltic lavas

C. Emplacement of arc-related intrusions (870–740 Ma)

Guandaoshan pluton (860 Ma)
Gaojiacun and Lengshuiqing plutons (810 Ma)
Dadukou pluton (740 Ma)

D. Deposition of Sinian–Permian strata (<740 Ma)

Sinian–Permian cover

Fig. 16 Sun et al.